BIOCHEMICAL AND PHYSIOLOGICAL ANALYSIS OF ONCOGENIC CONSTITUTIVE ACTIVE VARIANTS OF GP130

Dissertation

zur Erlangung des Doktorgrades

der Mathematisch-Naturwissenschaftlichen Fakultät

der Christians-Albrechts-Universität

zu Kiel

vorgelegt von

Antje Michaela Schütt

Kiel, 2012

Erster Gutachter: Prof. Dr. Stefan Rose-John

Zweiter Gutachter: Prof. Dr. Thomas Röder

Tag der mündlichen Prüfung: 21.12.2012

Zum Druck genehmigt: 21.12.2012

gez. Prof. Dr. Wolfgang J. Duschl, Dekan

INDEX

1 INTRODUCTION

1.1 Interleukin 6

Interleukin 6 (IL-6) is the best characterized member of the IL-6 cytokine family. IL-6 was cloned in 1986 and is described as a four α-helix bundle protein with a mass of 21-28 kDa dependent on its glycosylation (1, 2). A common structural feature for all IL-6-type cytokines are four long α-helices (A, B, C, D), which are arranged in an up-up-down-down topology (Fig. 1.1) (3). The majority of the IL-6 family members binds directly to heterodimers of gp130 with LIF-R, OSM-R, WSX-1 or GPL (Tab. 1.1). IL-6 requires the IL-6 receptor (IL-6R), which exists as a membrane (mIL-6R) and as solube form (sIL-6R) (4). Initally IL-6 binds to its alpha-subunit IL-6R and the IL-6/IL-6R complex binds subsequently to homodimers of the common signal transducing beta-subunit gp130, initiating signal transduction (5).

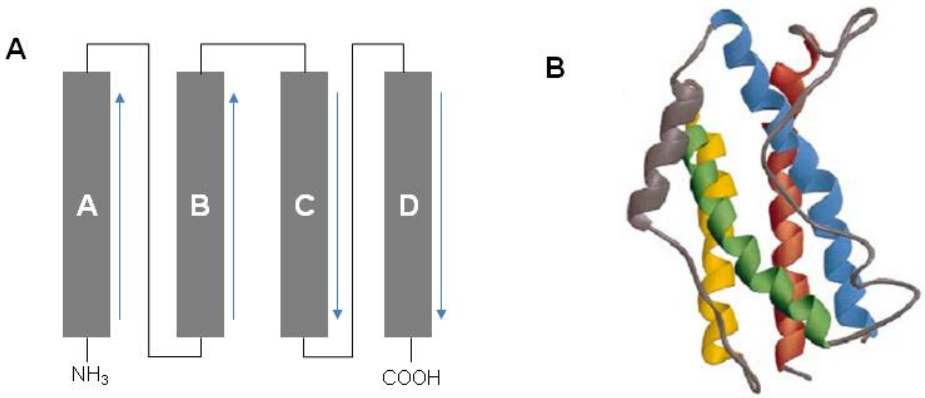

Figure 1.1: Structure of Interleukin 6. (A) Schematic representation of a four helix bundle cytokine with up-up-down-down topology. The four helices are designated A, B, C and D. (B) Ribbon representation of the four long α-helices of IL-6 solved by X-ray crystallography and NMR spectroscopy (6, 7). Helix A is highlited in red, B in green, C in yellow, D in blue. Picture was taken from Heinrich et al. (3).

Viral IL-6 (vIL-6) is an orthologue to human IL-6, sharing about 25% identity of amino acid sequence and is expressed by the *human herpesvirus* (HHV) type 8, which is associated with Kaposi's sarcoma and Castlemans disease (8). vIL-6 can directly bind to gp130 homodimers without the requirement of an alpha-receptor (9). Therefore, vIL-6 is able to stimulate every cell and mimicking the effect of IL-6 and the soluble IL-6 receptor (sIL-6R). However, the affinity of vIL-6 to gp130 is 1000-fold lower compared to IL-6/sIL-6R. Viral IL-6 was used to characterize the binding sites of the three membrane distal domains (D1-D3) of gp130 in structural analysis (5, 10).

Table 1-1.1: Members of the IL-6 cytokine family.

cytokine		alpha-receptor	beta-receptors
Interleukin 6	IL-6	(s)IL-6R	gp130/gp130
Viral IL-6	vIL-6		gp130/gp130
Interleukin 11	IL-11	(s)IL-11R	gp130/gp130
Ciliary neutrotrophic factor	CNTF	(s)CNTF-R	gp130/LIF-R
Leukemia inhibitory factor	LIF		gp130/LIF-R
Cardiotropin-1	CT-1		gp130/LIF-R
Neuropoietin	NP	(s)CNTF-R	gp130/LIF-R
Novel neurotrophin-1/	NNT-1/	(s)CNTF-R	gp130/LIF-R
B cell stimulating factor 3	BSF-3		
Cardiotropin-like cytokine	CLC	(s)CNTF-R	gp130/LIF-R
(+ Cytokine like factor)	(+ CLF-1)		
Oncostatin M	OSM		gp130/OSM-R or gp130/LIF-R
Interleukin 27	IL-27		gp130/WSX-1
Interleukin 31	IL-31		GPL/OSM-R

1.2 IL-6 signaling

Gp130 has been described as preformed dimer. Hence its activation is induced by cytokine binding (Fig. 1.2 A) (11, 12). Previous studies suggested that two molecules of each, IL-6, IL-6R and gp130 are forming a hexameric signaling complex (Fig. 1.2 C) (5, 13, 14). Additionally, the assembly of a tetrameric complex consisting of one molecule of IL-6, one molecule IL-6R and two molecules gp130, is discussed (Fig. 1.2 B) (15). Pflanz *et al.* demonstrated that heterodimers of gp130 mutants lacking either one of two cytokine binding sites are active (16). This leads to the suggestion, that a tetrameric complex is sufficient to induce signaling as shown for CNTF (17). It is under debate that the hexameric complex is built by an excess of IL-6 and represents an inactive assembly (15).

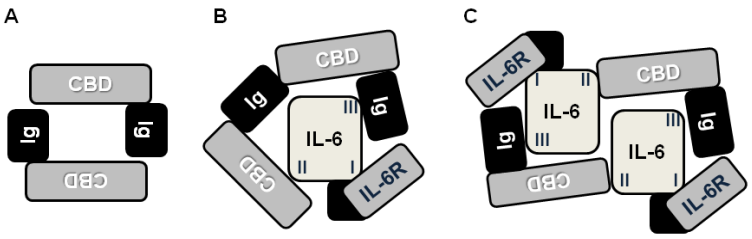

Figure 1.2: Schematic representation of gp130 dimers (top view). The cytokine binding domains of gp130 include domain D1 (Ig) as well as the domains D2 and D3 (CBD). (A) Preformed inactive dimers of gp130. (B) Tetrameric assembly of IL-6/sIL-6R/$(gp130)_2$. (C) Hexameric assembly of $(IL\text{-}6/sIL\text{-}6R/gp130)_2$.The binding sites of IL-6 are subdivided in site I (contacting the IL-6R), site II (contacting the CBD of gp130) and site III (contacting the Ig of gp130).

Assembly of the IL-6/IL-6R/gp130 receptor complex leads to the activation of the intracellular associated Janus kinases (JAK1, JAK2), which become auto-phosphorylated. Subsequently distinct tyrosine residues of gp130 are phosphorylated (Y^{683}, Y^{759}, Y^{767}, Y^{814}, Y^{905} and Y^{915}) and represent binding sites for proteins containing phospho-tyrosine binding motifs, such as Src-homology (SH) 2 domains. The Signal Transducer and Activator of Transcription 3 (STAT3), as the prominent transcription factor in IL-6 dependent signaling, binds to phospho-YXXQ motifs in gp130 (Y^{767}RHQ, Y^{814}FKQ, Y^{905}LPQ and Y^{915}MPQ) and is trans-phosphorylated by JAK1/JAK2 at Y^{705}, which leads to its homodimerization and translocation into the nucleus. In addition, phosphorylation of Y^{759} of gp130 generates a binding site for the protein tyrosine phosphatase SHP2, which becomes phosphorylated by JAK1/JAK2 as well and recruits the adaptor protein Grb2, thereby initiating the mitogen-activated protein kinase (MAPK) pathway (Fig. 1.3).

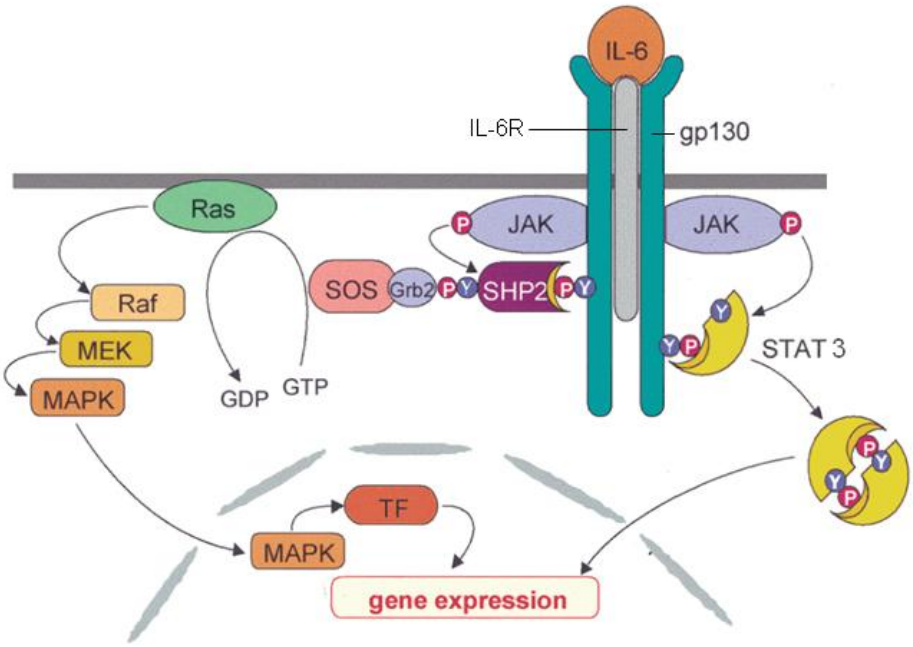

Figure 1.3: IL-6 induces the JAK/STAT pathway and the MAPK cascade. JAK1/2 mediated phosphorylation of distinct tyrosine residues of gp130 initiates either STAT3 or SHP2 mediated signaling. Picture was adapted from Heinrich *et al.* (18).

One hallmark of IL-6 is its ability to activate cells in two different ways, due to the differential expression of the alpha-subunit IL-6R, which is exclusively expressed on hepatocytes and distinct leukocyte populations. Therefore, only a small subset of cell populations can be activated via the binding of IL-6 to the membrane bound IL-6R, thereby initiating the activation of gp130, which is described as 'classic signaling' of IL-6 (Fig. 1.4). However, a soluble form of the IL-6R (sIL-6R) can be generated by alternative splicing or proteolytic cleavage (shedding) via A Disintegrin And Metalloprotease (ADAM) (19, 20). This soluble receptor binds free IL-6 molecules to form complexes, which subsequently bind the membrane associated beta-receptor subunit gp130 (Fig. 1.4). This process has been designated 'trans-signaling' and has the potential to activate a wide spectrum of cells. Obviously, IL-6 classic signaling represents more specificity as IL-6 trans-signaling. The significance of the different ways of signaling in the context of inflammation, regeneration or tumor development is part of ongoing investigations (21, 22).

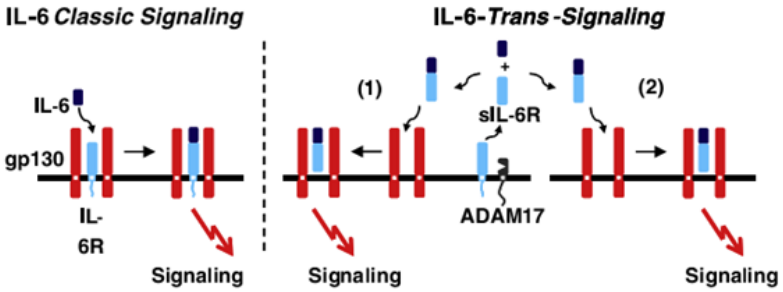

Figure 1.4: Classic signaling and trans-signaling of IL-6. In the classic signaling gp130 is activated by a complex of IL-6 and the membrane bound IL-6R. The trans-signaling is elicited by IL-6 in a complex with soluble IL-6R, which is cleaved from the membrane by ADAM 17. Thereby, the activation of gp130 can occur in (1) an autocrine or (2) a paracrine manner. Picture was taken from Scheller *et al.* (23).

To investigate the role of trans-signaling, a fusion protein consisting of IL-6 and the sIL-6R was generated in our laboratory. This molecule, named Hyper-IL-6 (HIL-6), is a potent stimulator of all gp130 expressing cells and reveals its full activity at 100 to 1000-fold lower concentrations than unlinked IL-6 and sIL-6R (24, 25). Peters *et al.* showed that Hyper-IL-6 binds with high affinity to gp130 and is less efficiently internalized (26).

1.3 The pathophysiological role of IL-6 signaling

IL-6 is secreted by cells of the immune system, e.g. lymphocytes, monocytes and macrophages and other mesenchymal cells like adipocytes, endothelial cells, fibroblasts, keratinocytes, myocytes and osteoblasts, thereby acting in an autocrine, paracrine and endocrine manner (27). Under physiological conditions the serum level of IL-6 is low, whereas tissue damage or pathological stimuli result in a significant increase (28).

IL-6 has been identified as an important factor for the immune system. Initially IL-6 has been described to be crucial for the terminal differentiation of B cells into antibody secreting cells (29, 30). In addition, it has

been shown that IL-6 promotes the generation of $CD8^+$ cytotoxic T cells from mature as well as immature human T cells (31). Furthermore, IL-6 orchestrates the transition from innate to acquired immunity by the attraction of distinct immune cells to the site of inflammation. Endothelial cells activated by microbes produce various cytokines including IL-6 acting in an autocrine manner. IL-6 signaling is linked to the induction of chemokine expression in endothelial cells leading to the attraction of neutrophiles to the site of infection, which are then replaced by monocytes and T cells in the cause of infection. Differentiation of monocytes into macrophages, the resolution of neutrophiles and the attraction of T cells to the site of infection are essentially triggered by IL-6 signaling (32, 33). Another crucial role of IL-6 has been shown in the context of autoimmune diseases, where IL-6 in combination with TGF-β induce the development of Th17 cells (34). An overproduction of IL-6 is often associated with pathological conditions caused by Th17 cells, such as multiple sclerosis (MS) and rheumatoid arthritis (RA) (35, 36). Additionally, high levels of IL-6 and sIL-6R in the serum of patients often correlate with the severity of disease, seen in arteriosclerosis and liver diseases. Moreover, it has been shown that IL-6 knock-out mice ($IL\text{-}6^{-/-}$) were not capable to clear bacterial infections from *L. monocytogenes* (37, 38). In addition, Okuda *et al.* showed that $IL\text{-}6^{-/-}$ mice are protected against autoimmune diseases, such as experimental autoimmune encephalomyelitis (EAE), reflecting the bivalent role of IL-6 (39).

The liver represents a privileged site for IL-6 stimuli due to the expression of the membrane bound IL-6R on hepatocytes and their susceptibility to IL-6 classic signaling. Activation of the IL-6 dependent pathways in hepatocytes initiates the acute phase response and leads to the upregulation of acute phase genes, such as serum amyloid A (SAA), haptoglobin, C-reactive protein (CRP), fibrinogen, and complement factors (40, 41). These factors are important for opsonization and killing of microbes, as well as for attraction of immune cells (chemotaxis). Unchallenged $IL\text{-}6^{-/-}$ mice showed no obvious phenotype, besides a massively suppressed acute phase response following infection with a vaccine virus or with the bacterium *L. monocytogenes* (42). Furthermore IL-6 is involved in regenerative processes and the central role of IL-6 signaling for liver regeneration is well known (43). Liver failure and defective hepatocyte regeneration was observed in $IL\text{-}6^{-/-}$ mice (44). The importance of IL-6 for liver regeneration following tissue damage due to toxins, alcohol abuse or viral infection (HCV) is well described (22, 45, 46). This correlates with the necessity of STAT3 for the induction of the acute phase response during inflammation and liver regeneration (44, 47, 48). Moreover, it has been shown that liver regeneration was improved by a Hyper-IL-6 therapy following partial hepatectomy or D-Galactosamine caused liver injury (45, 49). Additional an adenoviral vector encoding for Hyper-IL-6 was used for gene therapy to reverses fulminat hepatic failure in mice (50). The positive effect of IL-6 on liver regeneration is linked to its impact on hepatocyte proliferation.

However, persistent overexpression of IL-6 seems to be associated with cancer. It has been shown that formation of adenomas and hyperplasia of the liver is connected to an overexpression of IL-6 and sIL-6R in mice (51, 52). This stands in line with previous clinical studies, which reported elevated levels of circulating IL-6 in patients with chronic hepatitis, alcoholic liver diseases, and liver cirrhosis (53–56). In

addition, elevated IL-6 serum levels were found in patients with hepatocellular carcinoma (HCC), which has been shown to correlate with the tumor mass, cancer invasiveness and with the impairment of liver function as well as with the degree of liver fibrosis (57–60). Furthermore, IL-6 has been implicated in many diseases, e.g. diabetes, obesity, arteriosclerosis, rheumatoid arthritis, psoriasis and is connected to different types of cancer (61–66). Elevated serum levels of IL-6 has been shown to correlate with the stage of colorectal cancer and distinct tumors, such as esophageal cancer, renal cell carcinoma, multiple myeloma, prostate and ovarian cancer have the characteristic of elevated IL-6 secretion (67). In this context, IL-6 has been identified as a growth factor for renal carcinoma and multiple myeloma cells (68, 69).

1.4 STAT3 as an oncogenic factor

IL-6 mediated activation of STAT3 induces the expression of a variety of genes, which are important for cell cycle, apoptosis, signaling, angiogenesis, inflammation, wound healing and invasion, e.g. c-myc and pim-1 (18, 70, 71). It is known that inflammation triggers tumor initiation and enhances tumor progression as well as metastasis (72, 73). In distinct tumor types exaggerated STAT3 activation is described and displays a major oncogenic factor (74–76). The persistent phosphorylation of STAT3 can be seen in human epithelial cancer cell lines as well as in primary tumors including hepatocellular carcinoma, breast, prostate, colon, head and neck cancers and in several hematological malignancies (77-81). In addition STAT3 activation is important for the development of epithelial cell tumors (82–84). Known before that STAT3 is a key player in liver inflammation and cancer, it has been recently shown by Pilati *et al.* that about 12% of inflammatory hepatocellular adenomas (IHCAs) carry STAT3 mutations, which seems to be associated with benign proliferation of hepatocytes in human (85, 86). Moreover, a constitutive active variant of STAT3 (STAT3C) was described leading to an increased VEGF expression and tumor angiogenesis in mice (72, 87, 88).

Recently a tumor suppressor role of STAT3 has been found in glioblastoma, which is a highly malignant brain tumor. De la Iglesia *et al.* reported that STAT3 plays a pro-oncogenic or tumor suppressive role depending on the mutational profile of the tumor (89). Furthermore, Ecker *et al.* demonstrated that a constitutive active version of Stat3alpha (Stat3alphaC) suppressed the c-myc dependent transformation of mEF cells, which were deficient for p53 (90).

1.5 SOCS3 as a competent inhibitor of IL-6 signaling

The members of the Suppressor Of Cytokine Signaling (SOCS) family are inhibitors of Janus kinases and their expression is upregulated by e.g. IL-6, LIF, IL-11 and OSM (18, 91). SOCS3 specifically affects the signaling mediated by IL-6 and gp130 (92). SOCS proteins contain a central SH2 domain, as well as a C-terminal domain (SOCS box). The SH2 domain of SOCS3 has a slightly higher affinity to the phosphorylated tyrosine Y^{759} at the intracellular domain of gp130 than SHP2. Thereby the activation of

the MAPK cascade is abrogated. Furthermore, it has been shown that the activity of JAK2 is inhibited by SOCS3 (93). Other studies suggest that SOCS proteins are interacting with elongin B and C and might be part of E3 ubiquitin ligases, which are involved in the degradation of their binding partners (94, 95).
SOCS3 deficient mice die at mid-gestation owing to placental insufficiency, which is linked to aberrant signaling through the LIF-R (96, 97). Furthermore, it has been shown that a conditional deletion of SOCS3 in hepatocytes promotes fibrosis and hepatitis-induced hepatocarcinogenesis (98, 99). Mice expressing a gp130 knock-in mutation ($gp130^{Y757F}$) are deficient in SHP-2 and SOCS3 binding and were examined by Tebbutt *et al.* (100). This hyperactivation of STAT3 leads to an age-dependent enlargement of the stomach, the proximal small intestine and the spleen as well as to the development of gastric adenomas. Jenkins *et al.* showed that the formation of gastric adenomas and the reduced survival of $gp130^{Y757F/Y757F}$ mice could be partially rescued in $gp130^{Y757F/Y757F}$ $STAT3^{+/-}$ mice (101). However, compared to STAT3 deficient mice, $gp130^{Y757F}$ mice were protected in a model of severe colitis (74, 101).

1.6 Glycoprotein 130

The members of the IL-6 family, besides IL-31, signal through the ubiquitously expressed type I cytokine receptor glycoprotein 130 (gp130, CD130) (Tab. 1.1). It is known that a complete deletion of gp130 is lethal to mice (102). Therefore, conditional gp130 knock-out mice ($gp130^{flox}$) were used to study the physiological function of gp130 *in vivo*. For instance, the lack of hepatic gp130 promotes liver injury, which was confirmed in a variety of studies (46, 103–105). Moreover, mice expressing a hyperactive variant of gp130, due to the lack of suppression via SOCS3 ($gp130Y^{757F}$), showed improved survival in a model of DSS colitis (100).

Structurally, the extracellular domain of gp130 is composed of one immunoglobulin-like domain (Ig, D1), a cytokine binding domain consisting of the domains D2 and D3 (CBD), three fibronectin domains (FNIII, D4 - D6) followed by the transmembrane (TM) and the intracellular domain (ICD), which is associated with a Janus kinase (JAK) (Fig. 1.5 A). Domain D1 of gp130 is involved in the binding of IL-6, such as the domains D2 and D3 (CBD). The FNIII domains D4 to D6 seem to be essential for the transmission of the signal to the cytoplasmatic portion (106–109). The basic structure of the CBD is a β-sandwich, consisting of a three-stranded (A, B, E) and a four-stranded (C, C', F, G) β-sheet. The domains are connected via a short helix (Fig. 1.5 B, C).

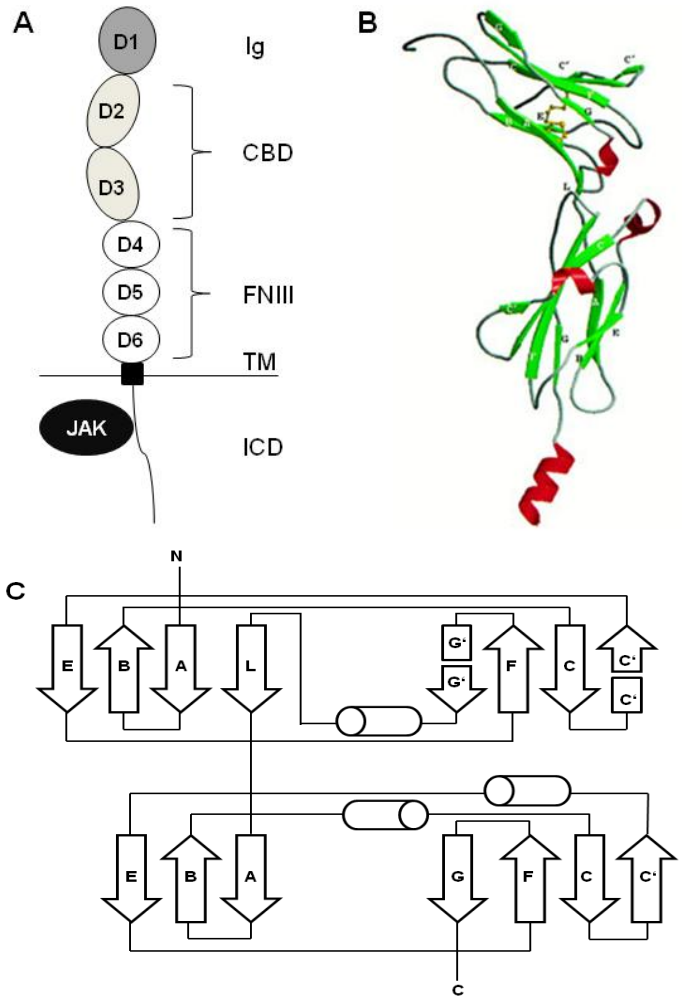

Figure 1.5: Structure of gp130 and the cytokine binding domain. (A) Schematic representation of gp130. Domain D1 represents the Ig-like domain, the domains D2 and D3 form the cytokine binding domain (CBD) and the domains D4 to D6 are fibronectinIII domains, which are followed by the transmembrane domain (TM) and an intracellular domain (ICD), associated to Januns kinase (JAK). (B) Ribbon representation of the crystal structure of the CBD. Helical segments are shown in red and β-strands in green. (C) Topology diagram of the CBD of gp130 (helices are represented by cylinders and β-strands by arrows). Pictures B was taken from Bravo *et al.* (106).

Three different binding sites are described for the human IL-6/sIL-6R/gp130 complex, which are based on the structure of vIL-6 bound to gp130 (5, 10, 110). Binding site I is generated between humen (h)IL-6 and the domains D2 and D3 of the sIL-6R, whereas site II describes the interaction of the IL-6/sIL-6R complex with the domains D2 and D3 of gp130 and site III the interaction with domain D1 of another gp130 molecule (Fig. 1.6). Site II consist of site IIa, which occurs only between the bound IL-6 and the domain D2 of gp130 and site IIb, which is between the bound sIL-6R and domain D3 of gp130 (Fig. 1.6). This assembly interacts with a second gp130 molecule forming the binding sites IIIa and IIIb. Both parts of site III are connected to domain D1 of gp130, which has been shown to be important for gp130 activation (16, 111). Furthermore, the structure of the site III interface reveals that the N-terminal tail of domain D1 can insert into a groove on the surface of IL-6 (112). Although the crystal structure of the gp130 domains D1 to D3 in complex with viral IL-6 is solved, it is not clear how the binding of the IL-6/sIL-6R complex leads to the activation of gp130 in detail (106, 113, 114). Thus, the binding of the

IL-6/sIL-6R complex to gp130 is a prerequisite for its activation and induction of the signaling via STAT3.

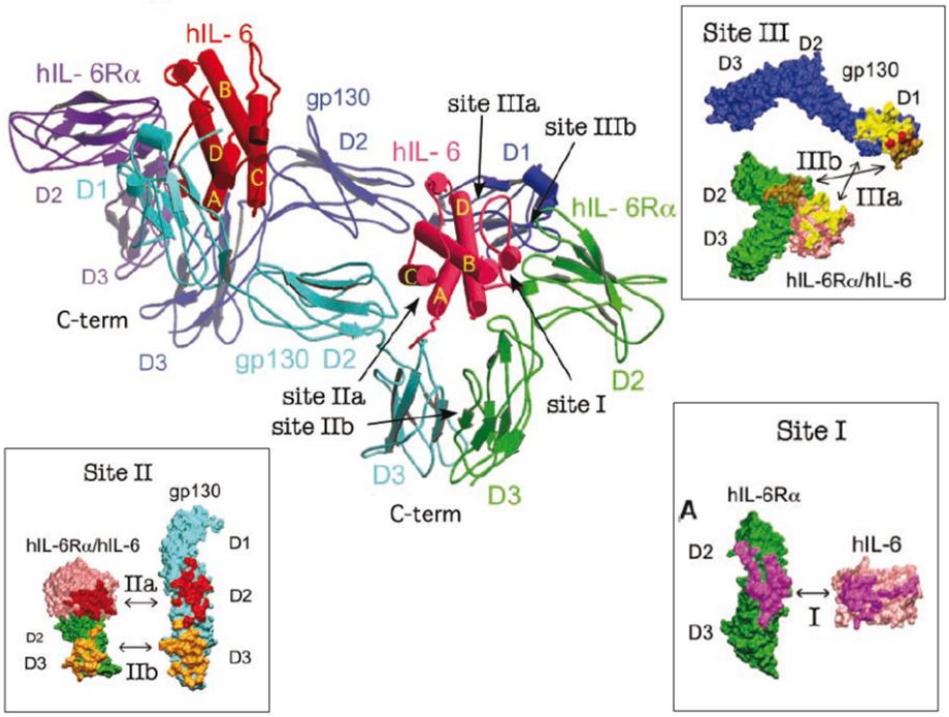

Figure 1.6: The signaling complex of human IL-6, hIL-6R and gp130. Representation of the ribbon structure of two molecules human IL-6 in complex with two molecules of human IL-6 receptor and two molecules gp130. Site I engages domain D2 and D3 of the human IL-6R (hIL-6R), site II the CBD (D2 and D3) of the first gp130 molecule and site III the Ig-like domain (D1) of a second gp130 molecule. Pictures were taken from Boulanger *et al.* (5).

It has been assumed since a long time that activation of the gp130 mediated signaling is triggered by its dimerization. However, preformed inactive homodimers were identified for gp130, as described for IL-17R, TNF-R1 and IFN-γR (115–118). Thereby, the formation of gp130 homodimers was found to be independent of the JAK activity. Blocking of gp130 dimerization and subsequent JAK activity was achieved by using the monoclonal anti-gp130 antibody B-R3, which binds to an epitope at domain D2 of gp130 (119, 120). Ligand independent homodimerization of gp130 and heterodimerization of gp130 and LIF-R was reported by Giese *et al.* using Bimolecular Fluorescence Complementation (BiFC), which detects predominantly stable protein-protein interactions (11). The used gp130 constructs were C-terminal tagged with the corresponding halves of YFP, therefore not signaling competent and did not reflect the natural gp130 activation. Tenhumberg *et al.* used Förster Resonance Energy Transfer (FRET) to detect dimerization of two fluorescently-tagged gp130 variants (12). Preformed but inactive dimers were found and the addition of the respective ligand led to enhanced dimer formation. Furthermore, this study revealed that gp130 could be co-precipitated with the LIF-R as well as with other gp130 variants in the absence of a ligand.

1.7 Natural occurring mutations of gp130

Recently, in-frame deletions of gp130 were found in 60% of human inflammatory hepatocellular adenoma (IHCA), which exhibit ligand independent activation (121). These deletions differ in length, but cluster all around the EF loop of domain D2 of gp130, representing the IL-6 contact site (Fig. 1.7). Out of twenty-six identified gp130 mutations found in IHCAs, 16 mutations were unique, small in-frame deletions and one mutation was a 33 base pair in-frame duplication in exon 6 (Tab. 1-2). Out of these 17 mutations, Rebouissou *et al.* analyzed two frequent deletions (delS187–Y190 and delY186–Y190) and two infrequent mutants (delV184–Y186, S187A and delK173-D177) in the hepatocellular Hep3B cell line. The expression of the gp130 deletion mutants was sufficient to activate STAT3 and the downstream acute phase inflammatory genes. Interestingly, SOCS3 expression, which normally suppresses IL-6 mediated STAT3 activation was induced as well, but had no effect on the constitutive STAT3 phosphorylation. Moreover, they showed in co-immunoprecipitation studies that the gp130 deletion mutant delS187–Y190 can form homodimers as well as heterodimers with wildtype gp130, in a IL-6 independent manner. Interestingly, the activity of the gp130 deletion mutant delS187–Y190 is driven by its homodimerization, as overexpression of wildtype gp130 impaired gp130 delS187–Y190 activity in a dose-dependent manner. Found frequently in IHCAs, only 1.8% of hepatocellular carcinoma (HCC) showed a correlation to these gp130 mutations. The most frequently activated oncogene in HCC is β-catenin, which was found in IHCAs as well (122). Furthermore, Pilati *et al.* showed that 12% of IHCAs lacking mutations for gp130 harbor somatic activating mutations for STAT3 (85).

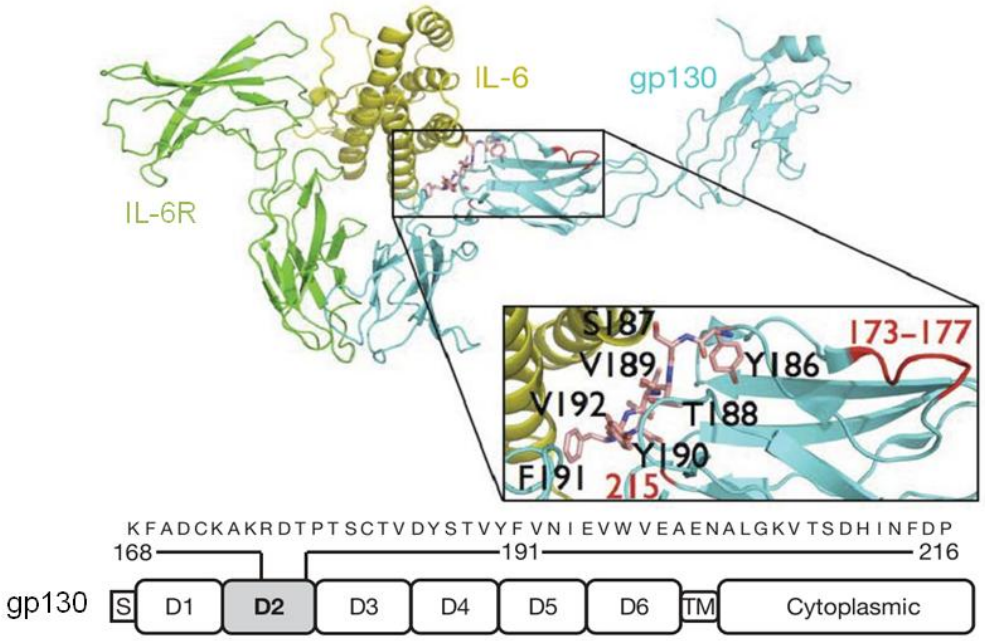

Figure 1.7: In-frame deletions of gp130 found in IHCAs. Overview of gp130 somatic mutations identified in inflammatory hepatocellular adenomas (IHCAs). Picture was taken from Rebouissou *et al.* (121).

Table 1-2: List of the deletions located in domain D2 of gp130.

Number of tumors	Amio acid change	Mutation
6	S187-Y190	Deletion
4	Y186-Y190	Deletion
3	V189-V192	Deletion
2	T188-F191, V192I	Deletion, point mutation
1	K168-N192	Deletion
1	K183-D177	Deletion
1	V184-Y186, S187A	Deletion, point mutation
1	Y186-F191, V192F	Deletion, point mutation
1	S187-F191	Deletion
1	T188-F191, V192T	Deletion, point mutation
1	Y190-V192, N193S	Deletion, point mutation
1	F191L, V192-I194	Deletion, point mutation
1	V192-I194	Deletion
1	N193, I194F	Deletion, point mutation
1	E195-V196	Deletion
1	K206-P216, G205R	Duplication, point mutation
1	D215	Deletion

1.8 A constitutive active variant of gp130

To point out the consequences of ligand independent gp130 activity and STAT3 signaling, an artificial constitutive active variant of gp130 was generated in our laboratory. This construct is named Leucin-gp130 (L-gp130). Here, the extracellular domain of human gp130 was truncated 15 amino acids above the transmembrane domain and replaced by the leucine zipper motif of c-Jun. C-Jun is known to form heterodimers with c-Fos, which constitute the transcription factor AP-1. However, c-Jun is able to form homodimers as well. The strong interaction relies on the coiled-coil structure with a hydrophobic core built by leucine residues. Additionally, cysteine residues were introduced to stabilize the leucine zipper (LZ) by a disulfide bond. An N-terminal Flag-tag was added for the detection of protein expression. The intracellular part and the transmembrane domain were left unchanged, to achieve normal signaling properties (Fig. 1.8). Expression of L-gp130 in different cell lines (HepG2, Cos-7 and Ba/F3 cells) showed IL-6 independent phosphorylation of STAT3 as well as a cytokine independent cell growth. These data indicate that L-gp130 is sufficient to activate a gp130-type signaling in an IL-6 independent manner. Moreover, *in vitro* differentiation of murine embryonic stem cells was completely suppressed in cells expressing L-gp130 (123).

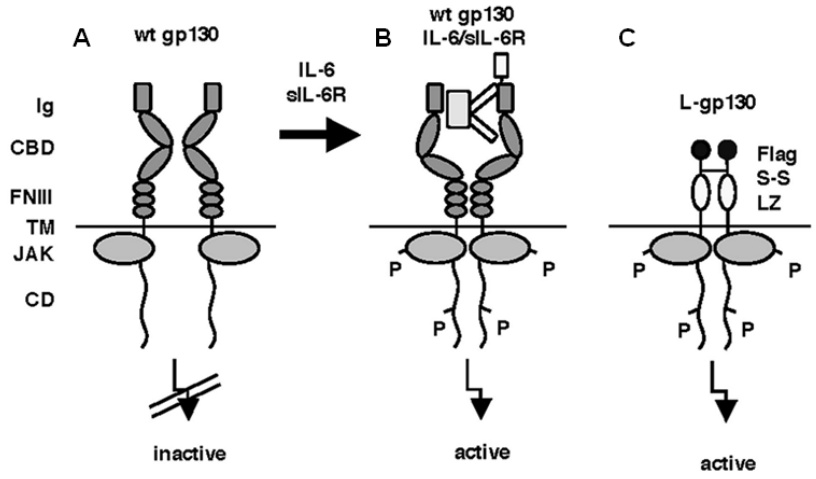

Figure 1.8: Schematic representation of L-gp130 signaling. (A) Inactive preformed homodimers of wildtype (wt) gp130. (B) The signaling competent complex of IL-6/sIL-6R/$(gp130)_2$ and (C) L-gp130, containing a leucine zipper (LZ) and a disulfide bond (S-S) instead of the wildtype extracellular domains. Picture was taken from Stuhlmann-Laeisz *et al.* (123).

1.9 Inducible regulation of gene expression via the Tet-system

The inducible regulation of gene expression *in vitro* and *in vivo* can be achieved by the Tet-system. The origin of this widely-used application is the antibiotic resistance of *E. coli*. This system was adjusted to be more specific in binding of eukaryotic DNA, so that it can be used in mammalian cells (124). The principle of inducible gene expression is the simultaneous application of two plasmids. One vector expressing the gene of interest under control of an inducible tetracycline responsive promoter element (TRE) is combined with a second vector, which expresses the tetracycline transactivator protein (tTA). tTA is a fusion protein, consistig of the Tet-repressor domain (TetR) from *E. coli* and the VP16 domain from the *herpes simplex* virus. The TetR unit is responsible for binding to the Tet operator (TetO), which is part of the promoter region. The VP16 domain is a strong activator of transcription. The reverse transactivator (rtTA) contains a modified TetR domain and exhibits altered binding properties to TRE (Fig. 1.9 A) (125).

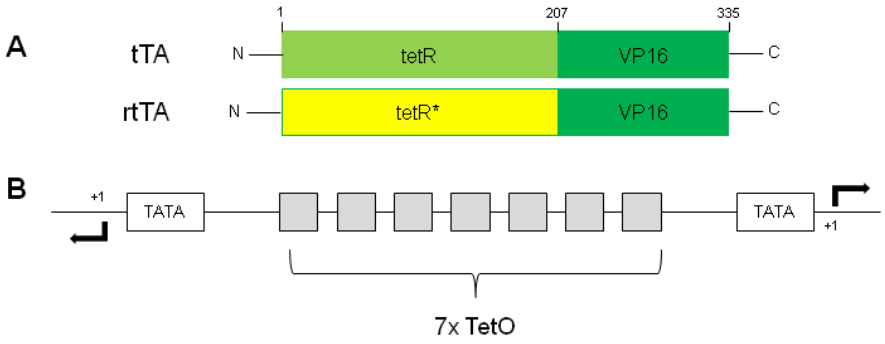

Figure 1.9: Schematic representation of: (A) The tetracycline transactivator proteins tTA and rtTA and of (B) The tetracycline promoter element (TRE). The TetR domain of rtTA is changed relating to its doxycycline affinity.

Selective expression of the transactivators (tTA/rtTA) can be achieved via a tissue specific promoter (Fig. 1.10). The expression of the gene of interest is controlled by the tetracycline responsive promoter element (TRE), which consists of seven repeats of TetO, separated by spacer sequences (Fig. 1.9 B). This sequence is flanked by two hCMV minimal promoters, which are responsible for an equal expression of two genes. Usually, a reporter gene (e.g. firefly luciferase) is used as second transgene. It has been shown, that these constructs can exhibit low basal expression in the absence of the activator.

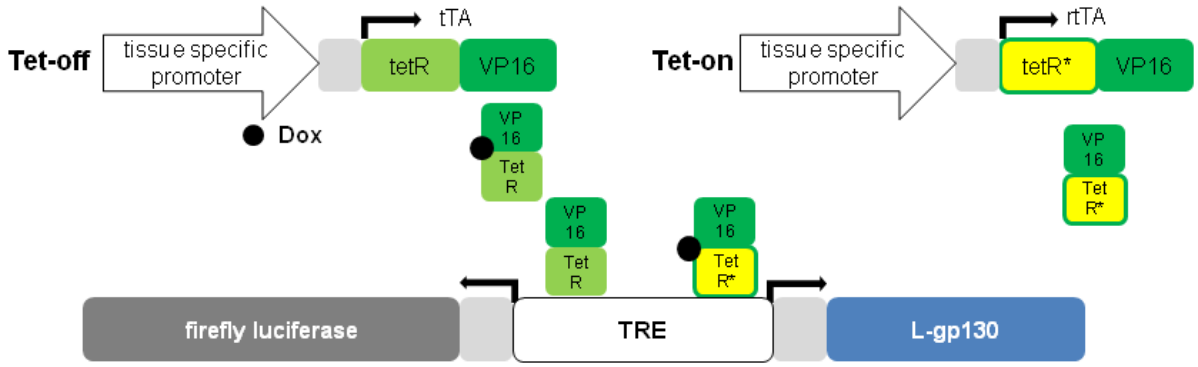

Figure 1.10: Inducible gene expression of L-gp130 and firefly luciferase via the Tet-system. Using the Tet-off system, the transgene is expressed in the absence of Dox, whereas in the Tet-on system Dox is needed for transgene expression. Dox: doxycycline, tTA: tetracycline transactivator protein, rtTA: reverse tetracycline transactivator protein, TetR: Tet repressor, VP16: activating domain, TRE: tetracycline responsive promoter element.

By means of tetracycline or its derivate doxycycline (Dox) the inducible gene expression can be switched. Thereby, initiation of gene expression is achieved in two different ways. Induction of gene expression in the absence doxycycline is designated as Tet-off. Thereby, the transactivator tTA binds to TRE and induces gene expression. Supplementation of doxycycline induces a conformational change of the tTA, which represses its binding to the promoter and results in inhibition of the gene expression. This system can be used *vice versa* (designated as Tet-on) by using the reverse transactivator (rtTA). Here, the binding properties of the tTA are changed to a doxycycline dependent binding to the promoter and therefore rtTA induces gene expression in the presence of doxycycline (Fig. 1.10). Recently, a second generation of rtTA (rtTA-M2) with higher sensitivity for doxycycline was found by mutagenesis.

As Gossen and Bujard showed, 0.1 to 1 µg/ml of doxycycline is an adequate concentration to repress luciferase activity using the Tet-off system *in vitro* (124). For induction of gene transcription via the Tet-on system a 10-fold higher concentration is required. *In vivo* studies, using the Tet-on as well as the Tet-off system, revealed a doxycycline concentration of 0.2 to 2 mg/ml, which was given to mice via drinking water (126).

Comparing both systems, the advantage of the Tet-off system is the requirement of low concentrations of doxycycline. The major disadvantage is the long term treatment of mice with doxycycline and the resulting incomplete clearance of doxycycline from the body, because initiation of gene expression is dependent on the fast clearance of doxycycline (K. Schönig, ZI Mannheim, personal communication). The advantage of

the Tet-on system is its fast induction capability but a 10-fold higher concentration of doxycycline is required compared to the Tet-off system (127).

1.10 Aim of this work

Recently, activating mutations of gp130 and less frequently activating STAT3 mutations have been found in liver adenoma (85, 121). Although crystal structures of gp130 and gp130 complexes are available, the detailed mechanism of gp130 activation is unresolved. Furthermore, it is unclear if ligand independent activation of gp130 in hepatocytes is sufficient to drive liver tumor formation.

1. We aimed to decipher the mechanism of ligand independent gp130 activation and to get an insight into the mechanism of gp130 activation in general. We therefore wanted to apply a rational driven mutagenesis approach based on available gp130 crystal structures. The aim was to identify amino acids that are critical for the autoinhibition of gp130 and therefore play a role in gp130 activation.

2. Using an artificial, constitutive active gp130 variant (L-gp130) we aimed to analyze the physiological consequences of persistent gp130 activation in the liver using transgenic mice. The aim was to generate and establish double transgenic mice that would allow for a tetracycline inducible expression of L-gp130 in the liver. The consequences of persistent gp130 activation in hepatocytes should then be analyzed by biochemical and histological methods.

2 MATERIAL

2.1 Chemicals

Basic chemicals were purchased from Carl Roth, Sigma-Aldrich or Merck, unless otherwise stated. Chemicals of particular interest are listed below.

AppliChem	3-(4,5-Dimethylthiazol-2-yl)-2,5-diphenyltetrazolium bromide (MTT)
	Leupeptin
	Aprotinin
	Pepstatin
Fermentas/	DreamTaq™ polymerase
Thermo Scientific	Phusion® Hot Start II polymerase
	Revert Aid™ reverse transcriptase
	Proteinase K
	Gene Ruler™ 1kb DNA ladder
	dNTPs (dATP, dCTP, dGTP, dTTP)
	CIAP alkaline phophatase
	FastAP™ alkaline phophatase
	T4 DNA Ligase
	T4 Polynucleotide Kinase
	Page Ruler™ Plus
	Pierce® Protein G Agarose
Sigma-Aldrich	Polybrene
	Puromycine
	Doxycycline hyclate
	PMSF
	Saponin
	Sodium orthovanadat (Na_3VO_4)

2.1.1 Enzymes

All other enzymes used including restriction enzymes were purchased from Fermentas/ Thermo Scientific.

2.1.2 Recombinant cytokines

Hyper-IL-6	fusion protein of the human IL-6 and the human sIL-6R; kindly provided by Dr. Inken Lorenzen and Prof. Dr. Achim Grötzinger (Department of Biochemistry, CAU Kiel)
Murine IL-3	Peprotech (#213-13), Immunotools (#12340032)

2.2 Solutions and buffers

2.2.1 Microbiology

LB medium	10 g NaCl 10 g Peptone/ Tryptone 5 g Yeast extract Ad 1 l ddH_2O Autoclave
LB Agar	20 g Agar-Agar 1 l LB medium Antibiotic (Ampicillin 100 µg/ml)
KCM buffer (5x)	500 mM KCl 150 mM $CaCl_2$ 250 mM $MgCl_2$

2.2.2 SDS-PAGE

Running gel (10%)	3.87 ml ddH_2O
(10 ml)	2.55 ml 1.5 M Tris-HCl (pH 8.8)
	100 µl 10% SDS
	3.3 ml 30% Acrylamide
	100 µl 10% APS
	10 µl TEMED

Stacking gel (4%)	3.72 ml ddH_2O
(5 ml)	625 µl 0.5 M Tris-HCl (pH 6.8)
	50 µl 10% SDS
	670 µl 30% Acrylamide
	50 µl 10% APS
	10 µl TEMED
SDS running buffer	25 mM Tris-HCl, pH 8.3
	192 mM glycine
	0.1% (w/v) SDS
Laemmli buffer (5x)	185 mM Tris-HCl (pH 6.8)
	50% glycerol
	10% SDS
	5% β-mercaptoethanol
	0.05% bromphenol blue

2.2.3 Western blot

NETG was used as buffer for blocking, washing and antibody dilution.

NETG	150 mM NaCl
	5 mM EDTA
	50 mM Tris-HCL, pH 7.5
	0.02% (v/v) Tween-20
	0.04% (w/v) gelatine
	Let gelatine soak in ddH_2O and boil before adding to the solution
Transfer buffer	25 mM Tris-HCl
(pH 8.3)	192 mM glycine
	20% (v/v) methanol
Stripping solution	15 g glycine
(pH 2.2)	1 g SDS
	10 ml Tween-20
	Ad 1 l ddH_2O

2.2.4 Lysis buffer

Tissue lysis buffer	150 mM NaCl
	50 mM Tris-HCl (pH 7.4)
	2 mM EDTA
	1% (w/v) Triton X-100
	1% (w/v) NP-40
	1 mM Na_3VO_4
	1 mM NaF
	1x tablet Complete (Roche)/ 50 ml lysis buffer (protease inhibitor cocktail)
Co-IP buffer	50 mM HEPES
(pH 7.4)	150 mM NaCl
	1 mM EDTA
	2 mM EGTA
	0.5% (w/v) NP-40
RIPA buffer	50 mM HEPES
(pH 7.4)	150 mM NaCl
	1 mM EDTA
	1% (w/v) NP-40
	0.5% (w/v) sodiumdeoxycholate
	0.1% (w/v) SDS

2.2.5 Inhibitors

1 mM (f.c.)	PMSF (in MetOH), serine protease inhibitor
1 μg/ml (f.c.)	Leupeptin, protease inhibitor
2 μg/ml (f.c.)	Aprotinin, trypsin inhibitor, serine protease inhibitor
10 μg/ml (f.c.)	Pepstatin, protease inhibitor
1 mM (f.c.)	Na_3VO_4 (Sodiumorthovanadat), protease inhibitor

2.2.6 Cell culture media and solutions

Cell culture media and solutions were purchased from PAA. Media was supplemented with 10% (v/v) heat-inactivated FCS.

DMEM	Dulbecco's Modified Eagle Medium (high glucose 4.5 g/l and stable glutamin)
RPMI 1640	Roswell Park Memorial Institute Medium
IMDM	Iscove's modified DMEM (with L-Glutamine)
FCS	Fetal Calf Serum

Trypsin-EDTA
Penicillin-Streptomycin

2.2.7 Flow cytometry (intracellular staining)

Staining buffer	PBS (Ca^{2+}, Mg^{2+}), pH 7.4 - 7.6
	2% (v/v) FCS (heat-inactivated)
	0.2% (v/v) sodium azide
Fixation buffer	PBS (Ca^{2+}, Mg^{2+})
	4% (v/v) formaldehyde
Permeabilization buffer	PBS (Ca^{2+}, Mg^{2+}), pH 7.4 - 7.6
	2% (v/v) FCS (heat-inactivated)
	0.2% (v/v) sodium azide
	0.5% (v/v) Saponin
Superperm buffer	PBS (Ca^{2+}, Mg^{2+}), pH 7.4 - 7.6
	2% (v/v) FCS (heat-inactivated)
	0.2% (v/v) sodium azide
	0.5% (v/v) Saponin
	25% (v/v) FCS

2.2.8 MTT cell viability assay

MTT solution	5 mg/ml MTT in PBS
Solubilization buffer	10 mM HCl
	10% (w/v) SDS

2.2.9 Southern blot

20 x SSC	3 M NaCl
(pH 7.0)	300 mM NaCitrat
	adjust pH with HCl
Depurination buffer	0.25 M HCl

Denaturation buffer	0.5 M NaOH 1.5 M NaCl
Neutralisation buffer (pH 8.0)	1 M Tris-HCl 1.5 M NaCl
Churchbuffer (1 l)	500 mM NaP_I (NaH_2PO_4, Na_2HPO_4) 7% (w/v) SDS 1% (w/v) BSA 1 mM EDTA (pH 8.0)

2.2.10 DNA buffer

TBE (0.5x)	44.5 mM boric-acid 10 mM EDTA, pH 8.0 44.5 mM Tris-HCl
DNA-loading buffer (5x)	20% (w/v) glycerol in TBE buffer 0.025% (w/v) bromphenol blue

2.3 Isotopes

Radioactive isotopes were used for radioactive labeling of nucleotides of DNA or RNA. The isotopes of phosphorus are the beta-emitter ^{33}P and ^{32}P. Thereby, ^{33}P is the long-lasting radioactive isotope although it has lower energy beta emission compared to ^{32}P. All isotopes were purchased from MP Biomedicals Europe.

Tabelle 2-1: Radioactive isotopes for Southern blot analysis used in this study.

Istotope	**Specific activity**	**Energy**	**Half-life**
alpha^{32}P dATP (#33002x)	25 Ci/ mmol; 925 GBq/mmol	1.71 MeV	14.263 days
alpha^{33}P dATP (#58200)	3000 Ci/mmol; 111 TBq/mmol	0.25 MeV	25.34 days

2.4 Plasmids and Primers

2.4.1 Plasmids

The bidirectional expression vector pBI5 contains of a tetracycline responsive promoter element (TRE). This promoter is composed of a heptameric Tet-operator sequence, which is flanked by two divergently orientated hCMV minimal promoters (Fig. 1.9). The expression vectors pBI5-GFP and pTan-Pur containing the sequence for the Green Fluorescent Protein (GFP) and the tetracycline transactivator (tTA), respectively were kindly provided by Anders Strom from the Department of Biosciences and Nutrition (Karolinska Institute, Sweden). The vector pTan-Pur was modified from Shockett *et al.* (125). The Tet-expression vectors hCMV-tTA (pUHD15-1), Lap-tTA (pUHD 15-30), hCMV-rtTA (pUHD 17-1) and Lap-rtTA (pUHD 61-30) containing the sequence for tTA or reverse tTA (rtTA) were kindly provided by Dr. Kai Schönig (*Zentralinstitut für seelische Gesundheit*, Mannheim) (Fig. 4.22). The mammalian expression vectors p409-gp130 wt and gp130 ΔYY were provided by Jan Sommer and Timo Effenberger (Departement of Biochemistry, CAU Kiel). All plasmids contain an ampicillin resistance gene. The mammalian expression vector pMOWs was used for retroviral transduction of eukaryotic cells. It contains a puromycine resistance cassette. For further details see Ketteler *et al.* (128).

Table 2-1: Plasmids used in this study.

name	promoter	transgene	description
		gp130 vectors	
p409	SV40	L-gp130	The constitutive active variant L-gp130 is expressed under control of the SV40 promoter.
p409	SV40	eYFP-gp130 wt	The wildtype variant of gp130 is fused N-terminally to eYFP and expressed under control of the SV40 promoter.
p409	SV40	eYFP-gp130 ΔYY	A constitutive active deletion mutant of gp130 (del Y186-Y190) is fused N-terminally to eYFP and expressed under control of the SV40 promoter. This mutant is explained in detail in section 4.1.3.
		Other	
pcDNA3.1	hCMV	GFP	The green fluorescent protein (GFP) is expressed under control of the human cytomegalovirus (hCMV) promoter.
pcDNA3.1	hCMV	myc- SOCS3	The suppressor of cytokine signaling (SOCS) 3 is fused N-terminally to c-myc and expressed under control of the human cytomegalovirus (hCMV) promoter.
pMOWs	5'MFG/MESV	myc-gp130	Different mutants of gp130 are fused N-terminally to

	LTR		c-myc and are expressed under control of 5'MFG/MESV LTR.
pMOWs	5'MFG/MESV LTR	GFP	The green fluorescent protein (GFP) is expressed under control of 5'MFG/MESV LTR.
TK-RL	Thimidin kinase	Renilla luciferase	Renilla luciferase is expressed under control of the promoter for the thimidin kinase.
SIEM-Luc	STAT3 senstive promoter	Firefly luciferase	Firefly luciferase is expressed under control of a STAT3 sensitive promoter.
		Tet-vectors	
pBI5-L-gp130	TRE	L-gp130/ Firefly luciferase	The constitutive active variant L-gp130 and the reporter gene firefly luciferase are expressed under control of the tetracycline responsive promoter element (TRE). L-gp130 is explained in detail in section 1.8.
pBI5-GFP	TRE	GFP	The Green Fluorescent Protein (GFP) is expressed under control of the tetracycline responsive promoter element (TRE).
pTan-Pur	TRE	tTA	The tetracycline transactivator protein (tTA) is expressed under control of the tetracycline responsive promoter element (TRE).
pUHD 15-1	hCMV	tTA	The tetracycline transactivator protein (tTA) is expressed under control of the human cytomegalovirus (hCMV) promoter.
pUHD 15-30	Lap	tTA	The tetracycline transactivator protein (tTA) is expressed under control of the promoter of the liver enriched activator protein (Lap).
pUHD 17-1	hCMV	rtTA	The reverse tetracycline transactivator protein (rtTA) is expressed under control of the human cytomegalovirus (hCMV) promoter.
pUHD 61-30	Lap	rtTA	The reverse tetracycline transactivator protein (tTA) is expressed under control of the promoter of the liver enriched activator protein (Lap).
pMOWs	5'MFG/MESV LTR	tTA	The tetracycline transactivator protein (tTA) is expressed under control of 5'MFG/MESV LTR.

2.4.2 Oligonucleotides

Oligonucleotides were synthesized by Metabion and Sigma-Aldrich.

Table 2-2: Primers used in this study.

Name	Sequence 5'-3'
	Myc tag
AgeI-myc-NotI sense	5'-CCGGTCGCCACC**GAACAAAAACTCATCTCAGAAGAGGATCTG**TAGGC-3'
AgeI-myc-NotI antisense	5'-GGCCGCCTA**CAGATCCTCTTCTGAGATGAGTTTTTGTTC**GGTGGCCA-3'
	Gp130 sequencing primers
gp130_N-term	5'-GGCCTGAGTGAAACCCAATG-3'
gp130_N-term_reverse	5'-TGACACTGGATGCTGTTCTG-3'
gp130_SP	5'-TCGCCGCCATGTTGACGT-3'
gp130_muta	5'-ACAATAATTTCGGGCTTG-3'
	Mutagenesis primers
gp130 C172S sense	5'-CACACAAGTTTGCTGAT**AGC**AAAGCAAAAC-3'
gp130 C172S antisense	5'-CGTTTTGCTTT**GCT**ATCAGCAAACTTGTGTG-3'
gp130 V189G sense	5'-GATTATTCTACT**GGG**TATTTTGTCAAC-3'
gp130 V189G antisense	5'-GTTGACAAAATA**CCC**AGTAGAATAATC-3'
gp130 Y190G sense	5'-GATTATTCTACTGTG**GGT**TTTGTCAACATTG-3'
gp130 Y190G antisense	5'-CAATGTTGACAAA**ACC**CACAGTAGAATAATC-3'
gp130 D215G sense	5'-CATATCAATTTT**GGT**CCTGTATATAAAGTG-3'
gp130 D215G antisense	5'-CACTTTATATACAGG**ACC**AAAATTGATATG-3'
gp130 V252G sense	5'-CAAGTATTAAGAGT**GGT**ATAATACTAAAATATAAC-3'
gp130 V252G antisense	5'-GTTATATTTTAGTATTAT**ACC**ACTCTTAATACTTG-3'
	Primers for gp130 deletions
ΔYYΔD1 sense	5'-TTGCCTCCAGAAAAACCTAAAAATTTG-3'
ΔYYΔD1 antisense	5'-ATCTAGAAGTTCACCTGTAGATTCAGTGGTG-3'
ΔYYΔE1-P5 sense	5'-TGTGGTTATATCAGTCCT-3'
ΔYYΔE1-P5 antisense	5'-ACCTGTAGATTCAGTGGT-3'
	Primers for mice genotyping
tTA sense (856)	5'-CGCTGTGGGGCATTTTACTTTAG-3'
tTA antisense (857)	5'-CATGTCCAGATCGAAATCGTC-3'
rtTA sense	5'-CCATGTCTAGACTGGACAAGA-3'
rtTA antisense	5'-CTCCAGGCCACATATGATTAG-3'

TET sense	5'-AATGAGGTCGGAATCGAAGG-3'
TET antisense	5'-TAGCTTGTCGTAATAATGGCGG-3'
L-gp130 full length sense	5'-CCACCATGTTGACGTTGC-3'
L-gp130 full length antisense	5'-TCACTGAGGCATGTAGCC-3'
luciferase sense	5'-AGGACCTATGATTATGTCCGGTTA-3'
luciferase antisense	5'-GTACTTCGTCCACAAACACAACTC-3'
Primers for gp130 probe (Southern blot)	
L-gp130 probe sense	5'-ACCTTGAAAGCTCAGAACTCGG-3'
L-gp130 probe antisense	5'-GGTAGACTCGGATCTTGAGAAG-3'
RT-PCR	
Oligo dT	5'-TTTTTTTTTTTTTTTTTTTT-3'

2.5 Antibodies

Specific antibodies were used for protein detection in Western blot analysis, in immunoprecipitation studies and in flow cytometry according to manufacturer's protocol.

2.5.1 Primary antibodies

Primary Antibodies were diluted 1: 1000 in NETG for Western blot analysis. For immunoprecipitation studies the antibodies anti-GFP and anti-myc were used at a final concentration of 0.8 µg. For flow cytometry analysis the anti-gp130 antibody B-P4 (100 µg/ml) was used at a final concentration of 50-100 ng/ $1x10^6$ cells. Inhibition studies with proliferating Ba/F3-gp130 cells were conducted with the anti-gp130 antibodies B-P4 (100 µg/ml) or C-20 (200 µg/ml) at a final concentration of 1 µg/ml**.**

Cell Signaling

anti -Phospho-STAT3 (D3A7)XP™ #9145	rabbit monoclonal antibody recognizes human, mouse and rat STAT3 only if phosphorylated at residue Tyr705.
anti-STAT3 #9139	mouse monoclonal antibody recognizes human, mouse, rat and monkey STAT3.
anti-P-Tyr-100 #9411	mouse monoclonal antibody recognizes phosphorylated tyrosine residues.

Roche

anti-GFP Cat.No. 11 814 460 001	mouse monoclonal antibody recognizes the green fluorescent protein (GFP) (*Aequorea victoria*), GFP derivatives such as e.g. YFP and EYFP.

Santa Cruz

anti-c-Myc (9E10) sc-40	mouse monoclonal antibody recognizes human, mouse and rat c-myc protein as well as Myc-tag, raised against the epitope EQKLISEEDLN.
anti-gp130 (B-P4) sc-57188	mouse monoclonal antibody recognizes the extracellular domain (D4) of human gp130.
anti-gp130 (C-20) sc-655	rabbit polyclonal antibody recognizes the intracellular domain of human, mouse and rat gp130.
anti-VP16 (1-21) sc-7545	mouse monoclonal antiobody recognizes VP16 and VP16 fusion proteins, raised against the epitope corresponding to amino acids 456-490 of VP16.

MoBiTech

anti-TetR(B) TET02	mouse monoclonal antiobody recognizes the Tet-repressor domain.

Millipore

anti-P-Y(4G10)	mouse monoclonal antibody recognizes phosphorylated tyrosine residues.

2.5.2 Secondary antibodies

All secondary antibodies were purchased from Thermo Fisher Scientific and used at a dilution of 1:5000.

ImmunoPure® Goat anti-rabbit igG, (H+L), Peroxidase Conjungated	#31462
ImmunoPure® Goat anti-mouse igG, (H+L), Peroxidase Conjungated	#31432
Goat-anti-mouse-Dylight 649	#35515

2.6 Organisms

2.6.1 Cell lines

Cell culture dishes and flasks were obtained from Sarstedt. All cells were cultivated at 37°C, 5% CO_2 and 90% relative humidity.

HepG2 cells and HEK 293T cells are human cell lines and were obtained from the German Resource Centre for Biological Material (DSMZ). Parental Ba/F3 cells do not express endogenous gp130 and acquired IL-3 as growth factor. Ba/F3-gp130 cells were stably transfected with a cDNA coding for human gp130 and grew in dependence of Hyper-IL-6 (explained in section 1.3). The ecotrophic phoenix cell line was used for the production of retroviraly supernatant, which exclusively infects murine cells.

Table 2-3: Cell lines used in this study.

HepG2	human	hepatocellular carcinoma cells	RPMI + 10% FCS
HEK 293T	human	embryonic kidney cells	DMEM + 10% FCS
Phoenix (Eco)	human	HEK 293T cell-derived retroviral packaging cell line	DMEM + 10% FCS
MEF	murine	embryonic fibroblasts	DMEM + 10% FCS
Ba/F3	murine	pre B-cells (IL-3 dependent)	RPMI + 10% FCS 10 ng/ml mIL-3
Ba/F3-gp130	murine	pre B-cells (Hyper-IL-6 dependent)	DMEM + 10% FCS 10 ng/ml Hyper-IL-6

2.6.2 Animals

Wildtype C57BL/6N mice were purchased from Charles River (Sulzfeld, Germany). Transgenic heterozygous L-gp130$^+$ tg mice were generated in the *Interfakultäre Biomedizinische Forschungseinrichtung* (IBF, University of Heidelberg) on a C57BL/6N background. The heterozygous LC-1 tg mice and the hCMV-rtTA tg mice (mixed background) were a kind gift of Prof. Dr. Saftig (Department of Biochemistry, CAU Kiel). LC-1 tg mice express the Cre-recombinase and firefly luciferase under control of a tetracycline-responsive promoter element. hCMV-rtTA$^+$ tg mice express the reverse tetracycline transactivator (rtTA) under control of the human cytomegalovirus promoter. Transgenic heterozygous Lap-tTA$^+$ tg mice were kindly provided by Lars Zender (Helmholtz Centre for infection research, Braunschweig) with NMRI background and were backcrossed to C57BL6/N background up to the 7th generation. These mice express the tetracycline transactivator (tTA) under control of a liver specific promoter. The heterozygous Lap-rtTA$^+$ tg mice (C57BL6/N background) were obtained from the European Mouse Mutant Archive (EMMA, Italy). These mice express the reverse tetracycline transactivator (rtTA) under control of a liver specific promoter.

Table 2-4: Mouse strains used in this study.

strain	transgene		tissue specificity	genetic background
Lap-tTA	Tg(Cebpb-rtTA2S*S2)1Bjd	tTA	liver, kidney	NMRI
rTALAP-1	Tg(Cebpb-tTA)5Bjd	rtTA	liver, kidney	C57Bl/6N
hCMV-rtTA	Tg(CMV-tTA)4Bjd	rtTA	ubiquitous	mixed
L-gp130		L-gp130, firefly luciferase	ubiquitous	C57Bl/6N
LC-1	Tg(tetO-cre)LC1Bjd	Cre-recombinase, firefly luciferase	ubiquitous	mixed

2.7 Kits

All kits were used according to the manufacturer's protocol.

Fermentas	GeneJET™ Plasmid Miniprep Kit
GE Healthcare	ECL-Plus ProbeQuant™ G-50 Micro Columns
Invitrogen	Mouse-SAA ELISA (Catalog Number KMA0021)
Macherey Nagel	NucleoSpin® RNAII (740955.250) NucleoSpin® RNA/Protein (740933.10) Nucleobond® XtraMidi (740410.100)
Pierce	BCA Protein Assay Reagent Super Signal ® West Pico Chemiluminescent Substrate
Promega	Dual-Glo® Luciferase Assay System (E2920) Luciferase Assay System (E1500)
Quiagen	Gentra Puregene Tissue Kit QIAquick Gel Extraction Kit QIAquick PCR Purification Kit
Stratagene	Prime-It II Random Primer Labeling Kit

3 METHODS

3.1 Molecular biology methods

3.1.1 Transformation of bacteria

10 - 100 ng of plasmid DNA or 5 µl of a ligation reaction was mixed with 10 µl of 5x KCM buffer in a total volume of 50 µl, added to 50 µl of chemical-competent *E.coli* DH5α and incubated for 30 min on ice. Bacteria were heat-shocked (42°C, 1 min), subsequently chilled on ice for 5 min and were then incubated with 500 µl LB w/o antibiotics for 1 h at 37°C under constant agitation. Bacteria were centrifuged (5 min, 6,000 x g) and supernatant was discarded. The pelleted bacteria were resuspended in 100 µl of the remaining LB media and spread on LB-agar plates with the indicated antibiotics. Plates were incubated at 37°C overnight.

3.1.2 Plasmid isolation

For plasmid preparation of transformed bacteria a single colony was inoculated in 2 ml LB medium with appropriate antibiotic and incubated at 37°C, under constant agitation over night. The bacteria cultures were pelleted by centrifugation (2 min, 6,000 x g). Isolation of DNA was done using the GeneJET™ Plasmid Miniprep Kit according to the manufacturer's protocol (Fermentas). The DNA pellet was dried for 10 min at 37°C and dissolved in 100 µl ddH_2O. DNA was analyzed by restriction digestion and verified by sequencing.

To prepare large amount of purified DNA, 100 ml bacterial cultures were inoculated and plasmid DNA was isolated using the Nucleobond® XtraMidi kit (Macherey Nagel) according to the manufacturer's protocol.

3.1.3 Digestion, blunting and dephosphorylation of vector DNA

The digestion of vector DNA and of PCR fragments was performed with the appropriate digestion enzyme at 37°C for 1 – 3 h according to the manufacturer's protocol (Fermentas). The enzymatic reaction was stopped at 65°C for 20 min. PCR fragments were purified using the QIAquick PCR Purification Kit (Quiagen), whereas vector DNA was purified via QIAquick-gel extraction kit (Qiuagen). The digested DNA-ends were filled by Klenow reaction (10 min, 37°C and 10 min, 75°C). For dephosphorylation 1 U calf instestinal alkaline phosphatase (CIAP) was added to the digested vector and the reaction was incubated for 30 min at 37°C followed by heat inactivation. Finally, the samples were loaded onto an agarose gel and purified using a QIAquick-gel extraction kit (Qiuagen).

3.1.4 Ligation of DNA fragments

Purified PCR fragments were ligated into digested, linearized plasmids (100 ng) using T4 DNA ligase (Fermentas) with five-fold molar excess of the insert according to the manufacturer's protocol. The reaction was incubated either at room temperature (RT) for 3 - 4 h or for 1h at RT following incubation at 16°C over night.

3.1.5 Purification of DNA fragments

For isolation and purification of DNA fragments from agarose gels, ethidium bromide stained gels were illuminated with UV-light. The appropriate DNA band was excised from the gel with a clean scalpel and transferred into a 1.5 ml tube. The DNA fragment was isolated by using the QIAquick-gel extraction Kit (Qiagen) following the manufacturer's instructions.
Purification of PCR fragments was done with the QIAquick PCR Purification Kit (Qiagen) according to the manufacturer's protocol.

3.1.6 Optimization of the Kozak sequence of pBI5-L-gp130

To achieve the best translation of the transgene L-gp130, the Kozak sequence was optimized from CUACC to CCACC. Therefore, L-gp130 was amplified via PCR using specific primers containing the new Kozak sequence as well as the restriction sites for NheI and Hind III (Fig 3.1, Tab. 3-1).

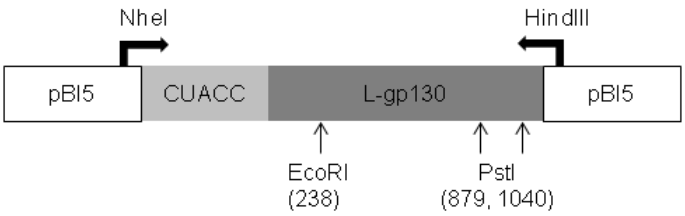

Figure 3.1: Primer binding sites for the introduction of a new Kozak sequence and restriction sites in the sequence of L-gp130. The restriction enzymes EcoRI and PstI were used to verified the orientation of the insert.

The vector pBI5 and the purified PCR fragment were digested by the restriction enzymes NheI and HindIII. The vector backbone was subsequently dephosporylated with CIAP to prevent re-ligation. Vector and PCR fragment were ligated and transformed into chemical-competent bacteria. Following successful transformation the DNA was isolated and the orientation of the insert was verified by digestion with the restriction enzymes EcoRI or PstI. Digestion with EcoRI resulted in four specific fragments (278bp, 563 bp, 1.609 bp, 4.796 bp) and digestion with PstI generated three specific fragments (161 bp, 1.488 bp, 5.597 bp).

Table 3-1: Primers for L-gp130 containing the new Kozak sequence (bold text) and the restriction sites for NheI and HindIII (underlined).

L-gp130 sense	NheI	5'-CTGAGCTAGC**CCACC**ATGTTGACGTTGCAGAC-3'
L-gp130 antisense	HindIII	5'-CAAGGCGGCTACATGCCTCAGTGAAAGCTTCTGA-3'

3.1.7 Cloning of pMOWs-tTA

The retroviral vector pMOWs-GFP was digested with EcoRI and EcoNI to remove the sequence coding for GFP. 5'-overhangs were filled via Klenow reaction to obtain a blunt ended vector. The vector pTan-Pur contains the sequence for the tetracycline transactivator (tTA) and was digested with HindIII and SpeI. The tTA fragment was purified via gel extraction and 5'-overhangs were filled via Klenow reaction. The blunted vector backbone of pMOWs and the blunted tTA fragment were ligated and transformed into chemical-competent bacteria. Following successful transformation the DNA was isolated and the orientation of the insert was verified by digestion with the restriction enzyme XbaI, which cuts the insert and the vector backbone. If the inserted tTA fragment is in the correct orientation, a fragment size of 1200 bp is expected, whereas a fragment size of 2200 bp identifies an incorrect orientation of tTA into the vector.

3.1.8 Generation of myc-tagged constructs

The expression construct p409-eYFP-gp130 was digested with AgeI and NotI to remove the sequence coding for eYFP and dephosphorylated using 1 U of FastAP™ (Fermentas) to prevent re-ligation. Oligonucleotides containing the sequence coding for the myc-tag (f.c. 3 mg/ml) were annealed in NEBuffer4 and phosphorylated using T4 polynucleotide kinase (Fermentas) according to the manufacturer's protocol. The annealed and phosphporylated myc-oligonucleotides were then ligated with the digested and dephosphorylated plasmid using T4 DNA ligase (Fermentas) at RT for 1 h and 16°C over night. The ligation mixture was transformed into chemical-competent *E.coli* DH5α bacteria, followed by plasmid isolation and sequencing.

3.1.9 Quantification of nucleic acids and sequencing

DNA and RNA concentrations were determined spectrophotometrically using Nano-Drop (PeqLab) technology by measuring the absorbance at 260 nm, 280 nm and 320 nm.
DNA sequencing was performed by SeqLab (Göttingen) and GATC Biotech AG (Köln) using single read sequencing by Sanger.

3.1.10 DNA gel electrophoresis

1% (w/v) agarose gels were prepared by heating of 1 g agarose (Biozym) in 100 ml of 0.5x TBE buffer supplemented by 0.05% (v/v) ethidium bromide. DNA sample was diluted with 6x DNA sample buffer

and loaded onto the agarose gel. DNA fragments were separated depending on their size, by horizontal agarose gel electrophoresis at constant voltage (100 V). Gel documentation was performed at the BioDoc system (Biometra).

3.1.11 Polymerase chain reaction (PCR)

Polymerase chain reaction (PCR) was used to amplify DNA sequences either for cloning or for detection. DNA for cloning was amplified using Pfu polymerase (Fermentas), while DreamTaq-polymerase (Fermentas) was used for detection of specific DNA sequences according to the manufacturer's protocol. The following reaction mixture was used for the different applications:

Template	10 – 100 ng plasmid DNA or 1 µl of cDNA
Forward primer	10 pmol
Reverse primer	10 pmol
dNTPs	10 mM each
PCR buffer (10x)	5 µl
Polymerase	1 U
ddH2O	ad 50 µl

The PCR was performed according to the following scheme:

95°C	5 min	initial denaturation	
95°C	45 sec	denaturation	30 cycles
55°C – 61°C*	45 sec	primer annealing	
72°C	1 min/1kb	elongation (1 min/1kb)	
72°C	5 min	final elongation	

*Primers used for different approaches required varying annealing temperatures.

3.1.12 Site directed mutagenesis PCR

Single amino acid exchange was performed via mutagenesis PCR. The point mutations were created by designing a mismatch in the mutagenic primer. For generating point mutations, the length of the correctly matched sequence in the mutagenic primers should be in average 24−30 nucleotides. The desired mutation should be in the middle of the primer with 10−15 perfectly matched nucleotides on each side. The reading frame must not be altered. Phusion® high fidelity polymerase (NEB) was used according to the manufacturer's protocol (Fermentas). The following reaction mixture was used with 50 ng template DNA for the different applications:

Template	50 ng plasmid DNA
Forward primer	10 pmol
Reverse primer	10 pmol
dNTPs	10 mM each
HF buffer (5x)	10 µl
Polymerase	1 U
ddH2O	ad 50 µl

The PCR was performed according to the following scheme:

95°C	3 min	initial denaturation	
95°C	20 sec	denaturation	20 cycles
44°C – 55°C*	20 sec	primer annealing	
72°C	30 s/1 kb	elongation	
72°C	5 min	final elongation	

*Primers used for different approaches required varying annealing temperatures.

Following PCR the non-mutated template vector was eliminated by digestion using the enzyme DpnI (37°C for 1 h, 80°C for 20 min), which exclusively digests methylated DNA. To verify the PCR, samples were analyzed on a 0.8% agarose gel and PCR products were transformed into bacteria *E.coli* DH5α, followed by plasmid isolation and sequencing.

3.1.13 Deletion PCR

Deletions are created by designing primers that border the deleted area on both sides. To generate a deletion, the primers should be perfectly matched on their entire length, which should be 24−30 nucleotides. The primers must be phosphorylated at the 5' end to ensure that the new generated plasmid can ligate after deletion PCR. The phosphorylation reaction was done using T4 kinase (Fermentas) according to the manufacturer's protocol. The reaction mixture was incubated for 20 min at 37°C and 10 min at 75°C and was subsequently used for mutagenesis PCR (1 ng template DNA, see 3.1.2), followed by ligation. Unchanged DNA was digested by DpnI as described above.

3.1.14 RNA Isolation

The NucleoSpin RNA II kit (Macherey-Nagel) was used for the isolation of ribonucleic acid (RNA) from different tissues and cells, e.g. 15 mg of liver tissue according to the manufacturer's instructions. 1 µg of total RNA was used as a template for the reverse transcription (RT-PCR) to generate cDNA.

3.1.15 Reverse transcription PCR (RT-PCR)

1 µg messenger RNA was reverse transcribed into complementary DNA (cDNA) using the reverse transcriptase. The generated single-stranded cDNA was further used for PCR analysis. The M-MuLV

Reverse Transcriptase (20 U/µl) or the RevertAid™ Reverse Transcriptase (200 U/µl) was used according to the manufacturer's protocol. The reaction was performed using oligo $(dT)_{18}$ primer, which anneal at the 3' poly (A) mRNA tail. 1 µl of the generated cDNA was used for the beta-actin (housekeeping gene) PCR as well as for a specific transgene PCR.

3.1.16 Protein extraction

Liver samples (30 – 50 mg) were homogenized in 500 µl tissue lysis buffer using ceramic beads. The amount of lysis buffer was adjusted to other organs. After homogenization with the Precellys® tissue homogenizer (Peqlab) the samples were incubated at 4°C under constant agitation for 1 h and subsequently cleared by centrifugation (15 min, 12,000 x g). The supernatant was transferred into a new tube and stored at -20°C.

3.1.17 Quantification of protein concentration

Protein concentration of tissue lysates was determined using the BCA kit (Pierce) according to the manufacturer's protocol. The protein concentration was calculated based on the extinction measured at 562 nm in a microtiter plate reader (Tecan).

3.1.18 SDS-polyacrylamide gel electrophoresis

Proteins were separated by discontinuous SDS-polyacrylamide gel electrophoresis (SDS-PAGE) using the Mini-PROTEAN system (BioRad). Protein samples were supplemented with 5x Laemmli buffer and loaded onto the gel. Electrophoresis was performed in 1x SDS running buffer and was carried out at 120-180 V for 90 to 120 min.

3.1.19 Western blot

Proteins separated by SDS-PAGE were transferred onto a PVDF membrane (GE Healthcare) using the wet blot Mini Trans-Blot Cell apparatus (BioRad) for 120 min (90 V, 4°C). Subsequently, the PVDF membrane was blocked with NETG at RT for 1h and incubated with the primary antibody diluted in NETG. After incubation at 4°C over night, the membrane was washed three times with NETG for 10 min and the appropriate secondary antibody linked to peroxidase (POD) was diluted in NETG and applied at RT for 1 h. The membrane was washed three times for 10 min with NETG to be subsequently developed using ECL Kit. The chemoluminescent signals were detected with the CCD camera system LAS-1000 (Fujifilm) or FluorChem®Q (Alpha Innotech). To analyze different proteins on the same membrane, the bound antibodies were removed by using an acidic mild stripping buffer. After the stripping procedure the membrane was washed several times with water, blocked again with NETG and was incubated with another primary antibody.

3.1.20 SAA-ELISA

The enzyme-linked immunosorbent assay (ELISA) was used to detect and quantify the amount of serum amyloid A (SAA) in mouse sera. The serum samples were diluted 1:20. The specific murine SAA-ELISA (Invitrogen) included an internal purified standard and was done according to the manufacturer's protocol. Quantification of the reaction was done by measuring the ELISA in a microtiter plate reader (Tecan) at 450 nm.

3.1.21 Southern blot

To detect specific DNA sequences in a sample, a single-stranded labeled DNA probe is used, which anneals to the gene or DNA fragment of interest. Therefore, genomic DNA was extracted from tail biopsy and 5 to 10 µg of genomic DNA was digested with NheI and XbaI (3 µl, 20 U/µl) at 37°C over night. The next day DNA was separated on a 0.7% agarose gel (4-6 h, 60 V) and subsequently depurinated with 0.25 M HCl for 15 min. Double stranded DNA was denatured for 30 min under alkaline conditions to improve the binding capacity of the negatively charged DNA to the positively charged nylon membrane (Amersham Hybond N+, GE healthcare). The single stranded DNA hybridizes better with the radioactively labeled probe at low pH.

Table 3-2: Protocol for Southern blot analysis.

Depurination	depurination buffer	1x 15 min
Denaturation	denaturation buffer	2x 15 min
Neutralization	neutralization buffer	1x 10 min
Washing	10x SSC	1x 5 min
Blotting	10x SSC	over night
Washing	5x SSC	1x 15 min
Baking		10 min, 65°C
Cross-linking	UV	2 min
Pre-hybridisation	20 ml churchbuffer	1 h, 65°C
Labeling (DNA probe)	Prime-It II Random Primer Labeling Kit	
Purification (DNA probe)	ProbeQuant™ G-50 Micro Colums	
Hybridization	Probe preparation	5 min, 95°C
		chill on ice
	20 ml churchbuffer (pre-warmed)	overnight, 65°C
	add 50 µl radioactive probe	
	discard hybridization solution	
Washing	2x SSC + 0.1% SDS	short time shaking
	2x SSC + 0.1% SDS	2x 15 min, 65°C
	0.1x SSC + 0.1% SDS	2x 10 min, 65°C

	2x SSC	1x short time shaking
Shrink-wrap in foil		
Stripping (membrane)	0.5% SDS	

The nylon membrane was labeled and placed below the gel. Several sheets of filter paper as well as a stack of paper towels were put on the top of the gel. Pressure was exerted by additional weights (1-2 kg). The whole sandwich was assembled according to Fig. 3.2.

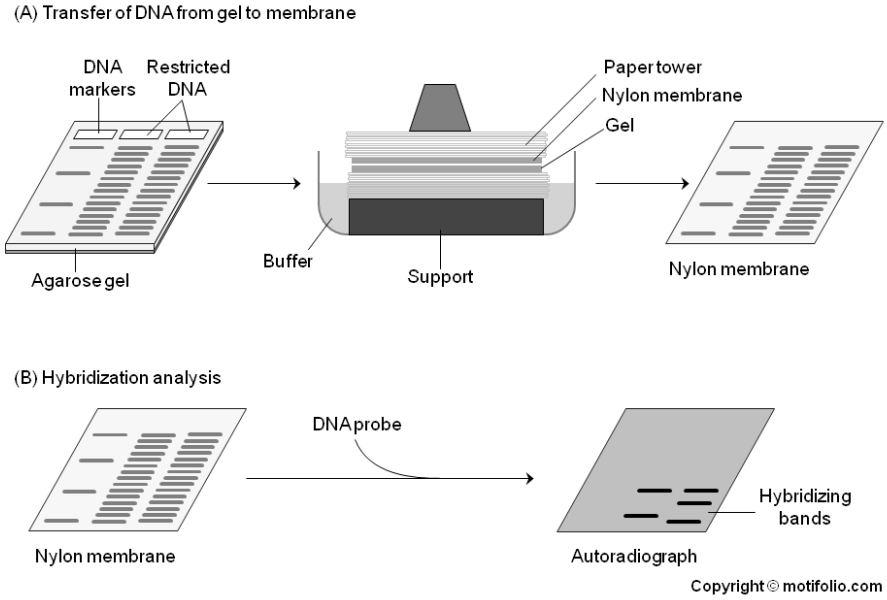

Figure 3.2: Performance of Southern blot analysis. (A) Restricted DNA was fragmented on an agarose gel, depurinated and denatured followed by blotting to a nylon membrane. (B) DNA was cross-linked to the nylon membrane by UV light and hybridized with a radioactively labeled probe. The labeld membrane was analyszed via a Phosphorimager (Fuji).

This stack was built on a glass bridge above a pan filled with buffer (10x SSC). A long filter paper bridge was used to connect the buffer with the membrane to prevent its dehydration. Due to capillary flow the DNA migrated from the gel to the membrane. The DNA bound to the membrane via ionic interactions. The transfer was performed at room temperature over night. The next day the membrane was washed and baked for 10 min at 65°C. The membrane was irradiated with UV light for 2 min to crosslink the DNA to the membrane and was pre-incubated with warm Church buffer using a glass container. Finally the membrane was hybridized with a radioactively labeled probe. To detect transgenic DNA, a specific probe for L-gp130 was generated using PCR with specific primers, which generated a 600 bp fragment of L-gp130. This PCR product was labeled with α-^{32}P or α-^{33}P-dATP using the Primer Labeling Kit (Stratagene) according to the manufacturer's protocol. The purification of radioactive labeled probe was done with ProbeQuant™ G-50 Micro Colums (GE Healthcare) according to the manufacturer's protocol. Analysis of the radioactive labeled membrane was done with a Phosphorimager (Fuji).

3.2 Cell culture methods

3.2.1 Conditions

Cell culture was conducted in flasks with the corresponding culture medium. Cells were passaged following confluency. For HEK 293T and phoenix cells it was sufficient to flush them vigorously with culture medium to detach them from the culture dish. In order to detach HepG2 cells, they were washed once with 1 ml trypsin and subsequently trypsinized in 2 ml trypsin at 37°C. Trypsinization was stopped with the addition of culture medium.

The detached cells were centrifuged (1,000 x g, 5 min) and the pellet was resolved in fresh medium. The cells were passaged in a ratio of 1:10 or seeded in dishes or 6-well plates for transfection at a ratio of 4 - 8x 10^5 cells/well. Suspension cells were split by transferring an appropriate amount of the cells into a new flask containing medium and the corresponding cytokine.

3.2.2 Transient transfection

Cells were seeded at a density of 4 – 8x 10^5 cells/well the day before transfection. Turbofect™ (Fermentas) was used to indroduce plasmid DNA into the cells according to the manufacturer's protocol. Medium of the cells was changed before the transfection. The appropriate amount of plasmid DNA (1 - 5 µg) was diluted in serum free medium (SFM) and a twofold amount of Turbofect™ was added. Following 15 - 20 min of incubation at RT this mixture was added drop wise to the cells, followed by an incubation period of 24 - 48 h at 37°C.

3.2.3 Starving and stimulation

Transfected cells were washed once and starved in serum free medium (SFM) in medium containing 0.5% FCS for 4 - 5 h or overnight. When indicated, cells were stimulated with 10 ng/ml of Hyper IL-6 for 10 to 15 min before cell lysis.

3.2.4 Retroviral transduction

Ba/F3 as well as mEF cells were transduced according these instructions. Prior, target cells were seeded and subjected to different puromycin concentrations ranging from 0.5 µg – 5 µg/ml to determine the lethal dosis. Phoenix cells were plated in 6-well plates at a cell density of 8x 10^5 cells/well and were transiently transfected with pMOWs retroviral expression constructs containing myc-tagged gp130 variants or tTA on the next day. pMOWs-GFP served as an appropriate control for transfection and transduction efficiency. 24 h after transfection the supernatant containing the retroviral particles was collected and filtered through a 0.2 µm pore size filter.

Ba/F3 cells were diluted to a cell number of 2x 10^6 cells/ml and 50 µl (1x 10^5 cells) were mixed with 250 µl of the corresponding supernatant. Polybrene was added at a final concentration of 8 µg/ml and

cells were centrifuged (2,000 x g) at RT for 2 h. The supernatant was discarded and the remaining pellet was resuspended in 5 ml medium containing the respective cytokine.
mEF cells were seeded at a densitiy of 4x 10^5 cells/well in a 12-well plate one day before transduction. The medium was removed and 1 ml of the filtered supernatant was supplemented to the cells and mixed with polybrene. Following centrifugation (2,000 x g) for 2 h at RT, 1 ml medium was added to the cells to dilute the supernatant.
48 h post transduction, cells were selected with puromycin at a final concentration of 1 – 1.5 µg/ml for Ba/F3 cells. mEF cells showed a higher resistance and were selected with 3 µg/ml of puromycin.

3.2.5 Surface expression analysis via flow cytometry

Ba/F3 cells were pelleted and washed once with PBS (5 min, 1,000 x g). Cells were resuspended in 1 ml PBS containing 5% FCS, counted using a hemocytometer and subsequently diluted to 1x 10^6 cells in 50 µl PBS+5%FCS. To block unspecific binding sites, 0.5 µl of rat-anti-mouse CD16/CD32 (Fc-block, BD) was added and incubated at RT for 5 min. Following blocking, cells were incubated with anti-gp130 antibody B-P4 (50 ng) at RT for 60 to 90 min. The cells were washed twice with 1 ml PBS+5%FCS, followed by incubation with the secondary antibody goat-anti-mouse-DyLight 649 (500 ng) for 30 to 60 min at 4°C in the dark. For the measurement cells were washed twice with 1 ml PBS+5%FCS and resuspended in 500 µl PBS 5%FCS. Analysis was performed on a BD FACSCanto.

3.2.6 Intracellular expression analysis via flow cytometry

Ba/F3 cells were adjusted to 1x 10^6 cells, washed once with PBS containing $Ca^{2+}$and Mg^{2+} (5 min, 1,000 x g) and resuspended in 0.5 ml PBS (Ca^{2+}, Mg^{2+}). Cells were fixed by adding 0.5 ml fixation buffer and gently mixing (20 min, RT). Cells were subsequently washed once with PBS (Ca^{2+}, Mg^{2+}), once with permeabilization buffer and once with super permeabilization buffer. The primary antibody (anti-gp130: B-P4) was used in twofold amount compared to surface staining (100 ng) and was incubated for 30 min at RT. Then the cells were washed twice with permeabilization buffer and incubated with the secondary antibody anti-mouse-DyLight 649 (500 ng) at 4°C in the dark for 30 min. Cells were then washed twice with permeabilization buffer, once with PBS (Ca^{2+}, Mg^{2+}), once with staining buffer and were finally resuspended in 500 µl staining buffer. Analysis was performed on a BD FACSCanto.

3.2.7 STAT3 reporter assay

To measure the transcriptional activity of STAT3, we used a STAT3 reporter construct in which firefly luciferase is expressed under the control of a STAT3 responsive promoter element (SIEM-Luc) (123, 129). A construct expressing renilla luciferase (TK-RL) was used to control the transfection efficiency. HepG2 cells were seeded at a density of 4 - 8x 10^5 cells/well in a 6-well plate. Next day the cells were co-transfected with 1 µg SIEM-Luc, 1 µg TK-RL and 1 µg of the p409-eYFP gp130 construct. The cells were analyzed for YFP expression using fluorescence microscopy. Following starvation cells

expressing gp130 wt were stimulated with Hyper-IL6 (10 ng/ml) for 4 h. Then the cells were washed with PBS and lysed using the passive lysis buffer of the DualGlo® luciferase Kit (Promega). Luciferase activity was measured according to the manufacturer's protocol.

3.2.8 Dual luciferase assay

The Dual-Glo® Kit (Promega) was used to measure firefly and renilla luciferase simultaneously according to the manufacturer's instructions. The bioluminescence was detected in a white 96-well plate using a plate injector system (GLOMAX®). 20 µl of cell lysates were dispensed per well and the injector added 50 µl of the first substrate D-luciferin per well. The firefly luciferase luminescence was quenched by adding 50 µl of the Stop&Glo Reagent to the sample after quantitation. This reagent includes coelenterazine and subsequently the renilla luciferase luminescence was quantified. A 2 sec premeasurement delay followed by a 10 sec measurement period for each reporter was performed. All samples were measured in duplicates or triplicates and were stored at -20°C.

3.2.9 Luciferase assay

The activity of firefly luciferase was measured in cell lysates and tissue homogenates using the Luciferase Assay System Kit (Promega) according to the manufacturer's protocol. The bioluminescence was detected in a white 96-well plate using a plate injector system (GLOMAX®). Murine liver sections (30 mg, median lobe) were homogenized in 500 µl 1x lysis reagent (CCLR, 4°C). 20 µl of cell lysates were dispensed per well and the injector added 50 µl of the substrate D-luciferin per well. A 2 sec premeasurement delay followed by a 10 sec measurement period was performed to quantify the firefly luciferase luminescence. All samples were measured in duplicates or triplicates and were stored at -20°C.

3.2.10 MTT cell viability assay

Proliferation of Ba/F3-gp130 cells stably transduced with the gp130 constructs was detected in the absence or presence of cytokines, inhibitors or antibodies by the MTT viability assay. The cells were washed three times (1,000 x g, 5 min) with PBS and resuspended in 1 ml appropriate medium for counting. Cells were resupendend in serum free medium containing the appropriate supplement and seeded with a density of 5x 10^3 cells/100 µl in a 96-well plate. Cells treated with 10 ng/ml of Hyper-IL-6 and 500 nM of the JAK inhibitor Pyridone 6 (P6) were used as controls. Inhibition studies were conducted with 1 µg/ml of either B-P4 or C-20 anti-gp130 antibody. Cells were incubated at 37°C for 72 h. To quantify proliferation 10 µl of the substrate MTT (5 mg/ml) were added and incubated for additional 4 h at 37°C. In living cells the MTT was reduced to insoluble purple formazan crystals, which were dissolved by adding 100 µl solubilization buffer followed by an incubation at 37°C over night. Finally, absorption was measured at 595 nm at microtiter plate reader (Tecan). The proliferation was calculated as fold induction. All experiments were made in triplicates or up to 8 times.

3.2.11 Cell lysis

Prior to lysis, cells were washed once in 1 ml PBS. If adherent cells were loosely attached, they were scraped into PBS, centrifuged at 2,000 x g for 5 min and subjected to cell lysis. Cells were lysed for 10 min on ice. Cell lysates were cleared by centrifugation at 12,000 x g for 15 min at 4°C.

3.2.12 Co-/Immunoprecipitation

Cells were lysed either in RIPA-buffer (Ba/F3 cells) or Co-IP buffer (HEK 293T cells). Immunoprecipitation was performed by the addition of 0.8 µg antibody (anti-GFP or anti-myc) and 30 µl washed protein G sepharose and incubated on a rotating wheel over night at 4°C. Sepharose beads were washed three times with 1 ml Co-IP-buffer (3,500 x g, 2 min) and the supernatant was completely removed using a Hamilton syringe. Beads were boiled in 30 µl of 2x Laemmli buffer and subsequently analyzed by SDS-PAGE.

3.2.13 Determination of doxycycline concentration in mouse serum

The serum concentration of doxycycline was analyzed *in vitro*. Therefore, HEK 293T cells were co-transfected with pBI5-L-gp130 and either hCMV-rtTA (Tet-on) or hCMV-tTA (Tet-off). Transfected cells were split onto 12-well plates 24 h after transfection. 24 h later 2 µl (for Tet-off) to 10 µl (for Tet-on) serum of Dox-treated mice as well as control serum of untreated mice was added to the cells. A defined doxycycline concentration was used as control. The cells were lysed 24 h later in luciferase lysis buffer (Promega) and luciferase activity was analyzed as described above.

3.3 Animal methods

All mice were bred at a 12-h light-dark cycle under standard conditions and provided with food and water *ad libitum*.

3.3.1 Generation of transgenic mice

The bidirectional vector pBI5, expressing the constitutive active variant L-gp130 and the reporter gene firefly luciferase, was chosen to generate transgenic mice. The plasmid was linearized by digestion with the enzyme PvuI and purified via gel extraction. 6 µg purified linearized DNA was sent to the *Interfakultäre Biomedizinische Forschungseinrichtung* (IBF, Heidelberg), where the pronucleii injection and implantation in C57BL/6N mice as well as the breeding of the foster mothers were performed. Genomic DNA was isolated from the tails of the offspring and genomic insertion of the gene cassette containing L-gp130 and firefly luciferase was analyzed via genotyping PCR.

3.3.2 Doxycycline treatment

Doxycycline was supplied either in drinking water containing 3% sucrose or via food pellets. The concentration differed in dependence on the mice. For all experiments with Lap-tTA$^+$ tg and LC-1$^+$ tg mice (Tet-off) doxycycline was given in low concentrations (Tab.3-3). It has been shown that doxycycline passes the placenta and is given to the pups via mother's milk. Therefore the doxycycline concentration was lowered to 1 μg/ml (in drinking water) during breeding, which was shown to suppress activation of the Tet-promoter. Mice at the age of 3 weeks received a higher dosage of doxycycline (10 μg/ml) to ensure a complete suppression. Later the administration was changed to food pellets containing doxycycline (50 mg Dox/kg) due to the better handling.
For all experiments with hCMV-rtTA$^+$ tg and Lap-rtTA$^+$ tg mice (Tet-on) doxycycline was given in high concentrations. Either they got food supplemented with 1 g Dox/kg or doxycycline was given in a concentration of 2 mg/ml in drinking water.
The food pellets were ordered from SNIFF using doxycycline hyclate (Sigma-Aldrich).

Table 3-3: Supply of doxycycline to the mice.

Tet-off	1 – 10 μg/ml (3% sucrose)	water
	50 mg/kg	food
Tet-on	1 g/kg	food
	2 mg/ml (3% sucrose)	water

3.3.3 *In vivo* imaging

The *in vivo* imaging of luciferase activity was performed in cooperation with the Molecular Imaging North Competence Center (MOIN-CC, UK-SH Kiel) under supervision of Dr. Christian Rosenkranz.
Initially, the mice were injected i.p. with 10 μl luciferin (15 mg/ml) per g bodyweight to ensure its transformation by luciferase and subsequently narcotized with ketamine and xylazine. Luminescence was measured with a CCD camera (Berthold NightOWL) for 2 min.

3.3.4 Isolation of genomic DNA from mouse tail

Mouse tails were lysed in cell lysis solution (Quiagen) containing 3 U Proteinase K (Fermentas) at 55°C overnight under constant agitation. DNA was isolated according to the manufacturer's protocol and was used for genotyping PCR or was stored for short term at 4°C and for long term at -20°C.

3.3.5 Generation of mouse embryonic fibroblasts

L-gp130^{+} tg mice were bred with C57BL6/N wildtype mice to obtain heterozygous L-gp130^{+} tg embryos, which were dissected at day 13.5 of pregnancy under sterile conditions. Heart, liver and all blood filled organs were removed. The embryos were washed in PBS to get rid of all blood. Afterwards the head was cut for further digestion and DNA isolation for genotyping PCR. Subsequently, the embryos were transferred in to 3 cm dish, cut in very small pieces with a fresh scalpel and incubated with 2 ml trypsin-EDTA for 15 min at 37°C. The tissue was shaken gently and resuspended with a shortened pipette tip to avoid cell damage. The dissolved tissue was transferred into a 15 ml tube and mixed with 10 ml warm DMEM medium containing 10% FCS and 1% Pen-Strep. The cells were pelleted (5 min, 1,000 x g) and the supernatant was discarded. Afterwards the cells were resuspended in fresh DMEM medium containing 20% FCS and 1% Pen-Strep and were seeded in 10 cm dish. MEF cells were split 1:5 once or twice a week and transfected with a vector containing the SV (simian virus) 40 large T antigen using Turbofect™ (Fermentas) to achieve immortalization, which was followed by selection with the antibiotic G418.

3.3.6 Plasma preparation of whole mouse blood

Whole mouse blood was obtained from either tail vein or heart puncture. Tubes coated with Lithium-Heparin (Sarstedt) were used to prevent coagulation. The plasma was obtained by centrifugation at 10,000 x g for 5 min at 4°C and stored at -20°C.

4 RESULTS

4.1 Point mutations of gp130

As shown in the crystal structure of the hexameric complex (IL-6/sIL-6R/gp130)$_2$, the domains D1 to D3 of gp130 are crucial for the recognition of the IL-6/sIL-6R complex (5, 108). One gp130 molecule contacts one IL-6/sIL-6R complex engaging its domains D2 and D3 (Fig. 4.1 A). Furthermore, a second gp130 molecule binds the IL-6/sIL-6R/gp130 complex via its domain D1 and is indispensable for the activation of gp130. Pflanz *et al.* could show that mutants of gp130 lacking domain D1 revealed impaired IL-6 induced signal transduction. Furthermore it has been shown that interference with the residues F191, located in domain D2 and V252, located in domain D3 resulted in inhibition of IL-6/IL-6R induced signaling, highlighting the importance of the domains D2 and D3 (16, 107). Recently, Rebouissou *et al.* identified gain-of-function mutations of gp130, which showed ligand independent constitutive activation. These deletion mutations cluster around the EF loop of domain D2, which represents one IL-6 contact site (Tab. 1-2) (130). We speculated that conformational changes of this particular IL-6 binding site triggers gp130 activation. We used a rational structure-based mutagenesis approach to interfere with EF loop flexibility in domain D2, as well as with the hydrophobic interactions between domains D2 and D3.

4.1.1 Structural analysis of activating gp130 point mutants

We analyzed the published crystal structure of gp130 and hypothesized that some amino acid residues might be crucial for the proper positioning of the EF loop (Fig. 4.1 B). The cysteine in position 172 (C172) preceding the EF loop, forms a disulfide bridge to the cysteine in position 182 (C182) and therefore stabilizes the EF loop (Fig. 4.1 E). Further, aspartate in position 215 (D215) seems to be a crucial residue, since it was found to be deleted in human liver adenoma and led to ligand independent activation of gp130 (130). As seen in the crystal structure D215 forms an ionic interaction to the backbone amide of F191 in the EF loop and therefore might affect its proper positioning, too (Fig. 4.1 D). Therefore, we performed mutagenesis studies to analyze the role of these crucial residues for ligand independent activation. The cysteine in position 172 was replaced by serine (C172S), whereas aspartate in position 215 was replaced by the small amino acid glycine (D215G) (Tab. 4-1). Moreover, many hydrophobic residues cluster around the interface of domain D2 and domain D3. The residues valine in position 189 (V189) and tyrosine in position 190 (Y190) of domain D2 as well as valine in position 252 (V252) of domain D3 are found in close proximity and might influence the hydrophobic connectivity between the domains D2 and D3 of gp130 (Fig. 4.1 C). The D3 BC loop containing V252 has been shown to be the only flexible region of domain D3 in a solution NMR structure (131). Horsten *et al.* could show a reduced binding of the IL-6/sIL-6R complex to the mutant gp130 V252D (107). In order to find out, if these residues and disruption of the hydrophobic core is involved in gp130 activation we replaced V189, Y190 and V252 by glycine (Tab. 4-1).

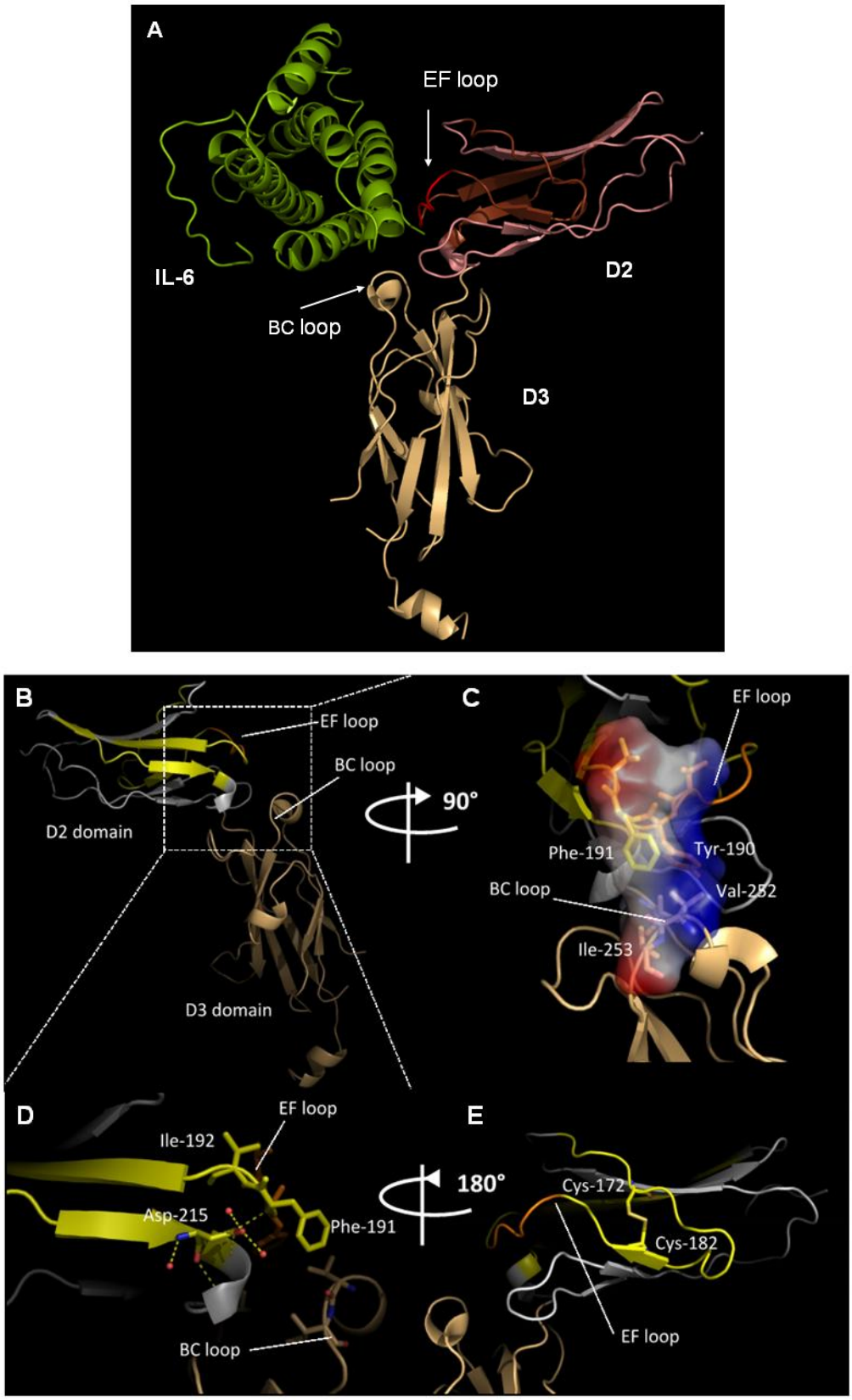

Figure 4.1: Activating gp130 deletion mutations cluster on the IL-6 contact site of gp130. (A) Crystal structure of the domains D2 and D3 bound to IL-6. (B) Domains D2 and D3 of gp130 without IL-6. The EF loop of domain D2 is formed by 2 β-strains (yellow). (C) The interconnecting hydrophobic interface of domain D2 (EF loop) and domain D3 (BC loop) including the residues V189, Y190 (Tyr-190), F191 (Phe-191), V252 (Val-252) and I253 (Ile-253). (D) The ionic interaction of D215 (Asp-215) to the EF-loop containing I193 (Ile-193) and F191 (Phe-191). (E) The disulfide bridge formed by C172 (Cys-172) and C182 (Cys-182) stabilizing the EF-loop (Schuett *et al.* submitted).

Table 4-1: Crucial residues in gp130 wildtype and their substitutions by mutagenesis PCR.

mutagenesis	function in gp130 wt
C172S	Disulfide bond with C182, stabilization of the EF loop in D2
V189G	Interconnecting hydrophobic area, in the IL-6 contact loop (T183-I193)
Y190G	Interconnecting hydrophobic area, in the IL-6 contact loop (T183-I193)
D215G	Ionic interaction to the backbone of the EF loop in D2 (F191)
V252G	Interconnecting hydrophobic area, in the BC loop of D3

4.1.2 Biochemical analysis of activating gp130 point mutations

The gp130 point mutations were generated by mutagenesis PCR. In order to analyze the expression of the generated mutants, we transfected HepG2 cells with expression constructs of C-terminal eYFP-tagged gp130 variants. Analysis was done by fluorescent microscopy. All mutants were expressed, shown by green fluorescence (Fig. 4.2).

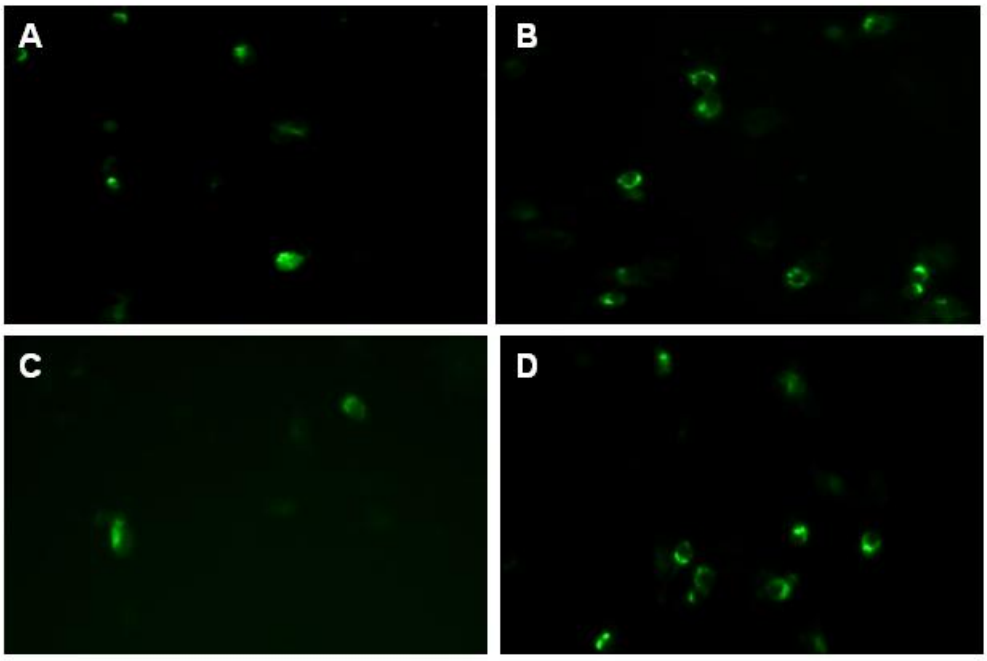

Figure 4.2: Microscopic analysis of HepG2 cells transfected with the expression constructs of eYFP-tagged gp130 variants. HepG2 cells were transfected with (A) gp130 wt, (B) gp130 V189G, (C) gp130 D215G and (D) gp130 V252G. 24 h post transfection cells were analyzed by fluorescence microscopy.

To analyze the activating potential of the generated gp130 mutants HEK 293T cells were transfected with the expression constructs of eYFP-tagged gp130 variants, starved over night and lysed. Cells transfected with gp130 wt were stimulated with Hyper-IL-6 (HIL-6) to achieve a positive control. STAT3 phosphorylation was analyzed by SDS-PAGE and subsequent Western blot analysis. Cells expressing the

point mutants gp130 C172S, D215G and V252G showed phosphorylation of STAT3 in an autonomous, ligand independent manner, whereas the point mutants gp130 V189G and Y190G did not promote any autonomous phosphorylation of STAT3 (Fig. 4.3). Differences in ERK phosphorylation were barely detectable (data not shown). All gp130 variants were equally expressed, as detected in Western blot analysis of cell lysates using anti-GFP antibody.

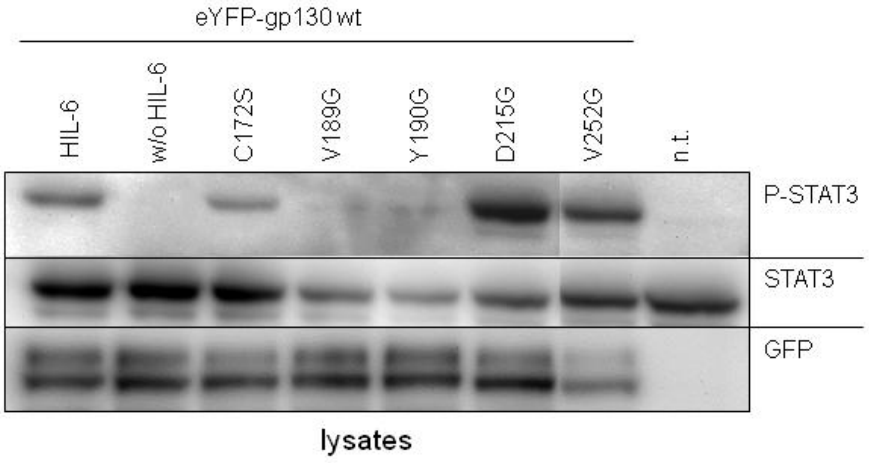

Figure 4.3: Analysis of STAT3 phosphorylation in cells expressing eYFP-tagged gp130 variants. HEK 293T cells were transfected with eYFP-tagged gp130 mutants. 24 h post transfection, cells were starved for 4 h in serum free medium (SFM). HEK 293T cells transfected with gp130 wt were stimulated for 10 min with Hyper-IL-6 (10 ng/ml) and served as positive control. Cell lysates were analyzed for phosphorylated STAT3 (P-STAT3), STAT3 and GFP by Western blot analysis. The anti-GFP antibody recognizes the YFP-tag. n.t.: non transfected

Furthermore, receptor phosphorylation of gp130 was analyzed in lysates of transfected cells by immunoprecipitation of the eYFP-tagged gp130 variants using either an anti-GFP or an anti-P-Tyr antibody. Following immunoprecipitation with an anti-GFP antibody, phosphorylation of the gp130 mutants C172S, D215G and V252G was observed by Western blot analyis using a specific anti-P-Tyr antibody. Gp130 wt and the gp130 variants V189G and Y190G showed receptor phosphorylation to a lower extent (Fig. 4.4). *Vice versa*, precipitation of phosphorylated tyrosine residues using an anti-P-Tyr antibody and subsequent Western blot analysis with an anti-GFP antibody showed the same result. Gp130 wt did not show autonomous activity, whereas the selected point mutants gp130 C172S, D215G and V252G displayed as ligand independent activation.

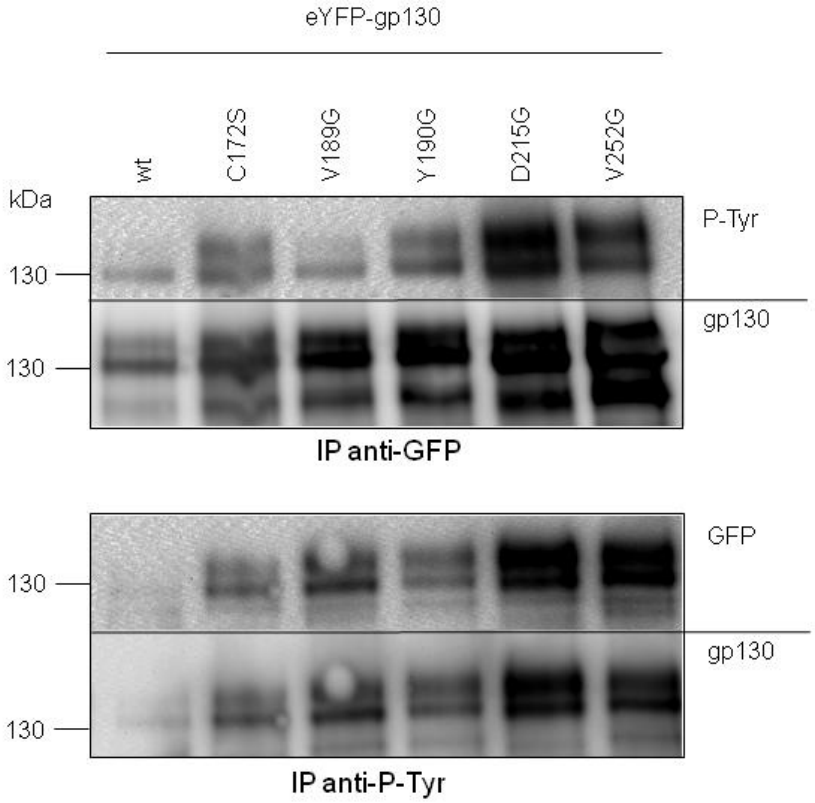

Figure 4.4: Immunoprecipitation of eYFP-tagged gp130 variants and analysis of tyrosine phosphorylation. HEK 293T cells were transfected with eYFP-tagged gp130 mutants. 24 h post transfection, cells were starved for 4 h in SFM. Cell lysates were analyzed by immunoprecipitation using either an anti-GFP or an anti-P-Tyr antibody, followed by SDS-PAGE and Western blot analysis for phosphorylated tyrosine (P-Tyr) or GFP, respectively and gp130. The upper band represents the complex glycosylated form and the lower band the high-mannose form of gp130. The anti-GFP antibody is crossreactive for the YFP-tag.

To confirm these data, we performed a STAT3 reporter assay in the human hepatoma cell line HepG2. In this assay the expression of firefly luciferase is under control of a STAT3 responsive promoter (SIEM-Luc). Renilla luciferase (TK-RL) was used as transfection control. Transfected HepG2 cells were starved overnight and luciferase expression was measured in cell lysates 24 h post transfection. The ratio between firefly and renilla luciferase was calculated and given as fold induction, with non stimulated gp130 wt set to 1. Cells transfected with gp130 wt were stimulated for 4 h with Hyper-IL-6. Cells expressing the gp130 mutants C172S, D215G and V252G showed increased firefly luciferase activity (Fig. 4.5 A). Hyper-IL-6 treatment of cells expressing gp130 wt led to a 4-fold induction of luciferase activity, whereas the point mutants gp130 C172S and V252G showed 5-fold and gp130 D215G 10-fold induction compared to non-stimulated gp130 wt. Cells expressing the point mutants gp130 V189G and Y190G showed no induction of firefly luciferase, which correlates with the absence of STAT3 phosphorylation in HEK 293T cells. All gp130 variants showed equal expression pattern in a specific anti-GFP Western blot (Fig. 4.5 B).

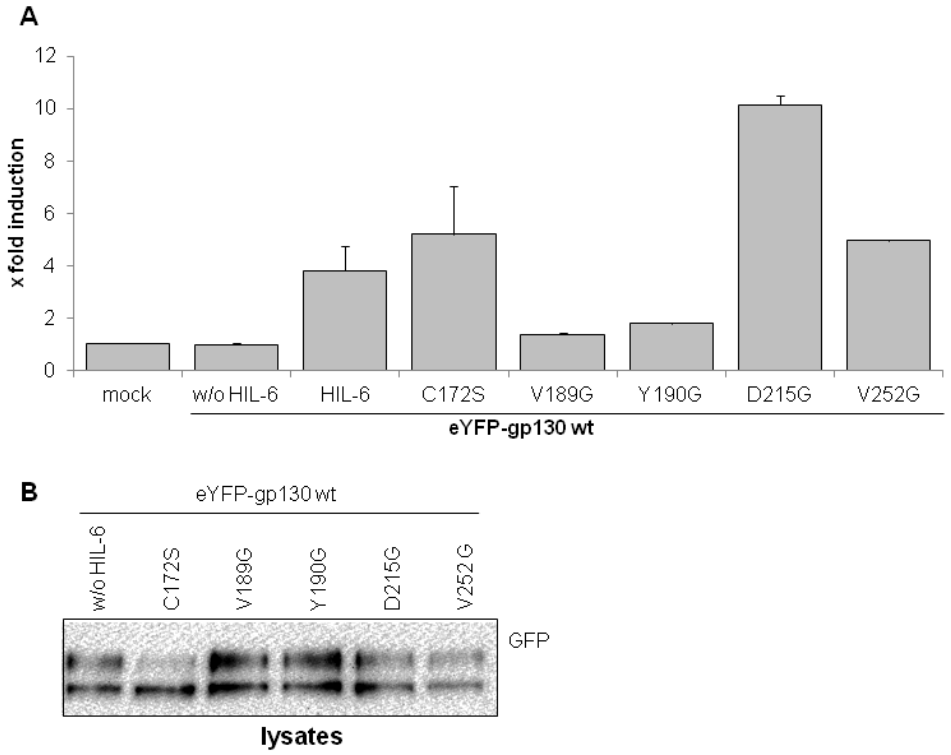

Figure 4.5: STAT3 reporter assay of gp130 point mutants. HepG2 cells were transiently co-transfected with a STAT3 responsive promoter construct, which express firefly luciferase (SIEM-Luc), renilla luciferase (TK-RL) and eYFP-tagged gp130 mutants. Cells were starved over night in SFM and cells expressing gp130 wt were stimulated for 4 h with Hyper-IL-6 (HIL-6, 10 ng/ml), serving as positive control (A) Luciferase activity was detected by using the Dual-Glo® assay (Promega). The fold induction was given with non-stimulated cells expressing gp130 wt set to 1. (B) Cell lysates were analyzed for the expression of eYFP-tagged gp130 mutants by Western blot analysis using an anti-GFP antibody. The upper band represents the complex glycosylated form and the lower band the high-mannose form of gp130. The anti-GFP antibody is crossreactive for the YFP-tag.

In order to analyse whether the gp130 variants can drive STAT3 dependent proliferation, Ba/F3-gp130 cells were stably transduced with C-terminal myc-tagged gp130 point mutants. Parental Ba/F3 cells do not express endogenous gp130 and exclusively proliferate in the presence of mIL-3, whereas Ba/F3-gp130 cells express gp130 and therefore respond to Hyper-IL-6. All transduced Ba/F3-gp130 cells expressing the myc-tagged gp130 mutants displayed comparable proliferation in the presence of Hyper-IL-6. Cells expressing gp130 wt did not show any cytokine independent proliferation, whereas cells expressing the gp130 mutants C172S, D215G and V252G were capable to proliferate without any cytokine (Fig. 4.6). The fold induction of their proliferation was calculated with non-stimulated gp130 wt set to 1. Cells expressing the mutants gp130 C172S and D215G showed a 3-fold induction of proliferation compared to non-stimulated Ba/F3-gp130 cells expressing gp130 wt. Furthermore, cells expressing the mutant gp130 V252G showed a 5-fold induction of cytokine independent proliferation. As expected, the mutations V189G and Y190G in gp130 were not sufficient to drive a cytokine independent proliferation.

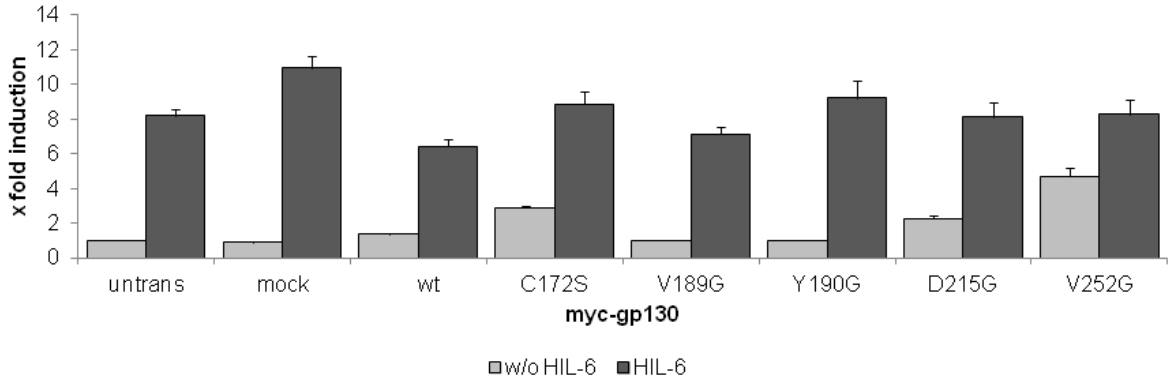

Figure 4.6: Proliferation of Ba/F3-gp130 cells expressing myc-tagged gp130 variants. Cells were stably transduced with myc-tagged gp130 wt, and the gp130 mutants C172S, V189G, Y190G, D215G and V252G. $5x10^3$ cells7well were seeded in a 96-well plate and proliferation was analyzed 72 h later using a MTT assay. Cells grew with or without Hyper-IL-6 (10 ng/ml).

To determine the surface expression, parental Ba/F3 cells were transduced with expression constructs for myc-tagged gp130 mutants and analyzed via flow cytometry. Cells were stained using the anti-gp130 antibody B-P4. Ba/F3-gp130 cells served as an internal positive control (data not shown). All gp130 variants were present at the cell surface of Ba/F3 cells (Fig. 4.7).

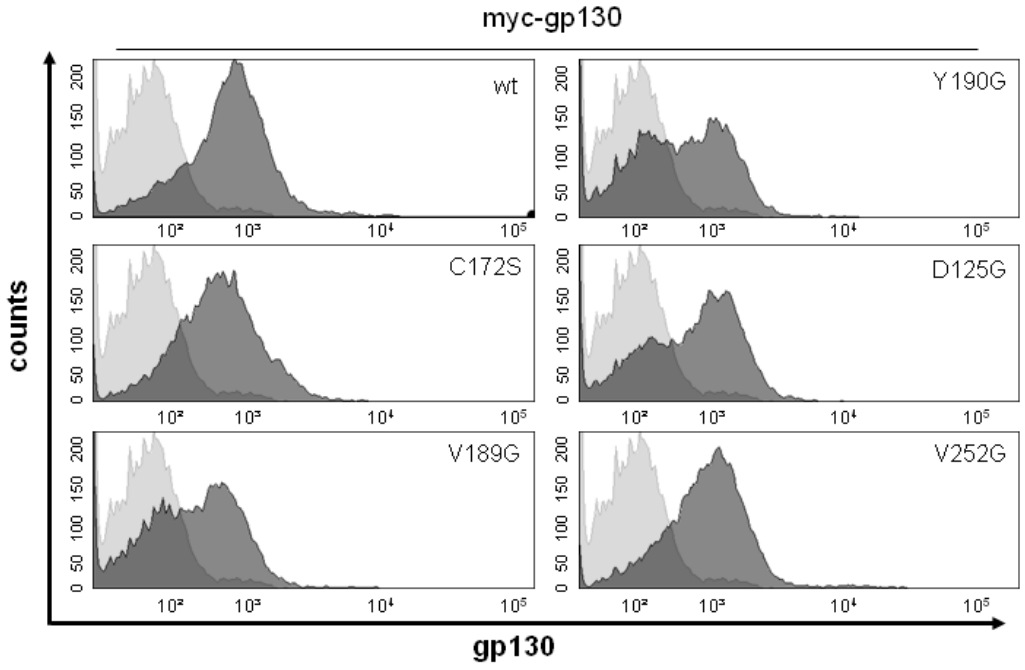

Figure 4.7: Surface expression of the myc-tagged gp130 variants on Ba/F3 cells measured by flow cytometry. Stably transduced Ba/F3 cells were analyzed for the surface expression of myc-tagged gp130 mutants. $1x10^6$ cells were stained with B-P4 (mouse-anti-gp130) antibody as primary and anti-mouse-DyLight 649 as secondary antibody. Light grey: parental Ba/F3 cells. Dark grey: Ba/F3 cells stably transduced with the myc-tagged gp130 variants.

The proliferation of Ba/F3-gp130 cells was in correlation with STAT3 phosphorylation (Fig. 4.8). To analyze the cytokine independent activation of Ba/F3-gp130 cells expressing the myc-tagged gp130

mutants, cells were starved in serum free medium. The mutations C172S, D215G and V252G led to a cytokine independent phosphorylation of STAT3 (Fig. 4.8 B). In contrast, Ba/F3-gp130 cells transduced with myc-tagged gp130 wt, V189G and Y190G showed no phosphorylation of STAT3. Stimulation with Hyper-IL-6 or the expression of a constitutive active variant, namely gp130 ΔYY, led to the activation and a robust phosphorylation of STAT3 (Fig. 4.8 A, B). Expression of the myc-tagged gp130 variants was verified using an anti-gp130 antibody. Due to the low expression levels of endogenous gp130 no interference was detectable.

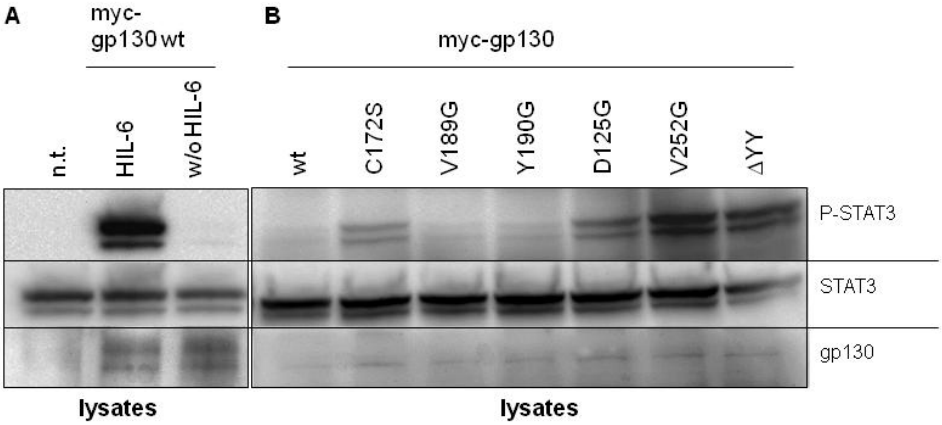

Figure 4.8: Analysis of STAT3 phosphorylation in Ba/F3-gp130 cells expressing myc-tagged gp130 variants. Ba/F3-gp130 cells were stably transduced and selected with puromycin. $5x10^6$ cells were seeded in a 6-well plate and starved for 4 h in SFM. Ba/F3-gp130 cells transduced with myc-tagged gp130 wt were stimulated for 10 min with Hyper-IL-6 (HIL-6, 10 ng/ml), which served as positive control. Cell lysates were analyzed for phosphorylated (P-) STAT3, STAT3 and gp130 by Western blot. (A) Western blot analysis of non-transduced (n.t.) Ba/F3-gp130 cells and HIL-6 stimulated and non-stimulated Ba/F3-gp130 cells expressing myc-tagged gp130 wt. (B) Western blot analysis of Ba/F3-gp130 cells stably transduced with myc-tagged gp130 wt and the myc-tagged gp130 mutants C172S, V189G, Y190G, D215G and V252G.

To exclude an unspecific proliferative effect of the transduced Ba/F3-gp130 cells, they were treated with the pan JAK inhibitor Pyridone 6 (P6). The cytokine independent proliferation of Ba/F3-gp130 cells expressing myc-tagged gp130 C172S, D215G and V252G could be inhibited with P6, indicating their dependence on Janus kinases (Fig. 4.9).

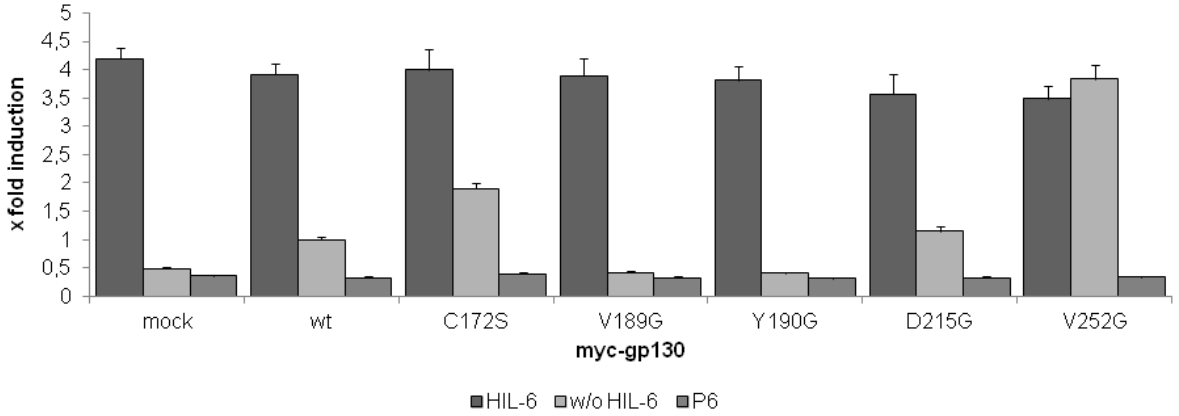

Figure 4.9: Inhibition of gp130 dependent proliferation by the JAK inhibitor Pyridone 6 (P6). $5x10^3$ cells/well were seeded in a 96-well plate and grew with or without Hyper-IL-6 (HIL-6, 10 ng/ml). Stably transduced Ba/F3-gp130 cells expressing myc-tagged gp130 wt, C172S, V189G, Y190G, D215G and V252G were treated with 500 nM of P6 as well as HIL6 and proliferation was analyzed 72 h later using a MTT assay.

Recently, it has been shown that the antibody B-P4, which binds to an epitope at domain D4 of gp130, can inhibit the proliferation of Ba/F3-gp130 cells expressing the constitutive active variant myc-gp130 ΔYY (132, 133). The anti-gp130 antibody B-P4 has been described to specifically inhibit IL-11 and, depending on the cells investigated, IL-6 responses (134–136). To examine if the antibody B-P4 is capable to inhibit the proliferation of Ba/F3-gp130 cells expressing the myc-tagged gp130 mutants, we analyzed the proliferation of these cells in the presence of B-P4. The antibody B-P4 was able to reduce, but could not completely abolish the proliferation of Hyper-IL-6 treated cells, as shown by Sommer *et al.*. Proliferation of cells expressing the point mutants gp130 C172S and D215G was low in the absence of the cytokine, compared to cells expressing the mutant gp130 V252G. However, the activity of all of them was reduced due to the B-P4 treatment (Fig. 4.10). Highly proliferative cells, expressing the mutants gp130 V252G or gp130 ΔYY responded best to the inhibitory potential of B-P4. Their proliferation was reduced to 80% and 50%, respectively.

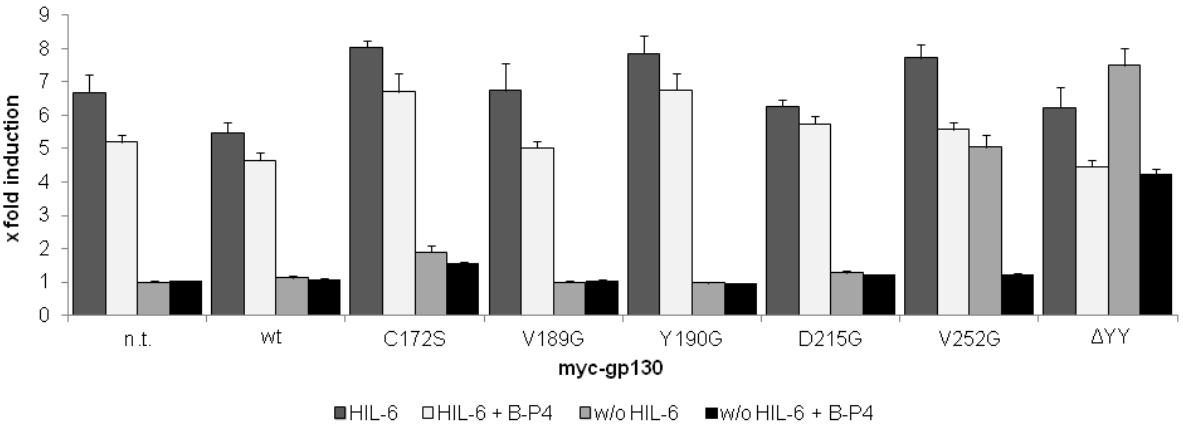

Figure 4.10: Proliferation of Ba/F3-gp130 cells expressing myc-gp130 variants is reduced by the anti-gp130 antibody B-P4. $5x10^3$ cells/well were seeded in a 96-well plate and grew with or without Hyper-IL-6 (HIL-6, 10 ng/ml). Stable transduced Ba/F3-gp130 cells were treated with 1 µg/ml of the anti-gp130 antibody B-P4 and proliferation was analyzed 72 h later using a MTT assay. n.t.: non transduced.

To exclude unspecific side effects of this antibody a different anti-gp130 antibody, which binds to an epitope at the C-terminus of gp130 (C-20) was used to examine the proliferation of transduced Ba/F3-gp130 cells. Proliferation of cells expressing myc-tagged gp130 wt as well as myc-tagged gp130 mutants was not affected by this antibody, indicating a specific blocking effect by the anti-gp130 antibody B-P4 (Fig. 4.11).

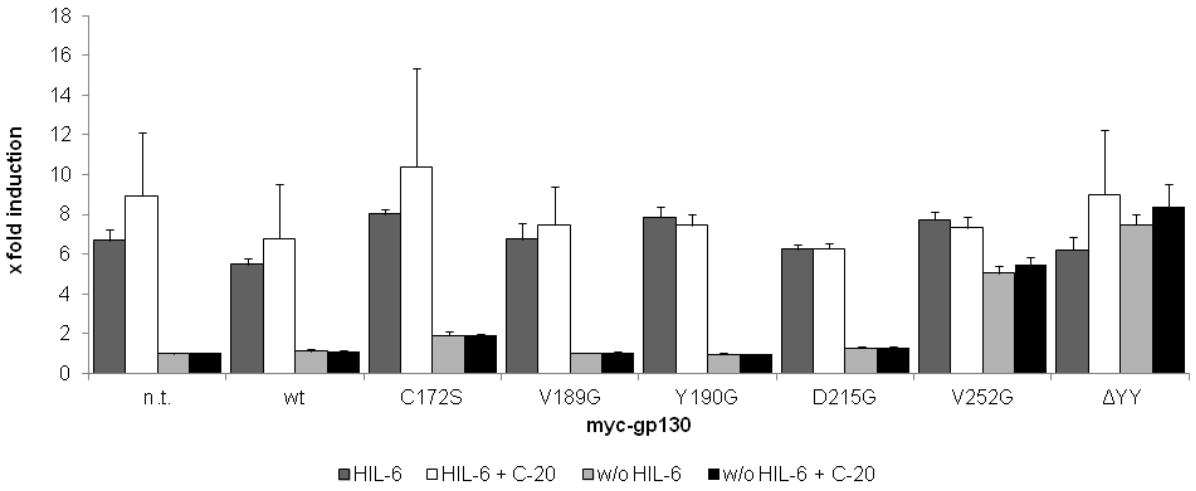

Figure 4.11: Proliferation of Ba/F3-gp130 cells expressing myc-tagged gp130 variants is reduced by the anti-gp130 antibody C-20. $5x10^3$ cells/well were seeded in a 96-well plate and grew with or without Hyper-IL-6 (HIL-6, 10 ng/ml). Stable transduced Ba/F3-gp130 cells were treated with 1 µg/ml of the anti-gp130 antibody C-20 and proliferation was analyzed 72 h later using a MTT assay. n.t.: non transduced. n.t.: non transduced.

The observations made in Ba/F3-gp130 cells confirm the results obtained from experiments with transfected HepG2 and HEK 293T cells. In each experimental setting, the expression of the mutants gp130 C172S, D215G and V252G resulted in a cytokine independent activation. This was shown by detection of phosphorylated STAT3 in lysates of transfected HEK 293T cells and stably transduced Ba/F3-gp130 cells by Western blot analysis. In addition, transfection of the gp130 mutants in HepG2 cells led to an activation of a STAT3 reporter. In this context, we furthermore observed an IL-6 independent proliferation of Ba/F3-gp130 cells, stably transduced with the mutants gp130 C172S, D215G and V252G.

4.1.3 Mutations in the constitutive active deletion mutant gp130 ΔYY

The active deletion mutant gp130 delY186–Y190 (ΔYY) was found in human liver adenoma (Fig. 4.12 A) (121). We took advantage of a previously generated eYFP-fusion of the gp130 ΔYY mutant, which showed cytokine independent activity *in vitro* (133). In order to test the impact of the described amino acid residues C172, D215 and V252 on the constitutive activation of the gp130 ΔYY mutant, we generated the same amino acid substitutions as in wildtype. Additionally, previous work in our laboratory has shown that deletion of the first N-terminal domain (ΔD1) of the gp130 ΔYY mutant completely abrogates the downstream signaling in HEK 293T cells and Ba/F3 cells (133). The gp130 crystal structure (PDB code: 1P9M) revealed that the first five N-terminal residues of domain D1 are implicated in IL-6 binding (Fig. 4.12 B). We hypothesized that domain D1, including the N-terminal residues E1 to P5, contacts the neighboring gp130 and is implicated in activation of gp130 ΔYY. Therefore, we deleted the first five

N-terminal amino acids (ΔN1-5) and analyzed the impact of the deletion on the activation of the gp130 ΔYY mutant.

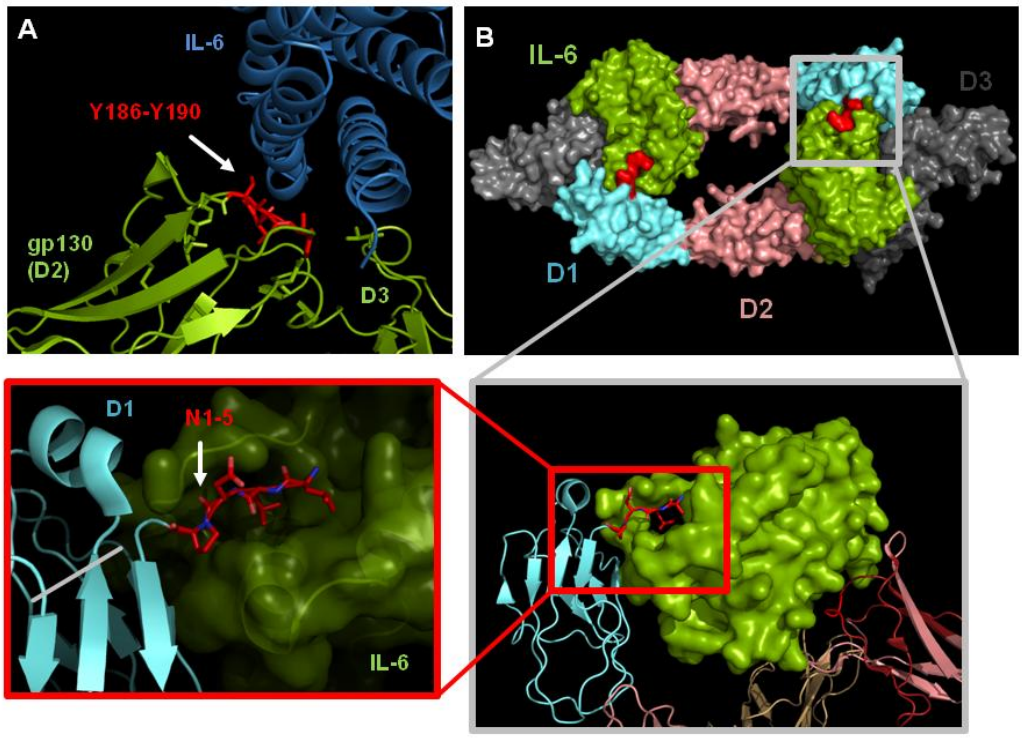

Figure 4.12: Crystal structure of gp130 wt depicting the deletion mutants ΔYY and ΔN1-5. (A) Contact area of IL-6 to domain D2 of gp130, where the residues Y186 to Y190 are deleted in the mutant gp130 ΔYY (marked in red). (B) Top view of the hexameric assembly of (gp130 D1-D3/IL-6/sIL-6R)$_2$ with zoom into the N-terminal portion (red) of domain D1 of gp130 and its contact side to IL-6 (green). The N-terminal tail (N1-5) of domain D1 intercalates into a groove of IL-6.

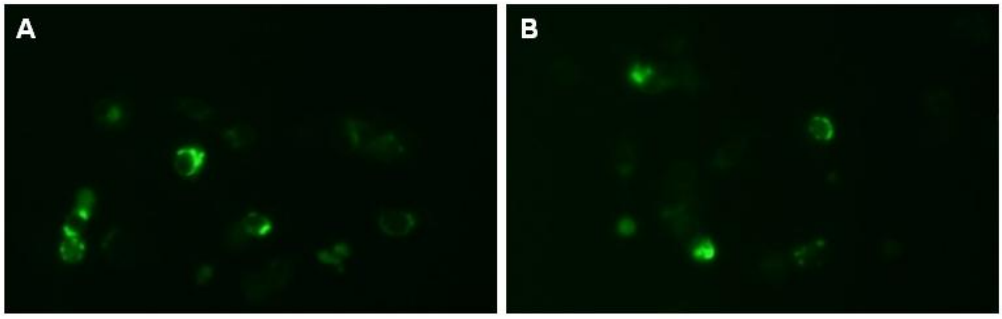

Figure 4.13: Microscopic analysis of HepG2 cells transfected with the expression constructs of eYFP-tagged gp130 ΔYY and ΔYYΔN1-5. The mutants (A) gp130 ΔYY and (B) gp130 ΔYYΔN1-5 were expressed in HepG2 cells. 24 h post transfection cells were analyzed by fluorescence microscopy.

EYFP-tagged constructs of the gp130 ΔYY variants were expressed in HepG2 cells as shown by fluorescence microscopy (Fig. 4.13). The analysis of cytokine independent activation of STAT3 in HEK 293T cells showed no difference between the mutants gp130 ΔYY, gp130 ΔYY D215G and gp130 ΔYY V252G. Cells expressing the mutant gp130 ΔYY C172S showed slightly reduced phosphorylation of STAT3. As expected, cells expressing the mutant gp130 ΔYYΔD1 showed impaired STAT3

phosphorylation, whereas the mutant gp130 ΔYYΔN1-5 was still active, but showed reduced STAT3 phosphorylation as compared to the gp130 ΔYY mutant. Equal expression of all gp130 variants were detected in Western blot analysis of cell lysates using anti-GFP antibody (Fig. 4.14).

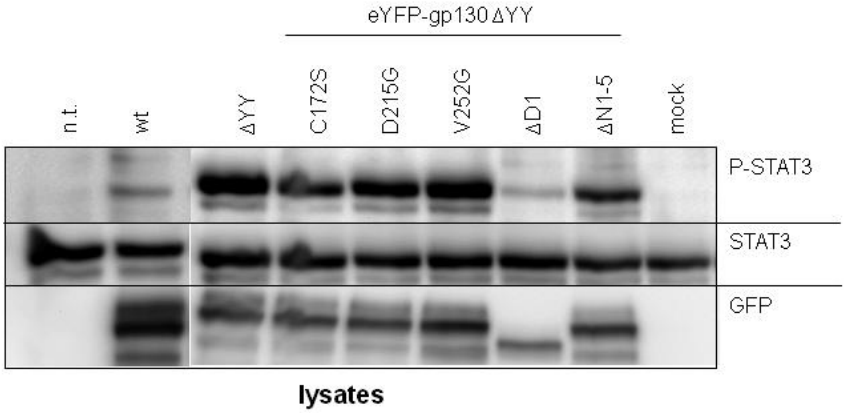

Figure 4.14: Analysis of STAT3 phosphorylation variants in cells expressing eYFP-tagged gp130 variants. HEK 293T cells were transfected with eYFP-tagged gp130 ΔYY mutants. 24 h post transfection, cells were starved for 4 h in SFM. HEK 293T cells transfected with gp130 wt were stimulated 10 min with Hyper-IL-6 (10 ng/ml) as a positive control. Cell lysates were analyzed for phosphorylation of STAT3 (P-STAT3), STAT3 and GFP in Western blot. Anti-GFP antibody is crossreactive for the YFP-tag. n.t.: non transfected.

In order to analyze STAT3 activation in a hepatic cell background, HepG2 cells were co-transfected with a STAT3 responsive promoter construct (SIEM-Luc) expressing firefly luciferase, a vector encoding renilla luciferase along with the indicated expression constructs for the gp130 ΔYY mutants. The ratio between firefly and renilla luciferase was calculated and the fold induction was given with non-stimulated gp130 wt set to 1. Cells transfected with gp130 wt were stimulated for 4 h with Hyper-IL-6. Cells expressing the mutant gp130 ΔYY showed 17-fold induction, which is twofold more than Hyper-IL-6 stimulated cells expressing gp130 wt. All gp130 ΔYY point mutations led to the activation of the STAT3 responsive promoter (Fig. 4.15 A). Interestingly, cells expressing the point mutants gp130 ΔYY D215G and V252G had a 1.5-fold elevated activation of STAT3 compared to cells expressing the mutants gp130 ΔYY. Surprisingly, the mutant gp130 ΔYY C172S displayed as well cytokine independent activation but showed one-third reduced activation compared to the gp130 ΔYY mutant. The deletion of domain D1 (ΔD1) in the gp130 deletion mutant ΔYY led to impaired luciferase activity due to no significant activation of the STAT3 responsive promoter. Deletion of the N-terminal portion (ΔN1-5) of the gp130 ΔYY mutant led to 10-fold induction of luciferase activity, which was reduced to 50% compared the mutant gp130 ΔYY. Equal expression of the gp130 variants was confirmed by anti-GFP Western blot (Fig. 4.15 B).

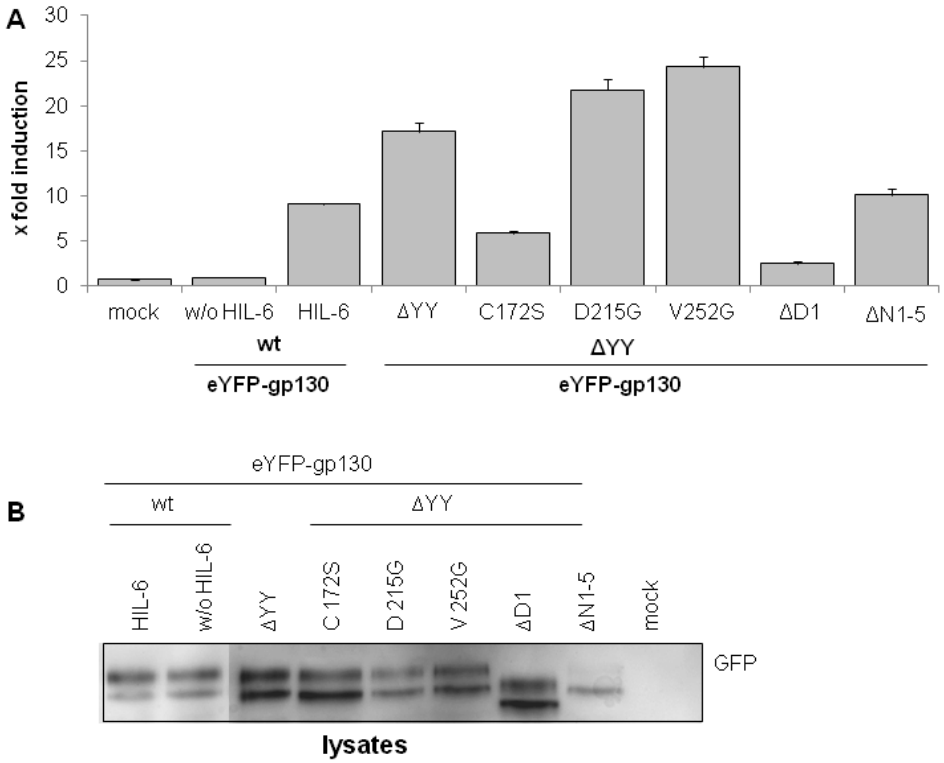

Figure 4.15: STAT3 reporter assay of gp130 ΔYY variants. HepG2 cells were transiently co-transfected with STAT3 responsive promoter construct expressing firefly luciferase (SIEM-Luc), renilla luciferase (TK-RL) and eYFP-tagged gp130 ΔYY mutants. Cells were starved over night in SFM and cells expressing gp130 wt were stimulated 4 h with Hyper-IL-6 (HIL-6, 10 ng/ml). (A) Luciferase activity was detected using the Dual-Glo® assay (Promega). (B) Cell lysates were analyzed for the expression of eYFP-tagged gp130 mutants by Western blot, using anti-GFP antibody. The upper band represents the complex glycosylated form and the lower band the high-mannose form of gp130. The anti-GFP antibody is crossreactive for the YFP-tag.

In order to find out if the gp130 ΔYY variants can drive STAT3 dependent proliferation, myc-tagged mutants were stably transduced into Ba/F3-gp130, as described for the gp130 wt variants. Cells expressing myc-tagged gp130 ΔYY displayed Hyper-IL-6 independent proliferation, which resulted in a 9-fold induction of proliferation compared to non stimulated Ba/F3-gp130 cells (Fig. 4.16). The deletion of domain D1 in the mutant gp130 ΔYYΔD1 led to an impaired proliferation in cytokine free medium, whereas the mutant gp130 ΔYYΔN1-5 showed cytokine independent proliferation, which was reduced by 50% compared to cells expressing the mutant gp130 ΔYY. This result stands in line with the results from the STAT3 reporter assay, indicating that the mutant gp130 ΔYYΔN1-5 is less active than the mutant gp130 ΔYY.

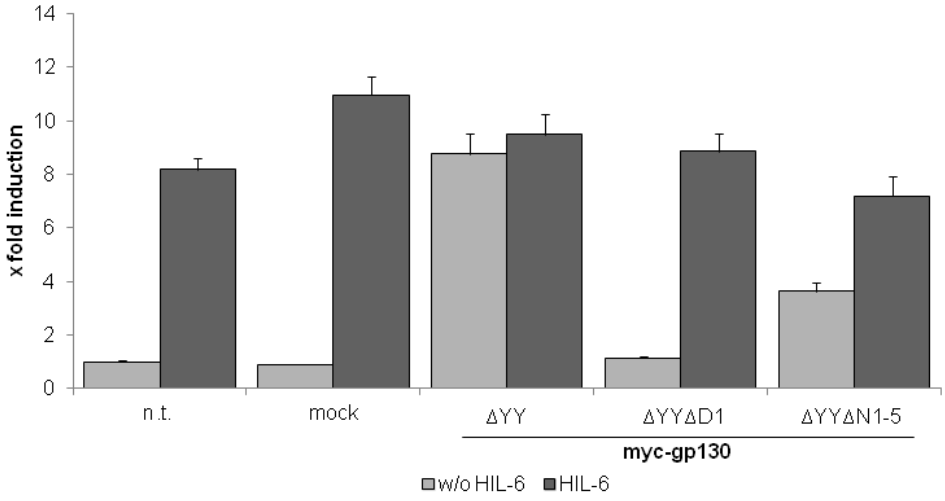

Figure 4.16: Proliferation of Ba/F3-gp130 cells expressing myc-tagged gp130 ΔYY variants. 5x10^3 cells/well were seeded in a 96-well plate, grew with or without 10 ng/ml of Hyper-IL-6 (HIL-6) and proliferation was analyzed 72 h later using a MTT assay. Cell were stably transduced with myc-tagged gp130 ΔYY, ΔYYΔD1 and ΔYYΔN1-5 selected with puromycin. n.t.: non transfected.

Furthermore, proliferation assays were conducted with Ba/F3-gp130 cells expressing the myc-tagged gp130 mutants ΔYY C172S, D215G and V252G. The latter mutants drove cytokine independent proliferation, whereas cells expressing the mutant gp130 ΔYY C172S showed an impaired proliferative potential. To exclude an unspecific proliferation of the stably transduced Ba/F3-gp130 cells, they were treated with the pan JAK inhibitor Pyridone 6 (P6). The cytokine independent proliferation of cells expressing the mutants gp130 ΔYY C172S, D215G, V252G and ΔN1-5 were inhibited with P6, indicating their dependence on Janus kinases (Fig. 4.17).

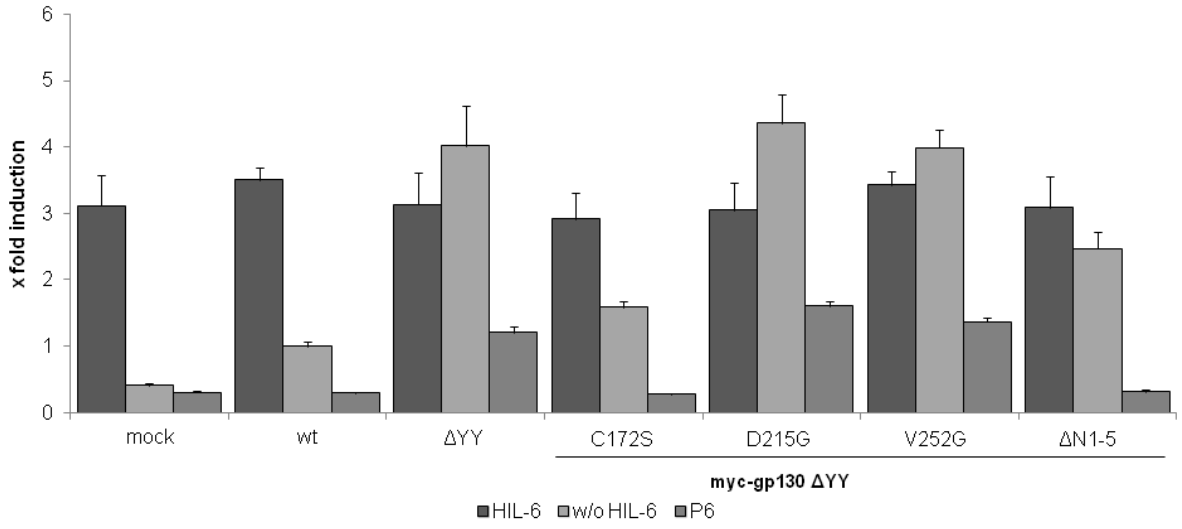

Figure 4.17: Inhibition of gp130 ΔYY dependent proliferation with the JAK inhibitor Pyridone 6 (P6). 5x10^3 cells/ well were seeded in a 96-well plate and grew with or without Hyper-IL-6 (10 ng/ml). Stably transduced Ba/F3-gp130 cells were treated with 500 nM of P6 and proliferation was analyzed 72 h later using a MTT assay.

In addition, analysis of STAT3 phosphorylation in Ba/F3-gp130 cells transduced with the myc-tagged gp130 mutants showed activation of all gp130 ΔYY mutants except for the mutant gp130 ΔYYΔD1 (Fig. 4.18 A, B). As seen in the STAT3 reporter assay and in the proliferation study, cells expressing the mutants gp130 ΔYY C172S and gp130 ΔYYΔN1-5 showed reduced STAT3 phosphorylation, indicating that the mutations interfere with constitutive activation of gp130 ΔYY deletion mutant. The expression of the myc-tagged gp130 constructs was confirmed in Western blot analysis using an anti-gp130 antibody. Due to the low expression levels of endogenous gp130 no interference was detectable (Fig. 4.18).

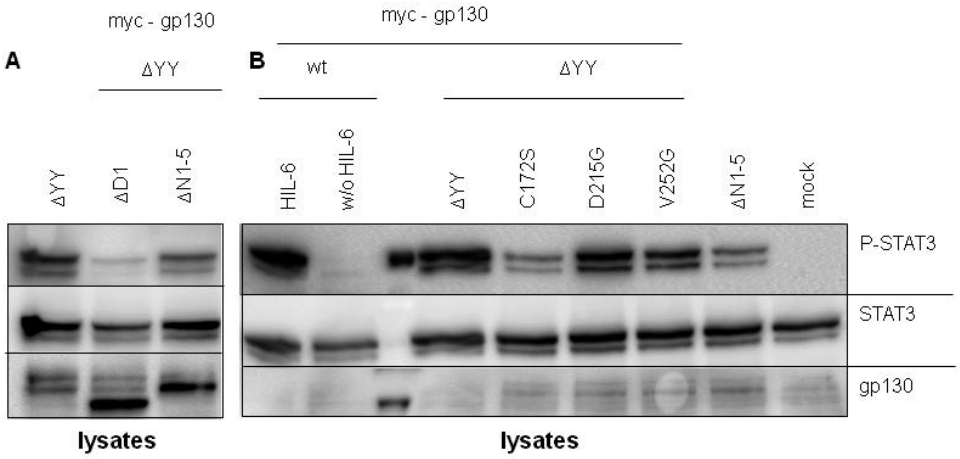

Figure 4.18: Analysis of STAT3 phosphorylation in Ba/F3-gp130 cells expressing myc-tagged gp130 variants. Ba/F3-gp130 cells were stably transduced and selected with puromycin. $5x10^6$ cells were seeded in a 6-well plate and starved for 4 h in SFM. Ba/F3-gp130 cells expressing myc-tagged gp130 wt were stimulated for 10 min with Hyper-IL-6 (HIL-6, 10 ng/ml). Cell lysates were analyzed for phosphorylated (P-) STAT3, STAT3 and gp130 (C-20) by Western blot analysis. (A) Western blot analysis of Ba/F3-gp130 cells stably transduced with the mutants gp130 ΔYY, ΔYYΔD1 and ΔYYΔN1-5. (B) Western blot analysis of Ba/F3-gp130 cells stably transduced with gp130 wt and ΔYY mutants.

Parental Ba/F3 cells were stably transduced with myc-tagged gp130 contructs and analyzed via flow cytometry to figure out, if the mutanted gp130 proteins are present at the cell surface. Cells were stained using the anti-gp130 antibody B-P4. Expression was compared to parental Ba/F3 cells. Cells stably transduced with GFP were used as control. For all gp130 mutants no cell surface staining was detectable. Therefore, cells were permeabilized and stained for intracellular gp130 using the antibody B-P4 as well. All cells transduced with the expression constructs of the myc-tagged gp130 variants showed detectable expression, indicating that the gp130 ΔYY variants were localized intracellularly (Fig. 4.19). These results correlate with an impaired maturation of the gp130 ΔYY mutant, which has been recently found in our laboratory (data not shown).

These data imply that the activity of the constitutive active deletion mutant gp130 ΔYY can be reduced. We discovered that the mutation C172S as well as the deletion of the N-terminal portion (ΔN1-5) interferes with the autonomous activity of STAT3 in the mutant gp130 ΔYY. These two mutants showed reduced phosphorylation of STAT3 in Western blot analysis of transfected HEK 293T cells. Furthermore, expression of gp130 ΔYY C172S and gp130 ΔYYΔN1-5 led to impaired luciferase activity in a STAT3 reporter assay in HepG2 cells. Retroviral transduction of Ba/F3-gp130 cells with these gp130 ΔYY

mutants resulted in a ligand independent but reduced proliferation as well as diminished STAT3 activation.

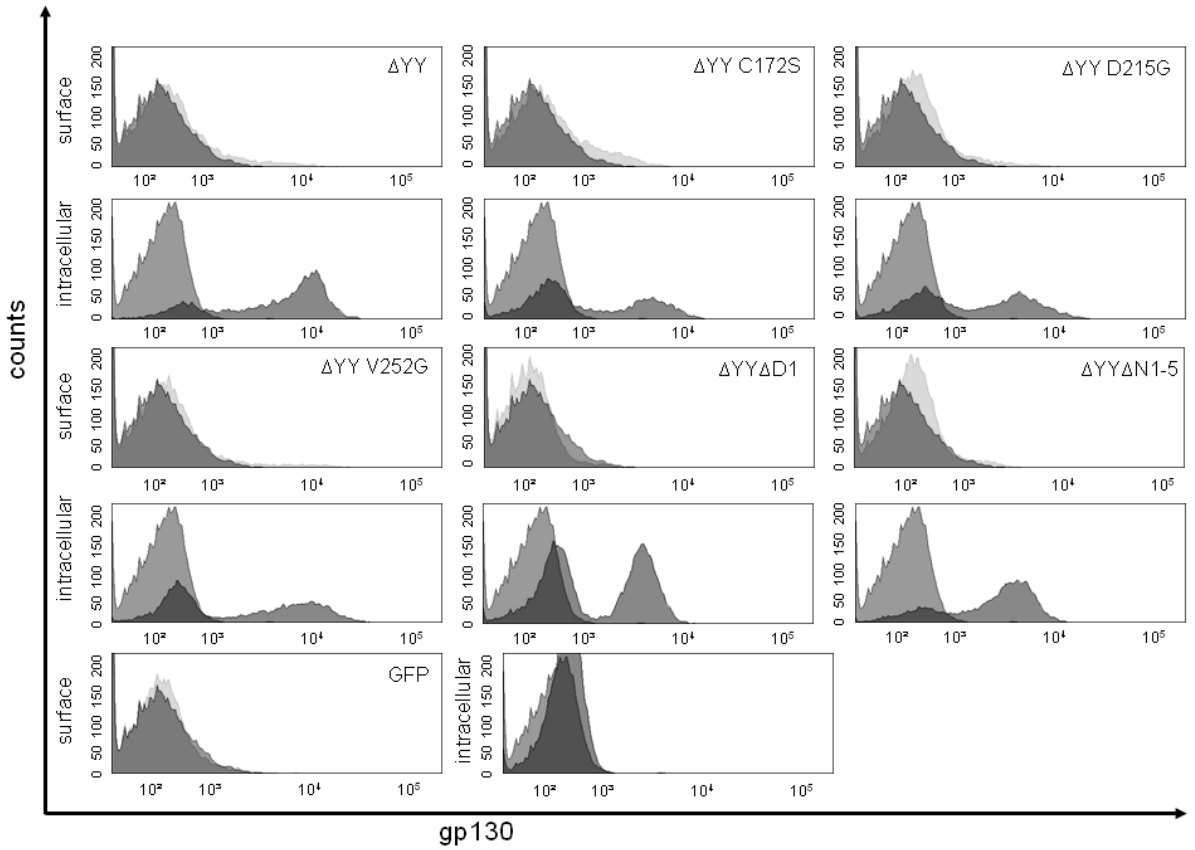

Figure 4.19: Flow cytometric analysis of the surface and the intracelluar expression of myc-tagged gp130 ΔYY variants. Ba/F3 cells were stably transduced with myc-tagged gp130 ΔYY variants. For detection of gp130 expression the mouse-anti-gp130-antibody (B-P4) was used as primary and anti-mouse-DyLight 649 as secondary antibody. Light grey: parental Ba/F3 cells. Dark grey: Ba/F3 cells stably transduced with myc-tagged gp130 ΔYY variants.

4.1.4 SOCS3 mediated suppression of STAT3 signaling

IL-6 induces the expression of SOCS3, which binds to JAK2 and is therefore a potent inhibitor of gp130 induced STAT3 phosphorylation. Constitutive active variants of gp130 such as the mutant gp130 ΔYY lead to the upregulation of SOCS3 (121). Nevertheless, STAT3 activation persists. In order to find out if constitutive active gp130 mutants are insensitive to SOCS3 inhibition, we co-expressed a myc-tagged SOCS3 construct with the gp130 point mutants C172S, D215G and V252G in HEK 293T cells. Overexpression of SOCS3 resulted in a strong reduction of phosphorylated STAT3 in cells expressing the constitutive active mutants gp130 C172S, D215G and V252D as well as in cells expressing the mutant gp130 ΔYY (Fig. 4.20). An equal expression of all gp130 constructs was confirmed by Western blot analysis of the cell lysates using an anti-GFP antibody.

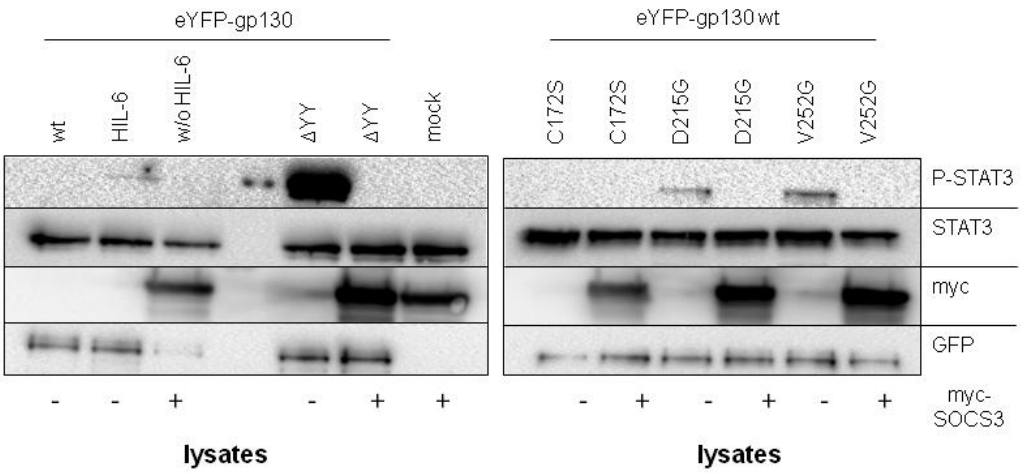

Figure 4.20: Inhibition of STAT3 phosphorylation due to SOCS3 overexpression in cells expressing the gp130 variants. HEK 293T cells were co-transfected with a myc-tagged SOCS3 construct and eYFP-tagged gp130 constructs. Cells transfected with gp130 wt were stimulated for 10 min with Hyper-IL-6 (HIL-6, 10 ng/ml). 24 h post transfection, cell lysates were analyzed for phosphorylated (P-) STAT3, STAT3, myc and GFP in Western blot. The anti-GFP antibody is crossreactive for the YFP-tag.

4.1.5 Dimerization studies of gp130 mutants

Previously, it has been shown by Tenhumberg *et al.*, that gp130 wt exists as preformed but inactive homodimer (12). The interaction was analyzed by co-immunoprecipitation and confirmed by FRET analysis. They postulated that ligand binding can enhance the dimer formation and is required for signal transduction. Rebouissou *et al.* showed that the gp130 ΔYY mutant can associate with itself and gp130 wt, resulting in dimer formation (121). To analyze dimerization of the generated point mutants the expression constructs of eYFP- and myc-tagged gp130 variants were co-expressed in HEK 293T cells. Cells were starved to analyze phosphorylation of STAT3 and gp130. Cells expressing gp130 wt were non-stimulated. The differently tagged proteins were co-immunoprecipitated, either using an anti-myc or an anti-GFP antibody. Western blot analysis of precipitated proteins indicated that the expressed mutants displayed a constitutive dimerization. Precipitation of eYFP-tagged gp130 variants with anti-GFP antibody resulted in the detection of myc-tagged gp130 variants and *vice versa*. Co-expression of the constitutive active eYFP- and myc- tagged mutants gp130 C172S, D215G and V252G resulted in receptor phosphorylation, which cannot be seen in gp130 wt (Fig. 4.21 B). These results were confirmed by Western blot analysis of cell lysates for phosphorylated STAT3 (Fig. 4.21 A). These data indicate a constitutive dimerization of gp130 variants irrespective of their activation status.

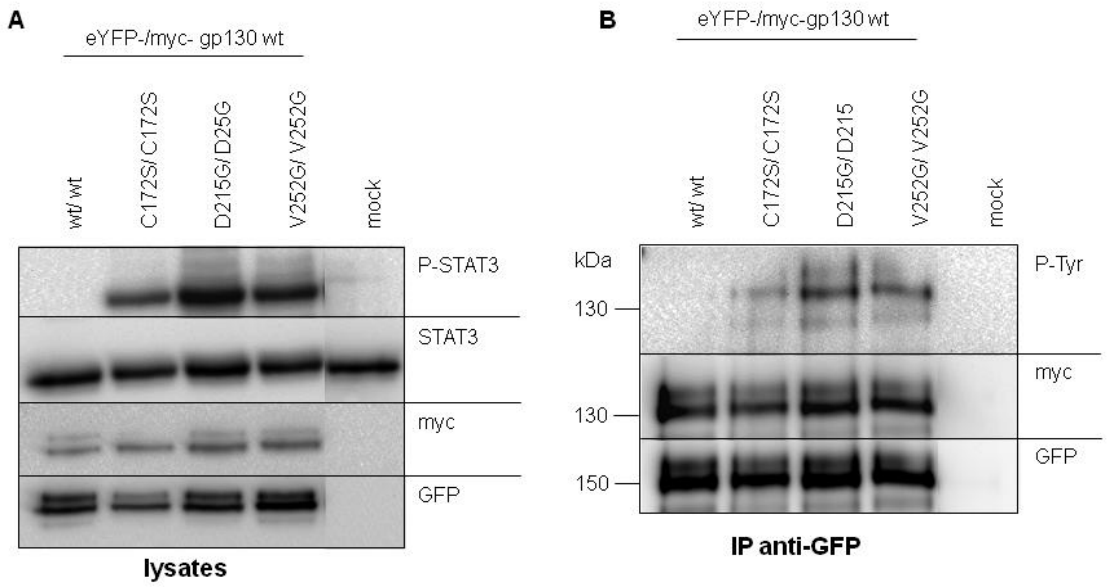

Figure 4.21: Immunprecipitation and detection of dimer formation of gp130 wt and the gp130 variants C172S, D215G and V252G. HEK 293T cells were co-transfected with the expression constructs of eYFP- and myc-tagged gp130 variants. Cells were starved 24 h post transfection and lysed. Cell lysates were used for Western blot analysis and for immunoprecipitation (IP). (A) Western blot analysis of lysates for phosphorylated (P-) STAT3, STAT3, myc and GFP. (B) Co-immunoprecipitation of cell lysates and detection of phosphorylated tyrosine (P-Tyr), GFP and myc using specific antibodies. The anti-GFP antibody is crossreactive for the YFP-tag.

It has been shown that the deletion of domain D1 in gp130 wt led to unresponsiveness to IL-6/sIL-6R stimulation and impaired the constitutive active signaling of the mutant gp130 ΔYY (16, 133). Therefore we postulate that domain D1 is potentially implicated in dimerization of gp130. To investigate gp130 dimerization, eYFP- and myc–tagged mutants gp130 ΔYY, ΔYYΔD1 and ΔYYΔN1-5 were co-expressed in HEK 293T cells and were analyzed for receptor phosphorylation under starving conditions. Formation of dimers was analyzed by precipitation of eYFP- and myc-tagged gp130 variants using an anti-GFP or an anti-myc antibody as described before. Immunoprecipitates were analyzed by Western blot using an antibody against the corresponding tag. Homodimer formation between the mutants gp130 ΔYY, ΔD1 and ΔN1-5 was detectable, concluding that the mutant gp130 ΔYY can dimerize irrespective of domain D1 and of its activation status (Fig. 4.22 A). Moreover, the mutant gp130 ΔYY was able to form heterodimers with the mutant gp130 ΔYYΔD1. The mutant gp130 ΔYYΔN1-5 as well as the mutant gp130 ΔYYΔD1 can be co-precipitated with the mutant gp130 ΔYYΔN1-5 (Fig. 4.22 B).

To sum up, gp130 ΔYY variants dimerize, when expressed in HEK 293T cells, irrespective of their activation status.

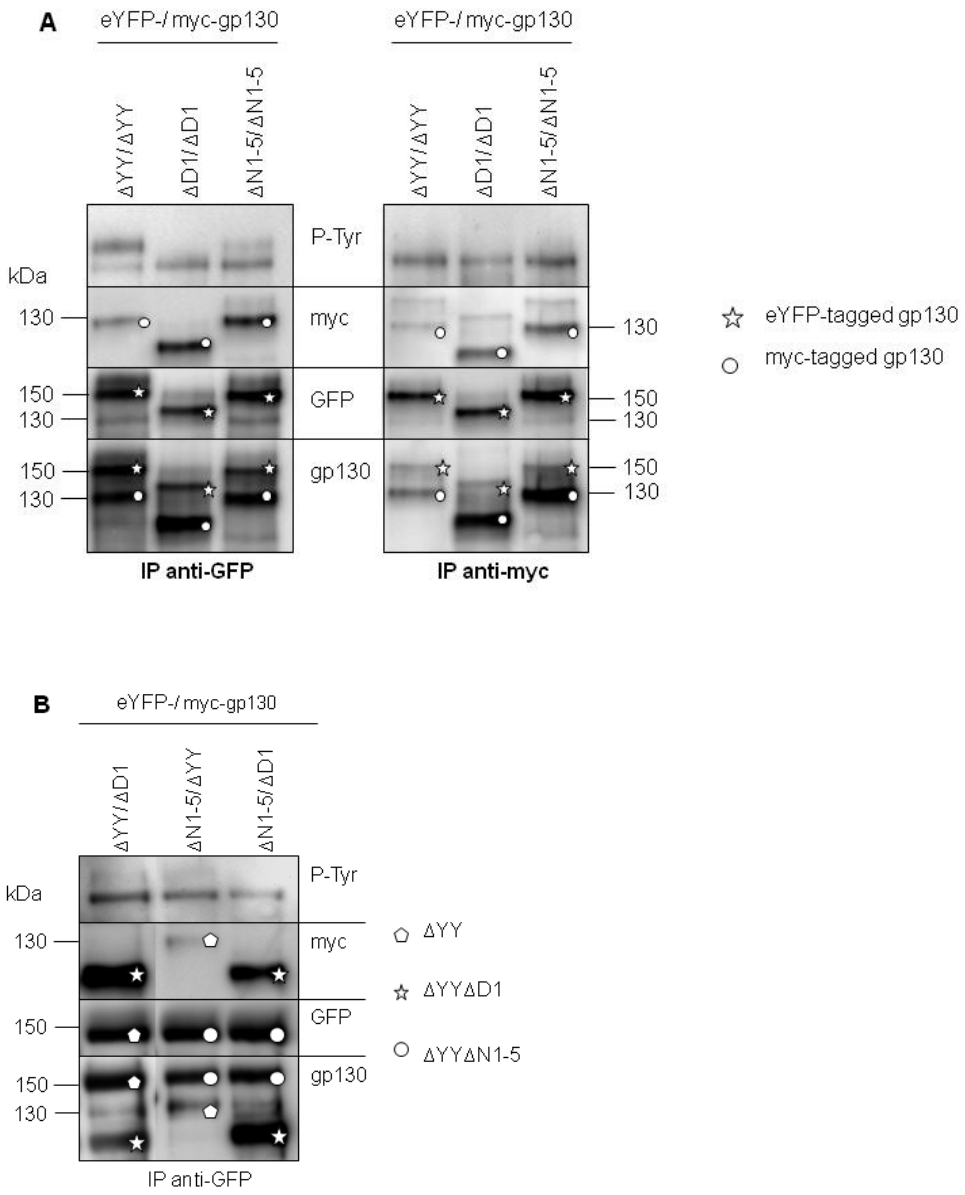

Figure 4.22: Immunoprecipitation and detection of dimer formation of the variants gp130 ΔYY, ΔYYΔD1 and ΔYYΔN1-5. HEK 293T cells were co-transfected with the expression constructs of eYFP- and myc tagged gp130 variants. Cells were starved and lysed 24 h post transfection. Cell lysates were analyzed using an anti-myc or an anti-GFP antibody for immunoprecipitiation. Precipitated proteins were analyzed for phosphorylated tyrosine residues in gp130 and for the corresponding tag in Western blot. Size of eYFP-tagged proteins is increased by 26 kDa. The anti-GFP antibody is crossreactive for the YFP-tag. (A) Homodimers of eYFP- and myc-tagged gp130 ΔYY, ΔYYΔD1 and ΔYYΔN1-5 mutants. (B) Heterodimers of eYFP- and myc-tagged gp130 ΔYY, ΔYYΔD1 and ΔYYΔN1-5 mutants. First named construct is eYFP-tagged and second named is myc-tagged.

4.2 Leucin-gp130: a ligand independent constitutive active gp130 variant

Previously an artificial constitutive active version of gp130 has been generated in our laboratory (see introduction point 1.8) (123). Replacing the extracellular domain with the leucine-zipper motif of c-Jun, which is stabilized by a cysteine bridge, led to the activation of an IL-6 like mediated signaling. This construct was named Leucin-gp130 (L-gp130). Expression of L-gp130 in HepG2 cells resulted in cytokine independent activation and phosphorylation of STAT3 and to ligand independent proliferation of stably transduced Ba/F3-gp130 cells. L-gp130 was able to suppress spontaneous differentiation of murine embryonic stem cells in the absence of LIF. In order to analyze physiological consequences of constitutive gp130 activation, we generated transgenic mice expressing a doxycycline inducible construct of L-gp130.

4.2.1 Inducible expression of L-gp130 via the Tet-system

Permanent activation of gp130 signaling is supposed to be cancerogenic due to constitutive active STAT3 (see introduction point 1.4). For this reason, the expression of L-gp130 was temporally restricted by using the inducible tetracycline sensitive (Tet-) system. The transgene L-gp130 as well as the reporter gene firefly luciferase were expressed under control of a tetracyline responsive promoter element (TRE). The Kozak sequence for L-gp130 was optimized to achieve optimal expression. Activation of TRE can be achieved via either the tetracycline transactivator protein (tTA) or the reverse tetracycline transactivator protein (rtTA) in dependence of doxycycline (Dox). These transactivator proteins were expressed by Tet-vectors. A selective expression of tTA or rtTA can be achieved by the use of a tissue specific promoter. (see introduction point 1.10 and Fig. 4.23 for further details)

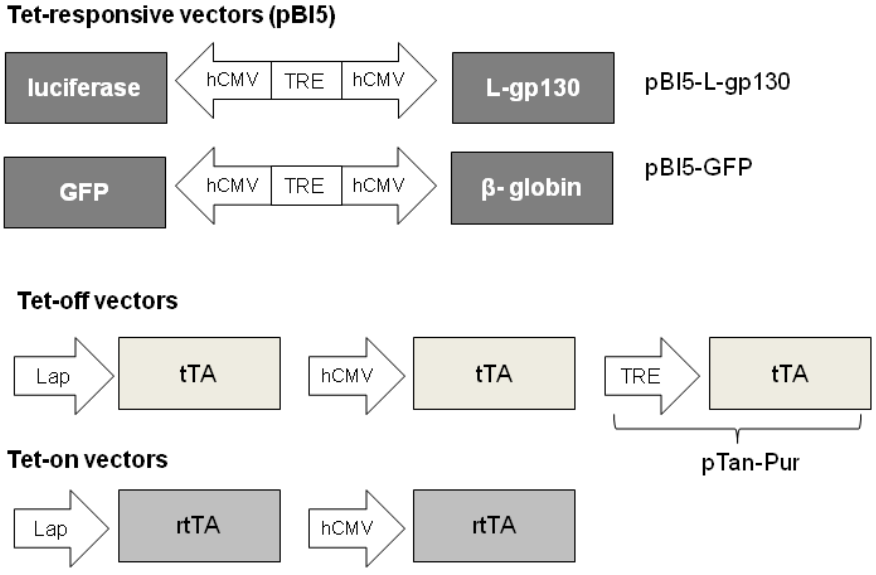

Figure 4.23: Used Tet-vectors in this study. The vector pBI5 contains a tetracycline responsive promoter element (TRE) fused to two differgently orientated hCMV minimal promoters. Tet-off vectors express the tetracycline transactivator protein (tTA) and Tet-on vectors express the reverse tetracycline transactivator protein (rtTA) under control of a specific promoter, respectively. A liver specific promoter (Lap) and a general promoter (hCMV) were used to induce the expression of tTA and rtTA.

4.2.2 Expression of pBI5-L-gp130

To test the inducible expression via the transactivator tTA, the human hepatoma cell line HepG2 was transfected with equal amounts of pBI5-GFP, expressing GFP under control of a tetracyline responsive promoter element (TRE) and the Tet-off vector pTan-Pur, which expresses the tetracycline transactivator (tTA). Transfected cells were analyzed by fluorescence microscopy using pcDNA3.1-eGFP transfected cells as control. Single transfection with pBI5-GFP did not drive the expression of the transgene GFP, which was observed by co-ransfection with the Tet-off vector pTan-Pur. The GFP expression of cells transfected with pBI5-GFP and pTan-Pur was comparable to cells transfected with pcDNA3.1-eGFP (Fig. 4.24).

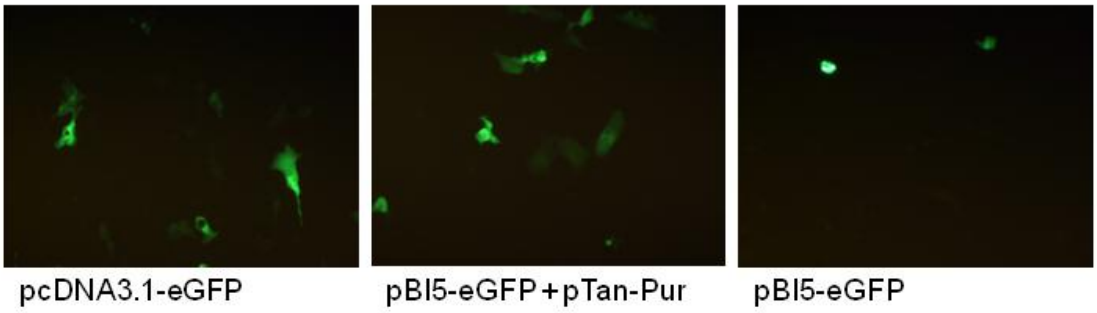

Figure 4.24: **Analysis of inducible GFP expression using the Tet-off sytsem.** Fluorescence microscopy images of HepG2 cells transfected with pcDNA3.1-eGFP and pBI5-GFP +/- the Tet-off vector pTan-Pur.

Furthermore, HepG2 cells were co-transfected with pBI5-L-gp130, which express L-gp130 as well as firefly luciferase and the Tet-off vector pTan-Pur. Luciferase levels were determined via luciferase assay. The co-expression resulted in high levels of L-gp130 already 24 h post transfection, analyzed in Western blot using anti-gp130 antibody (Fig. 4.25 A). Single transfection of HepG2 cells with the construct pBI5-L-gp130 did not lead to transgene expression. The expression of L-gp130 was completely inhibited by the addition of doxycycline (Dox). Analysis of the luciferase activity of transfected cells by luciferase assay confirmed this data. The dose response curve revealed that 1 μg/ml Dox was sufficient to suppress luciferase activity (Fig. 4.25 B). In time course experiments we identified the earliest time point of doxycycline dependent inhibition of luciferase expression. As shown in Fig. 4.25 C the luciferase activity decreased 3 h after Dox was supplemented and reached a minimum level after 6 h. A complete inhibition of luciferase activity and L-gp130 expression was achieved after 24 h. This experimental setting was chosen for futher experiments.

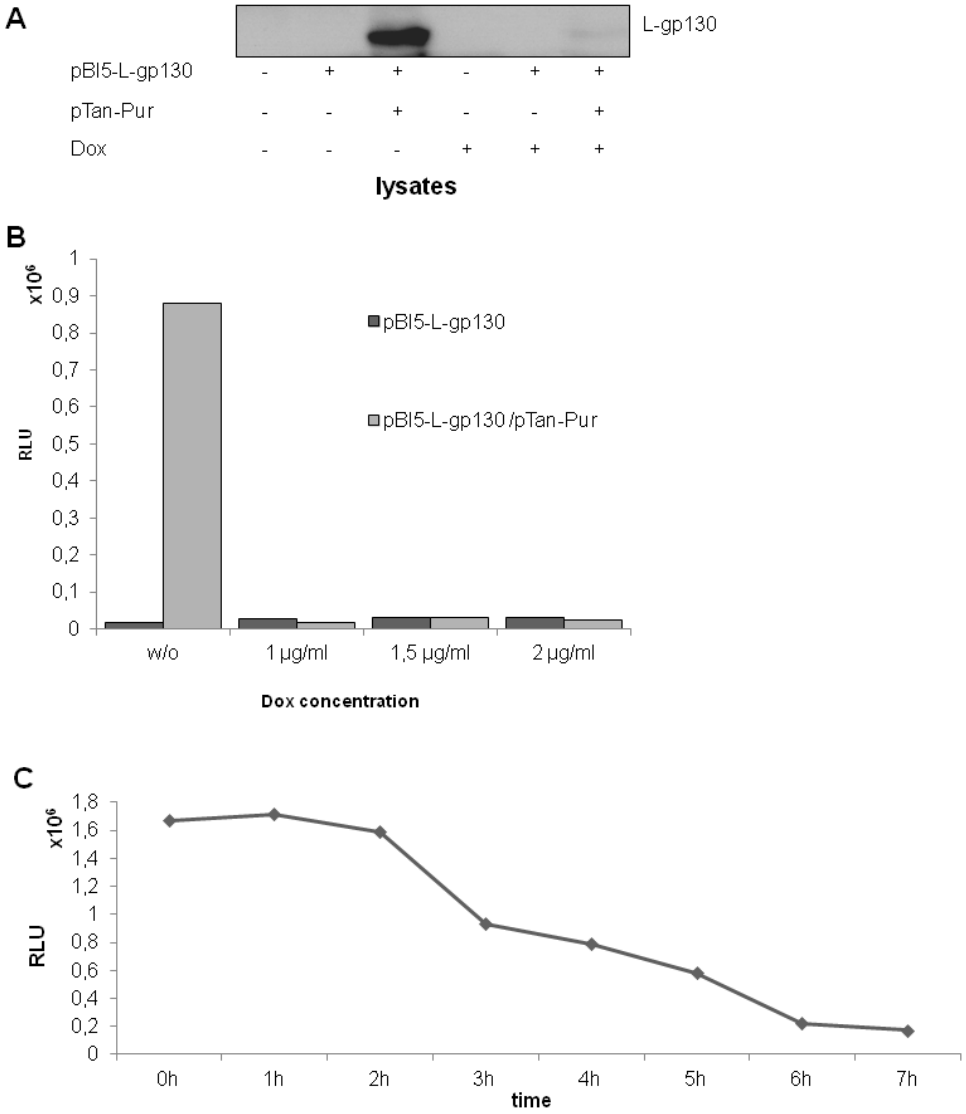

Figure 4.25: Analysis of inducible expression of pBI5-L-gp130. (A) HepG2 cells were transfected with pBI5-L-gp130 +/- pTan-Pur and treated with doxycycline (1 µg/ml) 24 h post transfection. Cell lysates were analyzed with anti-gp130 antibody (C-20) in Western blot. (B) HepG2 cells were transfected with pBI5-L-gp130 +/- pTan-Pur and treated with different concentrations of doxycycline (Dox, 1 - 2 µg/ml, n=1) 24 h post transfection. Cell lysates were analyzed using luciferase assay (Promega). (C) Time course of doxycycline dependent inhibition of gene expression. HepG2 cells were transfected with pBI5-L-gp130 and pTan-Pur (n=1), 1 µg/ml doxycycline was added 24 h post transfection and luciferase activity was analyzed hourly. RLU: relative light units.

Different Tet-off and Tet-on vectors expressing tTA or rtTA under control of either a general (hCMV) or a liver specific (Lap) promoter were co-transfected with pBI5-L-gp130 in HepG2 cells. Cells were treated with doxycycline immediately following transfection and lysed 24 h post transfection. Lysates were analyzed for luciferase activity by luciferase assay and for L-gp130 expression by Western blot using an anti-gp130 antibody. To analyse the fold induction, cells transfected with pBI5-L-gp130 and without Dox treatment were set to 1. Cells expressing pBI5-L-gp130 and hCMV-tTA, showed 40-fold induction of luciferase activity in the absence of Dox, which was downregulated to 4-fold induction by the addition of

Dox. A similar expression of luciferase was detected in cells expressing pBI5-L-gp130 and Lap-tTA. The co-transfection of HepG2 cells with pBI5-L-gp130 and the Tet-on vector hCMV-rtTA led to a significant induction of luciferase in the presence of Dox. Doxycycline treatment induced the expression of luciferase in cells expressing pBI5-L-gp130 and hCMV-rtTA up to 20-fold compared to non treated cells. Cells co-transfected with pBI5-L-gp130 and Lap-rtTA showed twofold higher luciferase activity compared to cells expressing rtTA under control of the hCMV promoter. Comparing both Tet-on vectors, the liver specific Lap promoter caused a stronger expression of luciferase compared to the hCMV promoter, which can be explained by the usage of a hepatocellular cell line. These data were confirmed by Western blot analysis of L-gp130 expression. Both Tet-systems worked properly, since tTA as well as rtTA were sufficient to induce expression of L-gp130 and firefly luciferase (Fig. 4.26).

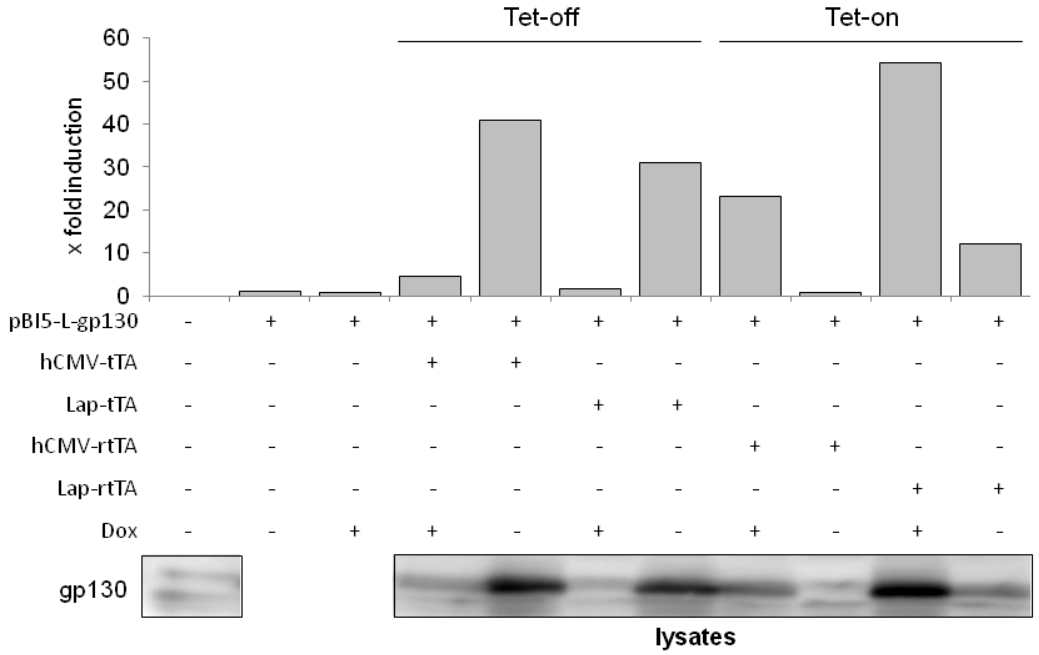

Figure 4.26: Analysis of luciferase activity and L-gp130 expression using different Tet-vectors. HepG2 cells were co-transfected with the indicated plasmids and were lysed 24 h after Dox treatment. Lysates were analyzed for luciferase activity using luciferase assay (Promega). Cells transfected with pBI5-L-gp130 without doxycycline treatment was set to 1. Lysates were analyzed for L-gp130 expression in Western blot using anti-gp130 antibody (C-20).

4.2.3 SOCS3 mediated suppression of L-gp130

It has been already shown that IL-6 signaling leads to upregulation of SOCS3. This potent inhibitor binds to phosphorylated Y^{759} in the intracellular domain of gp130 and down regulates the signaling of activated gp130. We threfore addressed the question, if the constitutive active L-gp130 is sensitive to SOCS3 mediated suppression. A myc-tagged SOCS3 construct was co-transfected with different L-gp130 expression contructs in HepG2 cells. The construct p409-L-gp130 as well as the inducible construct of pBI5-L-gp130 in combination with pTan-Pur were analyzed. In both cases the expression of L-gp130 led to a ligand independent activation and phosphorylation of STAT3. Mock transfected cells were stimulated with Hyper-IL-6 as a positive control. Overexpression of SOCS3 diminished L-gp130 mediated STAT3

phosphorylation. Interestingly, STAT3 phosphorylation induced by Hyper-IL-6 stimulation of mock transfected cells was not inhibited by SOCS3 overexpression (Fig. 4.27).

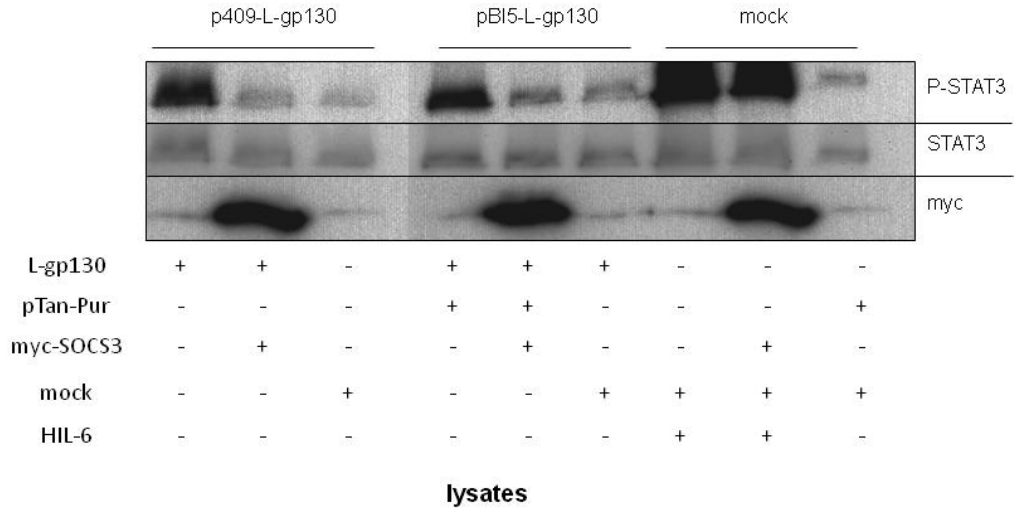

Figure 4.27: Overexpression of SOCS3 led to inhibition of L-gp130 mediated STAT3 phosphorylation. HepG2 cells were co-transfected with L-gp130 constructs and myc-tagged SOCS3 as indicated. Mock transfected cells served as control and were stimulated with Hyper-IL-6 (HIL-6, 10 ng/ml). Cells were lysed 24 h post transfection and lysates were analyzed for phosphorylated (P-) STAT3, STAT3 and myc in Western blot.

4.2.4 Generation of L-gp130^{+} transgenic mice

In parallel to the validation of the Tet-system *in vitro*, the construct pBI5-L-gp130 was linearized and used to generate transgenic mice via pronucleii injection (IBF, Heidelberg). The offspring were analyzed via genotyping PCR and Southern blot (Fig. 4.28 B, C). Genomic insertion was determined by specific primers for the *luciferase* gene and for the *L-gp130* gene. Primers used for PCR analysis bind to the sequence of leucine zipper and the intracellular domain of L-gp130. Primers used to generate a probe for Southern blot analysis amplified the full length *L-gp130* gene (Fig. 4.28 A).

Altogether, eleven strains were tested positive for the insertion of the L-gp130 gene as well as for the *luciferase* gene. The transgene was not expressed in the absence of the transactivator and therefore the L-gp130^{+} transgenic (tg) mice developed no visible phenotype. The fertility of some strains was either restricted to few generations or the generation size was limited. Finally, five strains (L2, L5, L9, L11 and L12) were selected to generate mEF cells and double transgenic (dtg) animals in order to analyze the inducible expression of L-gp130.

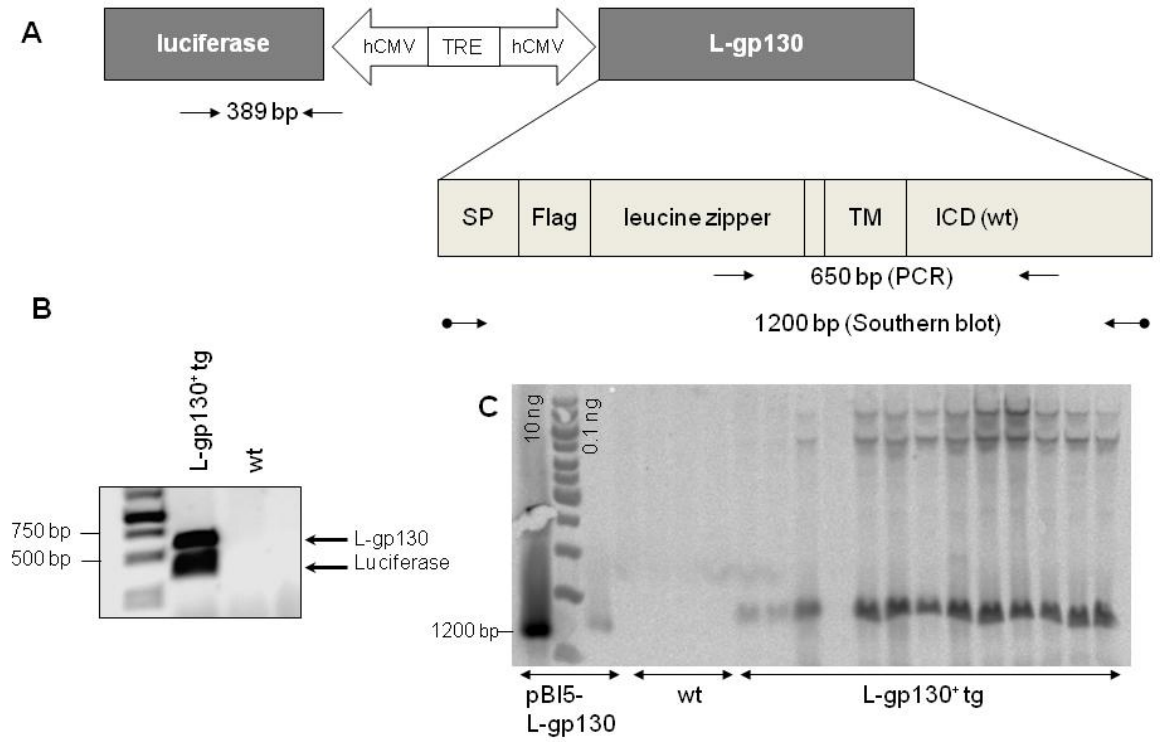

Figure 4.28: Genotyping of L-gp130$^+$ tg mice. Tail DNA was analyzed for insertion of the transgene firefly luciferase and L-gp130. (A) Primer design and expected PCR product size. (B) Genotyping PCR of L-gp130$^+$ tg and wildtype (wt) mice. (C) Southern blot analysis of L-gp130$^+$ tg and wildtyp (wt) mice. Plasmid DNA (10 ng/ 0.1 ng) of pBI5-L-gp130 was used as internal control.

4.2.5 Generation of L-gp130$^+$ murine embryonic fibroblasts

In order to analyze the inducible expression of L-gp130 and firefly luciferase *ex vivo*, we generated murine embryonic fibroblasts (mEF cells) from L-gp130$^+$ tg mice. Therefore, heterozygous L-gp130$^+$ tg mice were bred with wildtype mice and the embryos were sacrificed at day E13. Resulting mEF cells were either negative or positive for L-gp130 insertion revealed by genotyping PCR. MEF cells were generated from four L-gp130$^+$ strains (L2, L5, L9 and L11) to analyze differences in genomic integration among these strains. Different mEF cell clones (one embryo = one cell clone) of the corresponding L-gp130$^+$ tg mouse were tested for their background luciferase activity. In the absence of the transactivator (tTA), no luciferase activity was detectable in L-gp130$^+$ mEF cells of L2, L5 and L9. Only L-gp130$^+$ mEF cells of L11 showed tTA independent background luciferase activity (Fig. 4.29 A). To activate transgene expression, L-gp130$^+$ mEF cells were retrovirally transduced with the transactivator tTA. Stable cell lines were generated by puromycin selection. MEF cells expressing L-gp130 and tTA were analyzed for luciferase activity via luciferase assay as well as for L-gp130 expression by Western blot using an anti-gp130 antibody. L-gp130$^+$/tTA$^+$ mEF cells generated from strain 2 (L2) and 5 (L5) showed a tTA dependent induction of luciferase activity as well as an expression of L-gp130 revealed by luciferase assay and Western Blot, respectively. L-gp130$^+$/tTA$^+$ mEF cells of L5 showed higher induction of luciferase activity compared to L-gp130$^+$/tTA$^+$ mEF cells of L2 (Fig. 4.27 B, C). The luciferase activity detected in L-gp130$^+$/tTA$^+$ mEF cells from L5 was diminished by doxycycline (1 µg/ml) highlighting the inducible gene expression (Fig. 4.27 D).

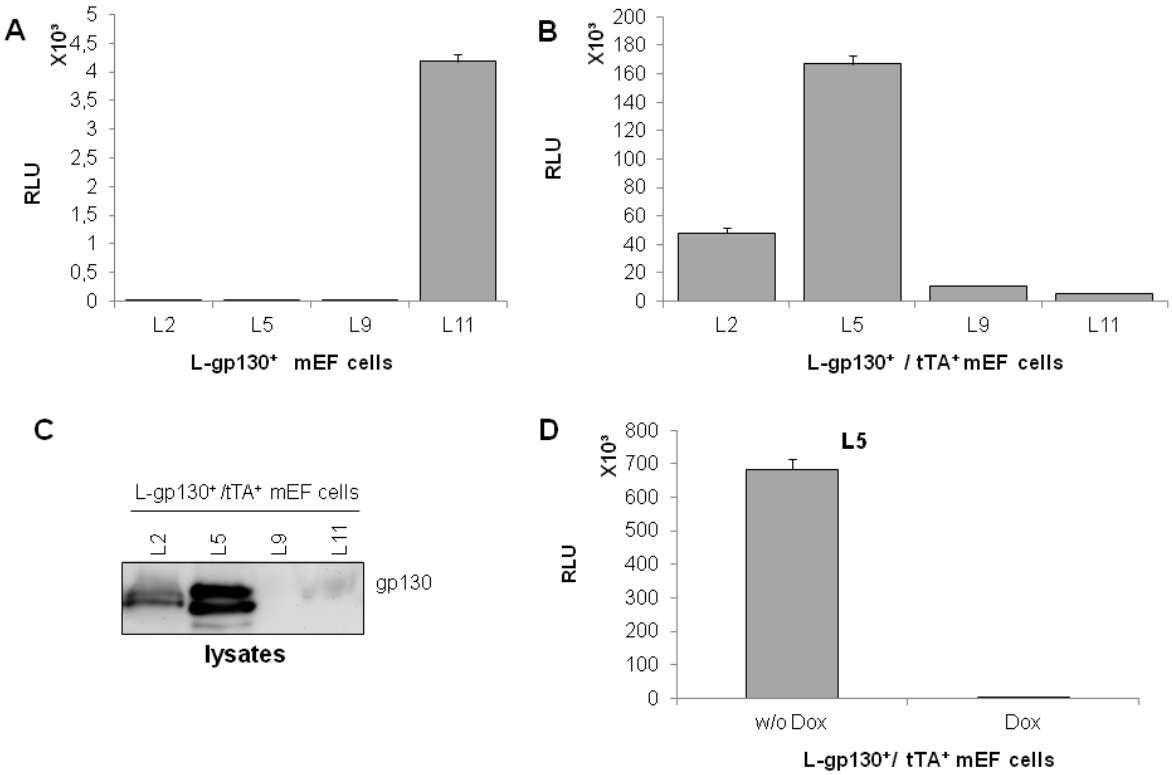

Figure 4.29: Expression of luciferase and L-gp130$^+$ in mEF cells. L-gp130$^+$ mEF cells were generated from L-gp130$^+$ tg mice of L2, L5, L9 and L11. (A) L-gp130$^+$ mEF cells were tested for background luciferase activity via luciferase assay (Promega). (B) Stably transduced L-gp130$^+$/tTA$^+$ mEF cells were analyzed for the expression of luciferase via luciferase assay (Promega). (C) Expression of L-gp130 in L-gp130$^+$/tTA$^+$ mEF cells was analyzed in Western blot using anti-gp130 antibody (C-20). (D) Analysis of luciferase activity following doxycycline treatment of L-gp130$^+$/tTA$^+$ mEF cells of L5 using luciferase assay (Promega). RLU: relative light units.

4.2.6 Generation of double transgenic mice to induce the expression of L-gp130

In order to achieve a tissue specific inducible expression of L-gp130 *in vivo*, transgenic mice were bred with different Tet-inducer strains. We used Lap-tTA$^+$ tg mice, expressing the transactivator tTA under the control of a liver specific promoter and hCMV-tTA$^+$ tg mice, which display an ubiquitous tTA expression (Fig. 4.30). All generated double transgenic (dtg) mice were bred heterozygous for their transgenes. The occurance of wt, tg and dtg mice were as expected according to Mendel's laws. We therefore expected 25% dtg mice.

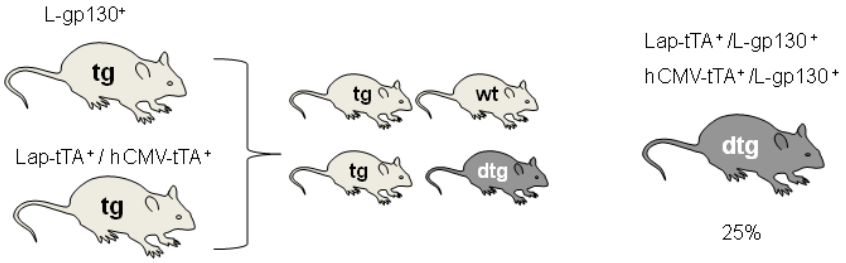

Figure 4.30: Generation of double transgenic mice. Mice heterozygous for L-gp130$^+$ or tTA$^+$ were bred to generate Lap-tTA$^+$/L-gp130$^+$ dtg mice or hCMV-tTA$^+$/L-gp130$^+$ dtg mice according to Mendel's law. Colors depicted in this scheme did not correlate with the hair color of the mice.

To suppress an early L-gp130 expression, breeding pairs were constantly kept on doxycycline supplemented nutrition (see methods). Four L-gp130$^+$ tg strains were used to generate double transgenic mice (Lap-tTA$^+$/L-gp130$^+$). We tested different conditions to induce transgene activation and analyzed the induction by measuring the luciferase activity in the liver. We varied the time point of doxycycline withdrawal (age of the mice) as well as the duration of induction (Fig. 4.31, Tab. 4-2). It has been shown that doxycycline persists in the body up to one week until it is eliminated via catabolic pathways, before causing a full and stable transgene expression (127).

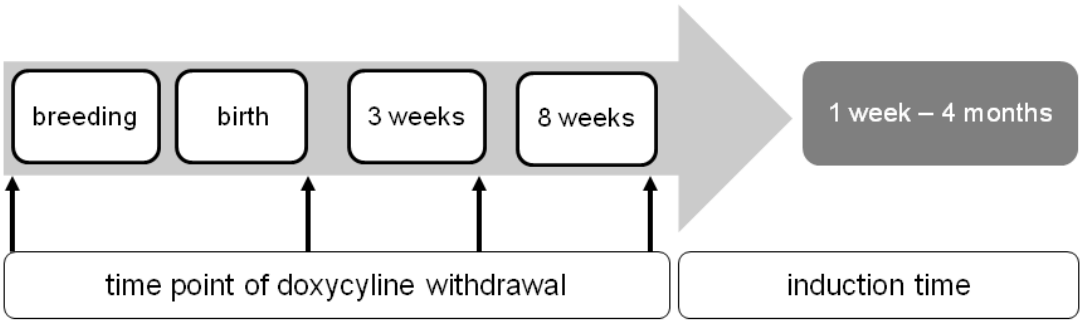

Figure 4.31: Scheme of doxycycline treatment and transgene induction time of double transgenic mice. Doxycycline was given in drinking water or food pellets. Either nutrion was not supplemented with doxycycline or was withdrawn at different age of the mice (see methods).

Table 4-2: Doxycycline treatment and induction time points of Lap-tTA$^+$/L-gp130$^+$ dtg mice.

Dox withdrawal (age of mice)	Induction time
8 weeks	3 weeks
	6.5 weeks (Fig. 4.32 B)
	16 weeks
3 weeks	1 week
	10 days (Fig. 4.32 C)
	4 weeks (Fig. 4.32 C)
	11 weeks
	14 weeks
2 weeks	16 weeks
Day 2	7 weeks
No Dox treatment	8 weeks

We analyzed livers of Lap-tTA$^+$/L-gp130$^+$ dtg mice for transgene expression. Both genders were used for all analyses. Liver samples were taken to analyze RNA, protein and luciferase expression. At no time point the expression of L-gp130 was detectable in the liver lysates of Lap-tTA$^+$/L-gp130$^+$ dtg mice by Western blot (data not shown). In accordance, no phosphorylated STAT3 was detectable (data not shown). The expression of the transactivator tTA was analyzed by Western blot of liver lysates, using antibodies specific for either VP16 or TetR. These antibodies failed to recognize their epitope, even in lysates of

cells, which show overexpressing of tTA (data not shown). The livers of Lap-tTA$^+$/L-gp130$^+$ dtg mice were tested for luciferase activity as well, due to the bidirectional expression of L-gp130 and firefly luciferase. L-gp130$^+$ tg mice were tested and a background luciferase activity was detectable in liver lysates of L-gp130$^+$ tg mice of strain 11 (L11) and 12 (L12), similar to what we detected in mEF cells (Fig. 4.32, Fig. 4.29 A). However, the level of luciferase was significantly lower comparing to published data.

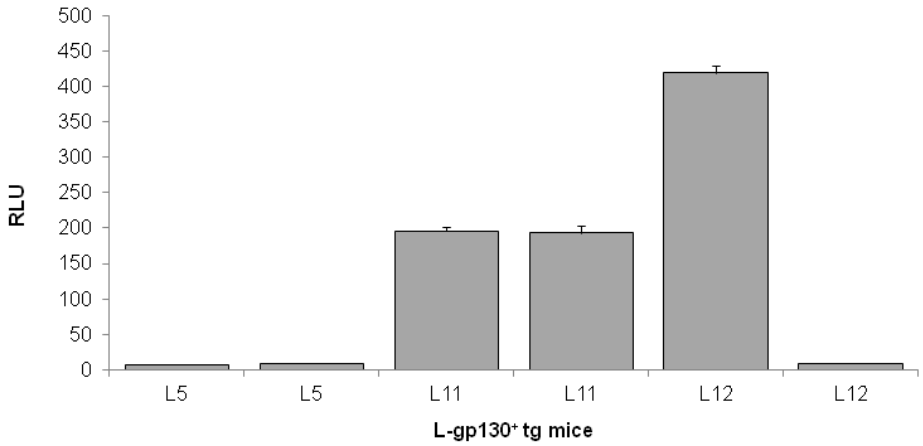

Figure 4.32: Analysis of luciferase activity in the liver of L-gp130$^+$ tg mice. Livers of L-gp130$^+$ tg mice (L5, L11, L12) were tested for background expression of firefly luciferase using luciferase assay (Promega). RLU: relative light units.

Wildtype mice showed no induction of luciferase expression in all experiments. No significant luciferase activity was detected in liver lysates of Lap-tTA$^+$/L-gp130$^+$ dtg mice compared to published data, although different parameters for transgene induction were analyzed (Tab. 4.2). Two experiments are depicted using Lap-tTA$^+$/L-gp130$^+$ dtg mice of strain 5 (L5) and 12 (L12) (Fig. 4.33 B, C). Nevertheless, a slightly increased luciferase expression was detected in Lap-tTA$^+$/L-gp130$^+$ dtg mice compared to L-gp130$^+$ tg mice and wildtype mice.

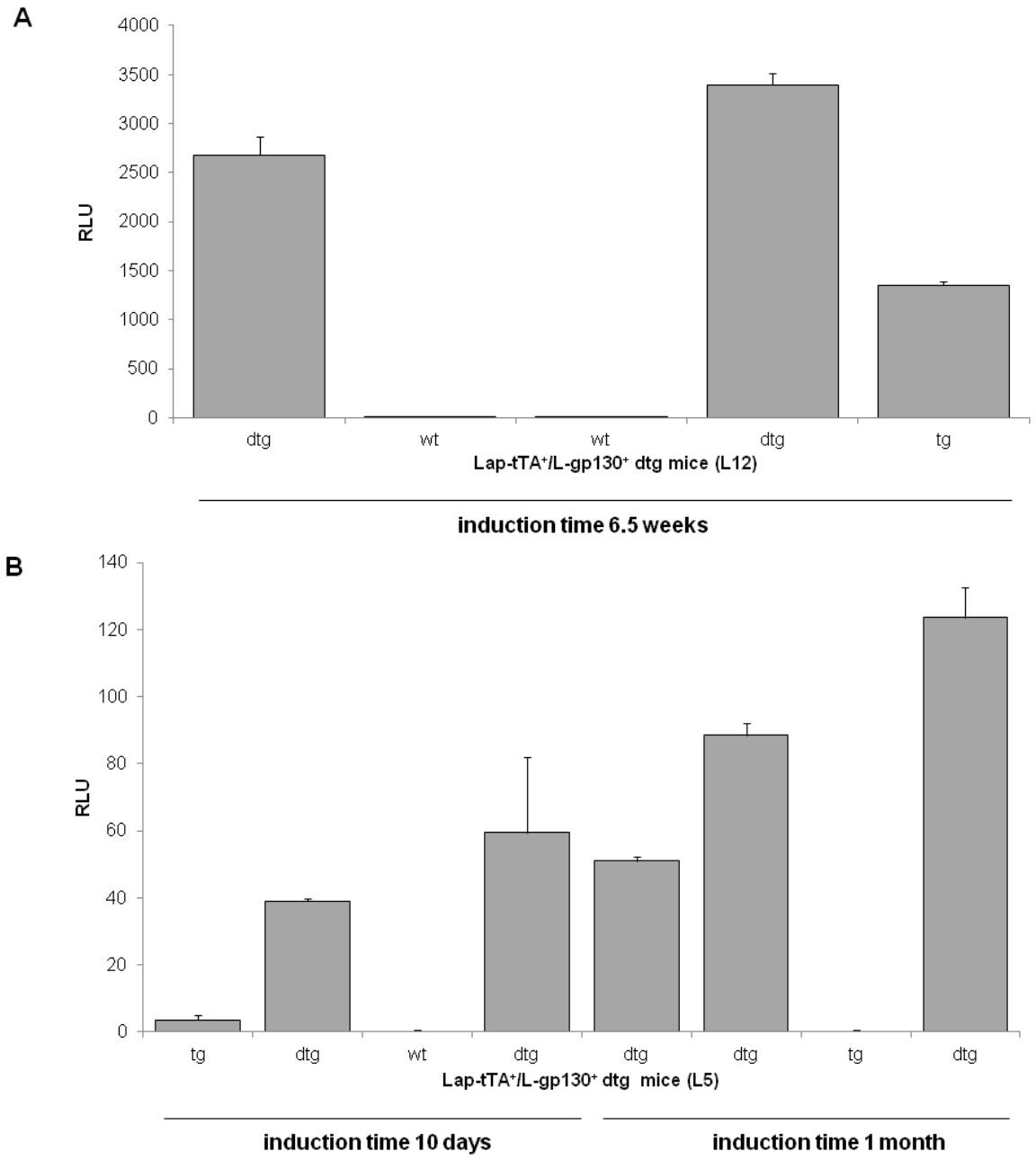

Figure 4.33: Analysis of luciferase activity in livers of Lap-tTA$^+$/L-gp130$^+$ dtg mice. (A) Livers of Lap-tTA$^+$/ L-gp130$^+$ dtg mice (L12) were analyzed 6.5 weeks after Dox withdrawal for luciferase expression by luciferase assay (Promega). (B) Livers of Lap-tTA$^+$/L-gp130$^+$ dtg mice (L5) were analyzed 10 days and 1 month after Dox withdrawal for luciferase expression by luciferase assay (Promega). RLU: relative light units.

4.2.7 *In vivo* imaging of Lap-tTA$^+$/L-gp130$^+$ dtg mice

To further analyze the transgene expression of Lap-tTA$^+$/L-gp130$^+$ dtg mice, luciferase activity was measured *in vivo* using a CCD camera. Mice were kept on doxycycline supplemented nutrition until the age of 8 weeks and analyzed 6.5 weeks later for the induction of luciferase in the liver. L-gp130$^+$ tg mice (L12) injected with luciferin showed background luminescence, whereas no luminescene was detectable in injected wildtype mice. Double transgenic Lap-tTA$^+$/L-gp130$^+$ mice did not show an increased induction of luminescence compared to L-gp130$^+$ tg mice (Fig. 4. 34). The detected bioluminescene was ubiquitous

and not restricted to the liver. These results were in line with the analysis of luciferase activity in liver lystates of L-gp130+ tg mice and Lap-tTA+/L-gp130+ dtg mice (Fig. 4.33 A).

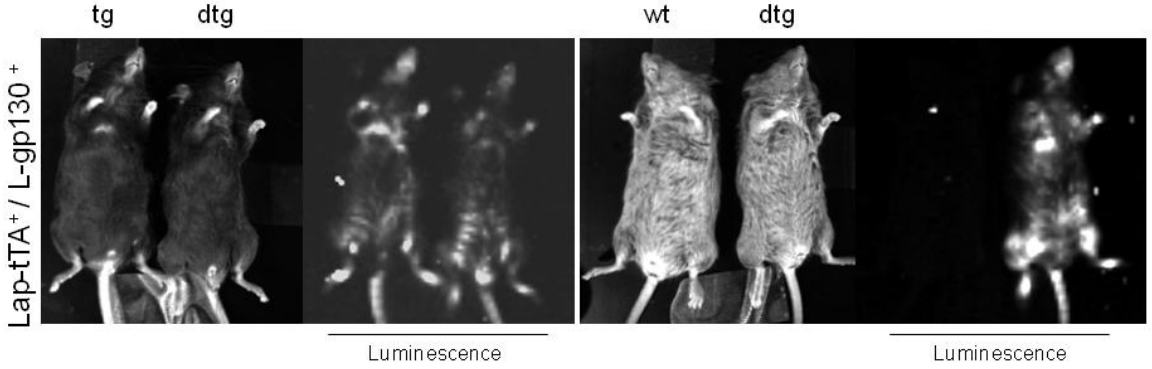

Figure 4.34: *In vivo* imaging of Lap-tTA+/L-gp130+ dtg mice (L12). Following an induction time of 6.5 weeks mice were injected with 150 µg luciferin/ g bodyweight. After an incubation period, while the substrate is converted by luciferase, mice were narcotized by ketamine and xylazine. The bioluminescence in living mice was measured with a CCD camera (Berthold NightOWL) and an integration time of 2 min.

Furthermore, liver RNA of Lap-tTA+/L-gp130+ dtg mice were tested for the expression of tTA and L-gp130. In our hands, it was impossible to detect the transcripts neither for tTA nor for L-gp130 using RT-PCR (data not shown).

4.2.8 Acute phase response of Lap-tTA+/L-gp130+ dtg mice

It is known that IL-6 mediated STAT3 signaling induces acute phase response in the liver resulting in an upregulation of acute phase proteins, such as serum amyloid A (SAA). The activation of a constitutive active gp130 variant in the liver may cause the induction of SAA as well. Since the concentration of SAA rises within hours and a short half life of SAA, it has to be measured subsequently. Hasan *et al.* showed that an inducible transgene expression is detectable one day following doxycycline withdrawal (127). Therefore the concentration of SAA was measured in the serum of Lap-tTA+/L-gp130+ dtg mice 24 h and 48 h after doxycycline withdrawal. The blood was collected via tail vein punctation and the serum was analyzed using a murine SAA ELISA (Invitrogen), including internal controls. No SAA was detectable in the serum samples obtained from Lap-tTA+/L-gp130+ dtg mice (data not shown).

4.2.9 Hydrodynamic injection of pBI5-L-gp130 into Lap-tTA+ tg mice

To test the inducibility of the expression plasmid pBI5-L-gp130 *in vivo* it was introduced into Lap-tTA+ tg mice via hydrodynamic injection (in cooperation with the group of Prof. Eithan Galun, Goldyne Savad Institute of Gene Therapy, Jerusalem, Israel). Hydrodynamic injection is used to introduce DNA into hepatocytes *in vivo* (137). Plasmid DNA was diluted in a high volume and injected into the tail vein in a short time (1 ml/10-20 sec) leading to a transient, liver restricted expression of the transgene. Wildtype mice were used as control and were co-injected with pBI5-L-gp130 and pTan-Pur, expressing the transactivaor tTA. Bioluminescence of injected mice was measured *in vivo* at day 1, day 2 and day 6 via

injection of luciferin and imaging using a CCD camera (Fig. 4.35 A). At day 1 all tg mice showed induction of luciferase activity, whereas the evaluation of bioluminescence of wildtype mice showed higher intensity compared to Lap-tTA$^+$ tg mice. At day 2 the expression of luciferase in Lap-tTA$^+$ tg mice was twofold higher than in wildtype mice, which remained until day 6 (Fig. 4.35 A, B). According to these data an inducible expression of luciferase in the liver can be achieved via hydrodynamic injection of pBI5-L-gp130 in Lap-tTA$^+$ tg mice as well as in wildtype mice, which were co-injected with an expression plasmid for tTA (pTan-Pur). Nevertheless, the detected luciferase level is 500-fold higher compared to luciferase activity measured in livers of L-gp130$^+$/Lap-tTA$^+$ dtg mice after induction.

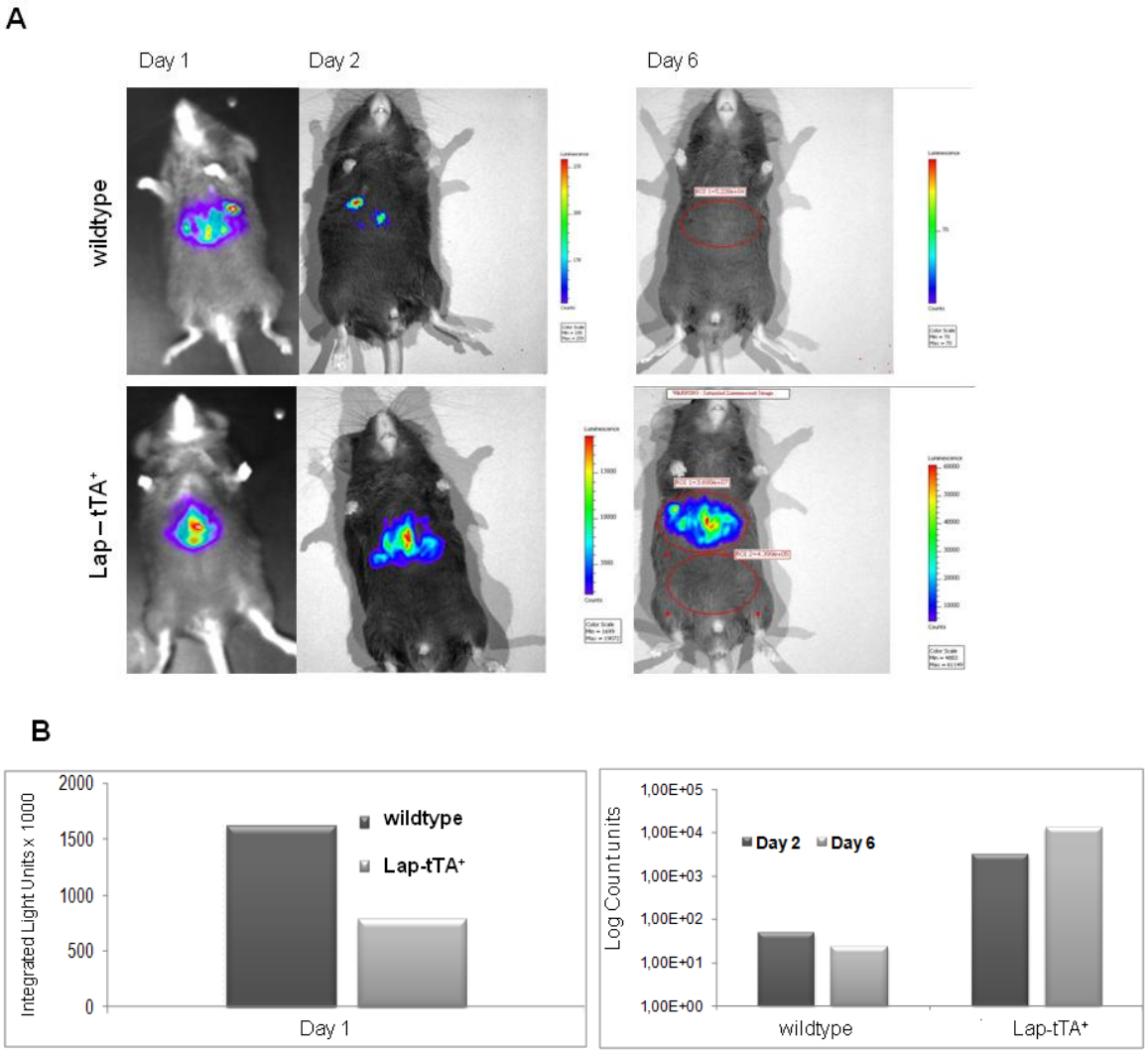

Figure 4.35: *In vivo* imaging of Lap-tTA$^+$ tg and wt mice following hydrodynamic injection of pBI5-L-gp130. (A) Wildtype mice (n=2) were injected with 5 µg of each pBI5-L-gp130 and the Tet-off vector pTan-Pur. Lap-tTA tg mice (n=2) were injected with 5 µg pBI5-L-gp130. Bioluminescence was measured in livig mice at day 1, 2 and 6 using a CCD camera. (B) Luciferase activity in the livers of injected mice was quantified at day 1, 2 and 6 after injection. Experiments were done in cooperation with the Goldyne Savad Institute of Gene Therapy, Jerusalem.

In order to further analyze the expression of L-gp130 in the livers of injected mice, RNA was isolated from liver samples obtained from two injected Lap-tTA$^+$ tg mice and two wildtype mice. The corresponding cDNA was analyzed by RT-PCR. The transcript of tTA was detectable in Lap-tTA$^+$ tg

mice at low levels as well as the transcript of luciferase (Fig. 4.36 A, B). However, the transcript for L-gp130 was not detectable in the liver of Lap-tTA+ tg mice (Fig. 4.36 B). Analysis of injected wildtype mice showed no expression of L-gp130, luciferase or tTA indicating that the expression of genes introduced via hydrodynamic injection in wildtype mice was not detectable via RT-PCR.

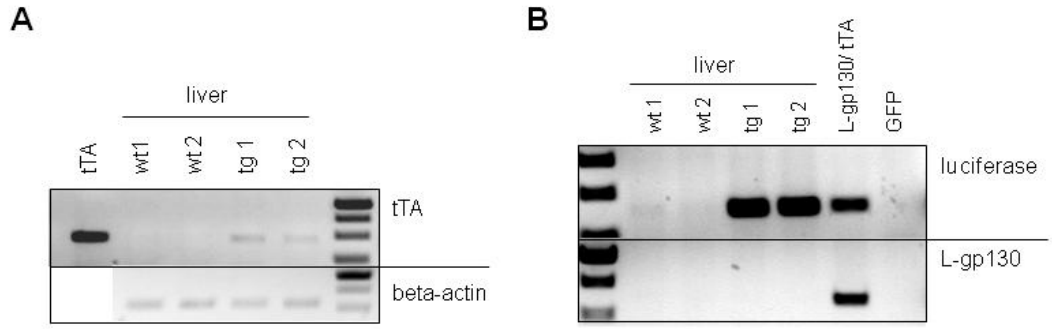

Figure 4.36: Analysis of gene expression for tTA, luciferase and L-gp130 in the liver via RT-PCR. The liver RNA of hydrodynamically injected wildtyp (wt) and Lap-tTA+ (tg) mice was analyzed for transcription levels of the indicated genes. (A) RT-PCR of liver cDNA for tTA and beta-actin. cDNA of HepG2 cells transfected with tTA was used a control for tTA. The house keeping gene beta-actin served as endogenous control. (B) RT-PCR of liver cDNA for luciferase and L-gp130. cDNA of HepG2 cells co-transfected with GFP or L-gp130 and tTA was used a control.

4.2.10 Analysis of Lap-tTA+ tg mice via Tet-reporter mice

Since we did no detect any transgene induction in Lap-tTA+/L-gp130+ dtg mice, but determined the functionality of the construct pBI5-L-gp130 *in vitro* and *in vivo*, we further tested Lap-tTA+ tg mice for the functionality of the transactivator. Therefore, Lap-tTA+ tg mice were bred with LC-1 reporter mice (126), which express firefly luciferase and Cre-recombinase under control of the tetracycline responsive promoter element (TRE). Three Lap-tTA+/LC-1+ dtg mice and control mice (wt, tg) were analyzed for luciferase activity in the liver but only one of the dtg mice showed expression of luciferase (Fig. 4.37). This result indicates that the transactivator tTA can initiate the gene expression of luciferase *in vivo,* which is under control of the tetracycline responsive promoter element. However, the expression of the transactivator in Lap-tTA+ tg mice is not homogenous within this strain because not all Lap-tTA+/LC-1+ dtg mice showed detectable levels of luciferase.

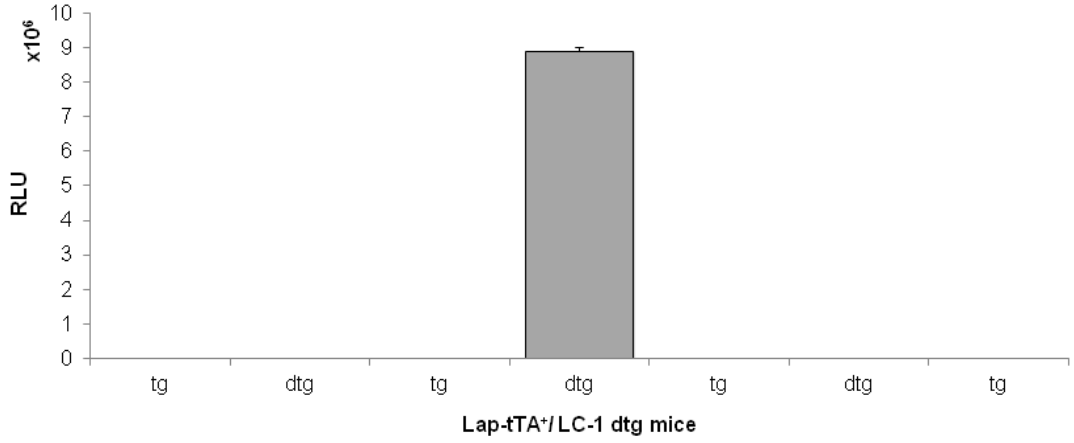

Figure 4.37: Luciferase activity in the liver of Lap-tTA$^+$/LC-1$^+$ dtg mice. Lap-tTA$^+$ tg mice were bred with LC-1$^+$ reporter mice, expressing luciferase and Cre-recombinase under control of TRE, to test the expression of tTA in the liver. Liver lysates of Lap-tTA$^+$ tg, wt and Lap-tTA$^+$/LC-1$^+$ dtg mice were analyzed for the expression of luciferase in the liver using luciferase assay (Promega). RLU: relative light units.

4.2.11 Analysis of L-gp130$^+$ tg mice via Tet-on mice

L-gp130$^+$ tg mice were analyzed regarding tetracycline responsive promoter (TRE) activity. Therefore we switched to the Tet-on system and L-gp130$^+$ tg mice (L2) were bred with hCMV-rtTA$^+$ tg mice, expressing the reverse tetracyclibe transactivator (rtTA) under control of a ubiquitous promoter. The gene expression of L-gp130 and firefly luciferase in hCMV-rtTA$^+$/L-gp130$^+$ dtg mice was induced by doxycycline given via nutrition. Initially, hCMV-rtTA$^+$/L-gp130$^+$ dtg and control mice (wt, tg) were analyzed 48 h after doxycycline treatment for luciferase activity in different tissues. hCMV-rtTA$^+$/L-gp130$^+$ dtg mice showed expression of luciferase in different tissues as described for the hCMV-promoter (126). Based on our data, tissues with different expression levels of luciferase were distinguished as followed: low expressing tissues liver, lung and spleen (< 2 x10^3 RLU), moderate expressing tissues heart, thymus and kidneys (< 20 x10^3 RLU) and high expressing tissues skin and stomach (> 200 x10^3 RLU). Single transgenic hCMV-rtTA$^+$ and L-gp130$^+$ tg mice as well as wildtype mice did not show any detectable luciferase activity (Fig. 4.38). Furthermore we analyzed hCMV-rtTA$^+$/L-gp130$^+$ dtg mice receiving doxycycline via nutrition for 7 days. Luciferase activity in the different tissues was detectable in three out of four double transgenic mice. The three hCMV-rtTA$^+$/L-gp130$^+$ dtg mice showed comparable activity of luciferase in the low, moderate and high expressing tissues as mentioned before. Only one dtg mouse exclusively showed luciferase induction in the skin. Less background luciferase activity was detectable in one L-gp130$^+$ tg mouse. Wildtype as well as hCMV-rtTA$^+$ tg mice showed no luciferase activity at all (Fig. 4.38). In addition, we analyzed hCMV-rtTA$^+$/L-gp130$^+$ dtg mice, which received doxycycline via nutrition for 2 months. Here, luciferase expression was detectable in one out of three dtg mice. Luciferase expression levels did not increase due to the longer induction time (data not shown). No expression of L-gp130 was detectable neither in Western blot nor in RT-PCR, although luciferase and L-gp130 should be equally expressed due to the bidirectional promoter (data not shown).

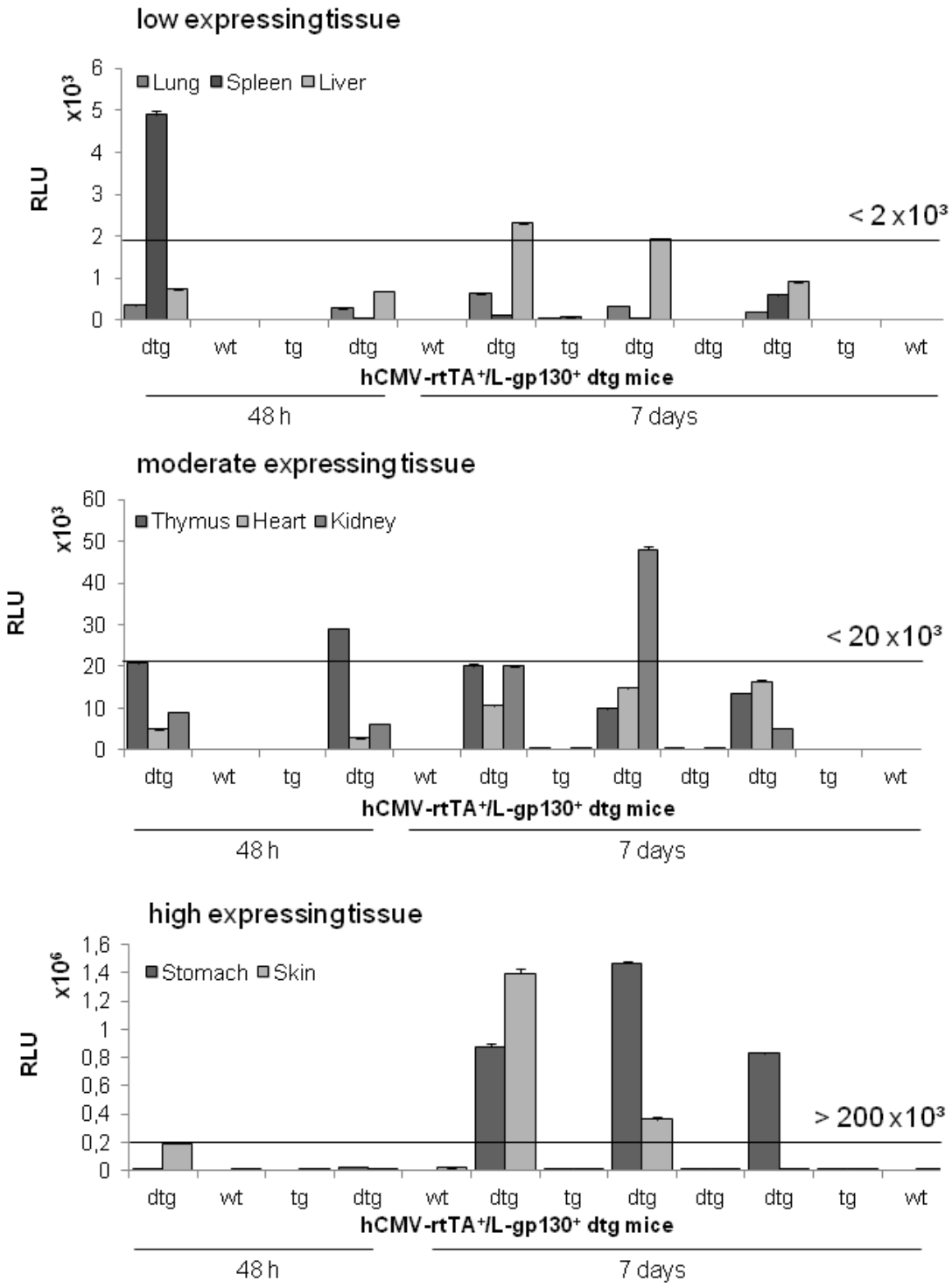

Figure 4.38: Analysis of luciferase activity in different tissues of hCMV-rtTA$^+$/L-gp130$^+$ (L2) dtg mice. Tissue lysates were analyzed for luciferase expression, following 48 h or 7 days of Dox treatment via luciferase assay (Promega). hCMV-rtTA$^+$/L-gp130$^+$ double transgenic (dtg) mice showed an expression of luciferase in selected tissues, whereas no luciferase activity was detectable in single transgenic (tg) and wildtype (wt) mice. According to different luciferase expression levels the analyszed tissues were grouped into low, moderate and high expressing tissues. RLU: relative light unit.

Taken together, luciferase expression was detectable in many tissues of hCMV-rtTA$^+$/L-gp130$^+$ dtg mice. Nevertheless not all dtg mice showed an expression of luciferase due to doxycycline treatment. Moreover, no further increase of luciferase activity was detected due to a longer induction period by doxycycline treatment.

4.2.12 Generation of Lap-rtTA$^+$/L-gp130$^+$ dtg mice

As hCMV-rtTA$^+$/L-gp130$^+$ dtg mice resulted in a robust luciferase expression, due to Dox treatment, we generated Lap-rtTA$^+$/L-gp130$^+$ (L2) dtg mice to achieve a liver specific expression of L-gp130. Double transgenic mice received doxycycline in varying concentrations and time intervals to achieve a sufficient induction of the transgene (Tab. 4-3).

Table 4-3: Doxycycline concentrations and administration for Lap-rtTA$^+$/L-gp130$^+$ dtg mice. Four experimental settings were done as indicated.

Experiment	Nutrition	Dox concentration	Duration
1	food	1 g/kg	6 days
2	food	1 g/kg	13 days
3	water (+ 3% sucrose)	2 mg/ml	6 days
4	i.p. injection	2 mg/0.5 ml	6 h

Independently of the doxycycline treatment parameters in the performed experiments, no induction of luciferase activity was detectable in the livers of Lap-rtTA$^+$/L-gp130$^+$ dtg mice. Even following i.p. injection of Dox, which is used for a short time induction, luciferase expression was undetectable (Fig. 4.39 A) (126). Furthermore, the expression of L-gp130 and rtTA could not be detected by Western blot (data not shown). Nevertheless, the rtTA transcript was detectable in the liver of Lap-rtTA$^+$ tg mice by RT-PCR, confirming that the mRNA of the activator was expressed (Fig. 4.39 B).

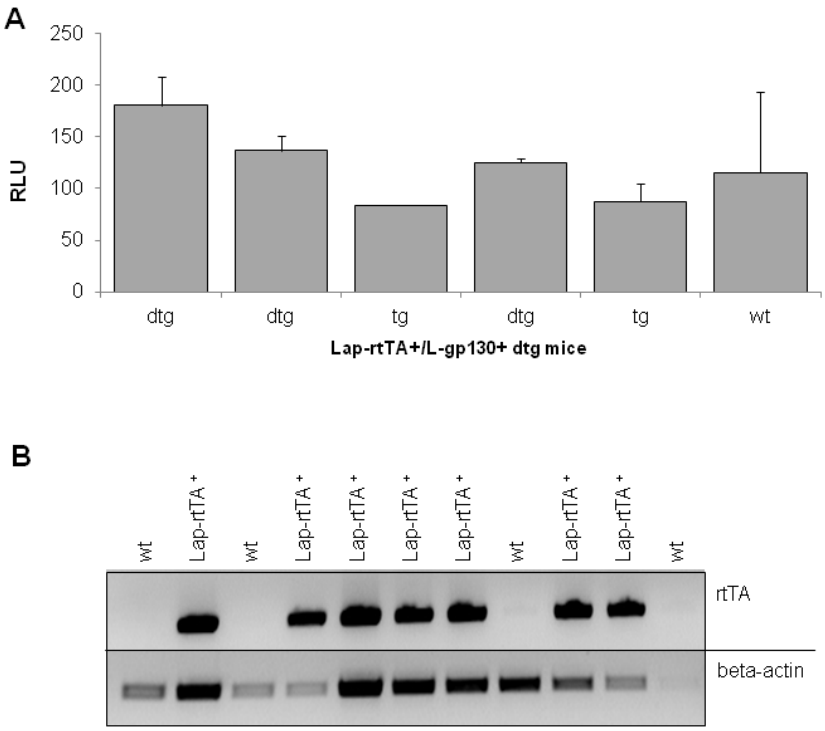

Figure 4.39: Analysis of Lap-rtTA$^+$/L-gp130$^+$ (L2) dtg mice. (A) Expression of luciferase in the livers of Lap-rtTA$^+$/L-gp130$^+$ dtg, L-gp130$^+$ tg and wildtype (wt) mice 6 h post i.p. injection of Dox via luciferase assay (Promega). RLU: relative light unit. (B) RT-PCR of liver tissue cDNA of Lap-rtTA$^+$ tg and wt mice for the transcript of rtTA. The house keeping gene beta-actin served as endogenous control.

4.2.13 Analysis of doxycycline concentration in mouse serum

The serum of treated mice was tested *in vitro* to analyze, if the doxycycline concentration of the serum was sufficient to initiate gene expression. Therefore, HEK 293T cells were transfected with the plasmids hCMV-tTA and pBI5-L-gp130. An appropriate amount of doxycycline would inhibit the transgene expression using the Tet-off system. Cells, covered with 1 ml of culture medium, were incubated with 2 µl of mouse serum obtained from the experiments listed in Tab. 4-3 and analyzed for luciferase activity. The serum from mice, which obtained 2 mg/ml Dox in drinking water (exp. 3) led to the strongest but not significant decrease of luciferase activity, compared to cells treated with doxycycline (1 µg/ml) (Fig. 4.40 A). This experimental setting was repeated *vice versa*. Therefore HEK 293T cells were transfected with the plasmids hCMV-rtTA and pBI5-L-gp130 and 10 µl of mouse serum was added to 1 ml culture medium. Doxycycline would induce the transgene expression using the Tet-on system. The strongest induction of luciferase expression was achieved with serum from mice injected i.p. with 2 mg doxycycline (exp. 4, Fig. 4.40 B). However, the luciferase activity of transfected cells was 10-times reduced compared to cells treated with a defined doxycycline concentration (1 µg/ml). These data revealed that the content of doxycycline in the serum of treated mice was sufficient to activate or inhibit inducible gene expression *in vitro* and indicated a comparable effect *in vivo* as well.

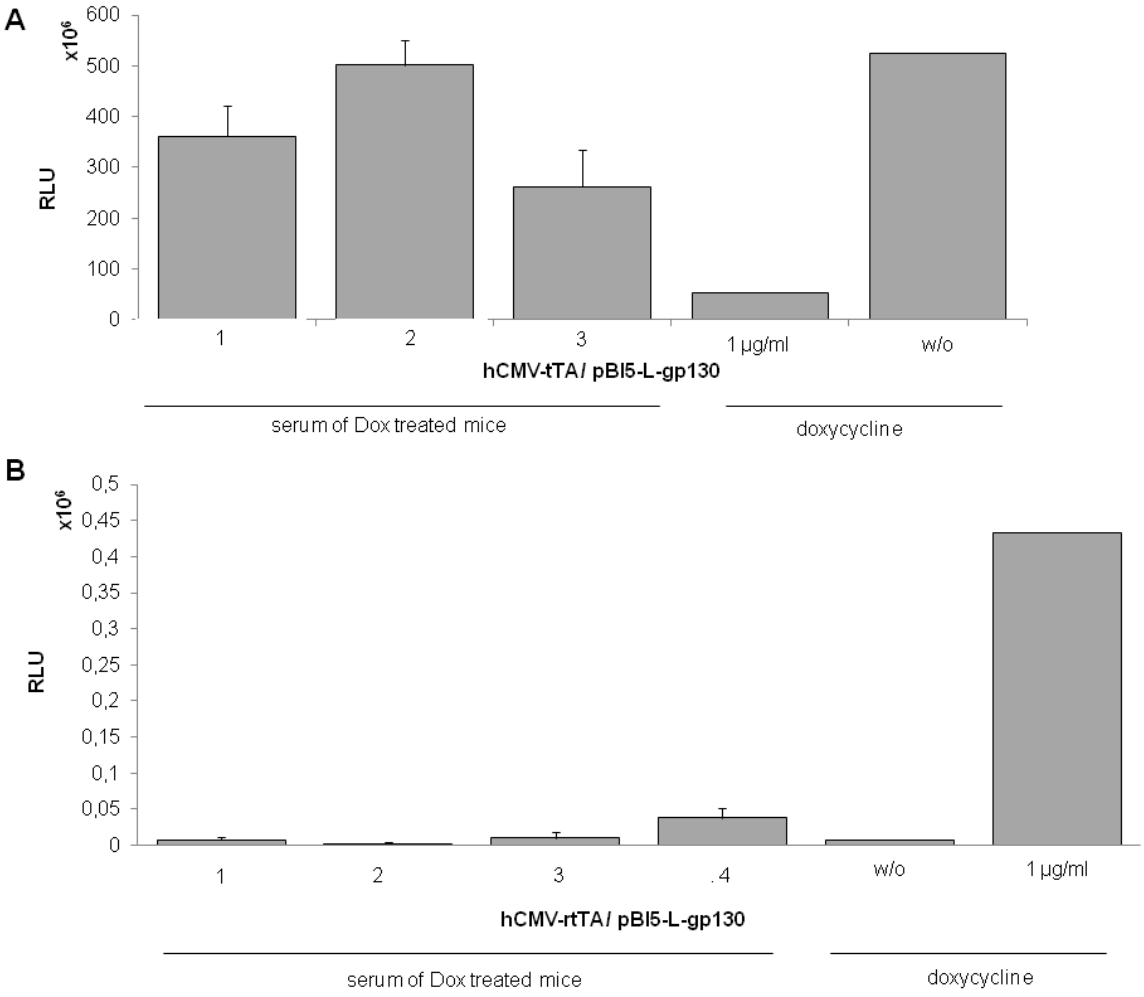

Figure 4.40: *In vitro* test of doxycycline concentration in serum of Dox treated mice. HEK 293T cells were transfected either with (A) hCMV-rtTA and pBI5-L-gp130 (Tet-on system) or (B) hCMV-rtTA and pBI5-L-gp130 (Tet-off system). Cells were incubated 48 h post transfection with mouse serum obtained from the experiments listed in Tab. 4-3 and were tested for luciferase activity after incubation of 24 h via luciferase assay (Promega). RLU: relative light unit.

To sum up, we could detect an inducible expression of L-gp130 due to doxycycline *in vitro*. Using L-gp130^{+} tg mice no transgene expression was obtained *in vivo* even though different mice expressing the transactivator in the liver were used to generate dtg mice.

5 DISCUSSION

5.1 Mutations in the IL-6 contact site of gp130 influence its activation

Activation of the cytokine receptor subunit gp130 is induced by IL-6 and corresponding cytokines of the IL-6 family. Thereby, IL-6 is a well known regulator of inflammation, autoimmune diseases and tissue regeneration (22, 138). Detailed mechanisms how cytokine binding to gp130 leads to activation of the intracellular associated Janus kinases is barely understood. Crystal structures and electron microscopy studies of gp130 (in complex with vIL-6 as well as with the IL-6/sIL-6R complex) revealed crucial interaction sites of the first three domains D1 to D3 of gp130 and defined three binding sites generated by the IL-6/IL-6R complex and two molecules of gp130 (5, 107). Recently, activating deletion mutations of gp130 have been discovered in patients with benign liver tumors, which were present in 60% of human inflammatory hepatocellular adenoma (IHCA) (121). Despite the knowledge that the mutations found in IHCAs were located in domain D2 of gp130, which represents the binding interface to IL-6, the structural mechanism of ligand independent gp130 activation is completely unknown. One frequently found deletion comprises the residues Y186 to Y190 (ΔYY) and was generated in our laboratory to investigate the functional and structural characteristics of ligand independent activation (Fig. 4.12 A) (133).

Based on the current crystal structure of the IL-6/sIL-6R/gp130 complex we assumed that a displacement or deletion of crucial residues around the EF loop of domain D2 results in ligand independent activation (139). We realized that the EF loop is stabilized by a disulfide bridge formed by C172 and C182, as well as by an ionic interaction of D215 to the backbone of the EF loop. We speculate that destabilization of the EF loop may result in aberrant signaling. Therefore we substituted the residues at position C172 and D215 in order to achieve molecular instability. We could show that the substitutions C172S and D215G led to ligand independent activation of gp130 in HEK 293T, HepG2 and Ba/F3-gp130 cells, which was monitored by STAT3 phosphorylation, STAT3 dependent proliferation and a STAT3 reporter assay. In cooperation with Martin Zacharias (Physics Department, TU Munich) we performed furthermore molecular dynamics simulations (100 ns) on gp130 wt, gp130 C172S and gp130 D215G to test our hypothesis that the described mutants enhance the EF loop flexibility. As a read out the D2/D3 interdomain angle flexibility and conformational fluctuations at the D2/D3 domain interface were recorded. We observed an increased rotamer flexibility of selected amino acid sidechains, which might result from an increased EF loop flexibility as well as an increased D2/D3 interdomain flexibility (data not shown). Given these data, the proper positioning of the EF loop in domain D2 seems to be crucial for an inactive gp130 conformation and interference results in activation (Fig. 5.1). We were interested if those mutations would alter constitutive activity of the gp130 ΔYY deletion mutant and introduced the point mutations C172S and D215G in the gp130 ΔYY mutant. Measuring gp130 activation by means of STAT3 phosphorylation, proliferation and activation of a STAT3 reporter, we could determine a slight decrease in ligand independent activation of the gp130 ΔYY mutant due to the substitution C172S. We wondered

why the mutation C172S led to ligand independent activation of gp130 wildtype but to diminished activation of the gp130 ΔYY mutant. We speculated that the disulfide bond formed by the residues C172 and C182 in gp130 wildtype is not present in the deletion mutant gp130 ΔYY, and that those cysteines could form alternative even intermolecular disulfide bonds instead, which are involved in the constitutive activity of the deletion mutant gp130 ΔYY. Therefore, we analyzed the influence of DTT, which is a strong reducing agent and leads to disruption of disulfide bonds. HEK 293T cells overexpressing the gp130 ΔYY mutant or gp130 wt (+ Hyper-IL6) were treated with DTT and lysates were analyzed under non-reducing conditions. We observed that DTT treatment led to a diminished phosphorylation of STAT3 in both gp130 ΔYY and Hyper-IL6 treated gp130 wt overexpressing cells. An equal reduction of STAT3 activity was detected in non treated HEK 293T cells expressing the mutant gp130 ΔYY C172S, indicating that disulfide bond formation is crucial for the activation of the gp130 ΔYY mutant (data not shown). Nevertheless we can not state at the moment if intermolecular disulfide bond formation is involved in gp130 ΔYY activation. So far, we could demonstrate that C172 in the extracellular portion contributes to the constitutive activity of the mutant gp130 ΔYY. The substitution D215G did not affect the signal transduction of the gp130 ΔYY mutant.

Moreover, it is unclear why constitutive active mutants of gp130 are not suppressed by endogenous inhibitors, such as SOCS3. Gp130 deletion mutants found in human liver adenoma led to upregulation of SOCS3 mRNA in comparable levels achieved with IL-6 treatment, but it remains unclear why these mutants still display constitutive STAT3 activation (121). When co-expressed with gp130 mutants, SOCS3 was still able to suppress ligand independent STAT3 phosphorylation, indicating that the gp130 mutants are still susceptible to SOCS3 mediated inhibition *in vitro*. Probably the balance of activating and inhibitory signals *in vivo* is shifted, leading to an incability of SOCS3 to suppress the downstream signaling of gp130 deletion mutants.

5.2 Disruption of the hydrophobic D2/D3 connectivity induces gp130 activation

Furthermore, we focused on the D2/D3 interface, which connects the D2 EF loop and the D3 BC loop through hydrophobic residues. We postulated that interference with the interconnecting hydrophobic area, comprising e.g. the amino acids V189, Y190 and V252 promote gp130 activation. This assumption is supported by previous reports, showing that the D2/D3 hinge region might function as a 'molecular switch'. The residue V252 is situated in the flexible and most exposed part of the BC loop in domain D3, which was revealed by NMR spectroscopy (131). Horsten *et al.* claimed that the substitution V252D destroys the central hydrophobic interaction between gp130 and IL-6. Indeed the mutant gp130 V252D showed 50% reduced affinity for the IL-6/sIL-6R complex compared to gp130 wt as well as a strong decrease of biological activity (107).

To underline the importance of this hydrophobic area for gp130 activation, we substituted the residues V189, Y190 and V252 and examined the signal transduction of the generated gp130 mutants in HEK

293T, HepG2 and Ba/F3-gp130 cells. Neither V189G nor Y190G displayed ligand independent induction of STAT3 phosphorylation or STAT3 dependent proliferation. Regarding these data, we conclude that substitution of V189 and Y190 did not alter the hydrophobic area and that these residues are not involved in gp130 activation. However, the substitution V252G resulted in an autonomous activation of gp130 and subsequent STAT3 activation, such as phosphorylation as well as proliferation and activation of a STAT3 reporter. Taken together, V252 is embedded in the hydrophobic core connecting the BC loop of domain D3 with the EF loop of domain D2 and substitution to glycine disrupts the conformation of this D2/D3 interdomain, resulting in activation of the intracellular associated Janus kinases (Fig. 5.1). Introduction of the mutation V252G did not alter the constitutive activity of the gp130 ΔYY mutant, which leads to the assumption that the hydrophobic interactions of D2/D3 are already loosened in the gp130 ΔYY mutant.

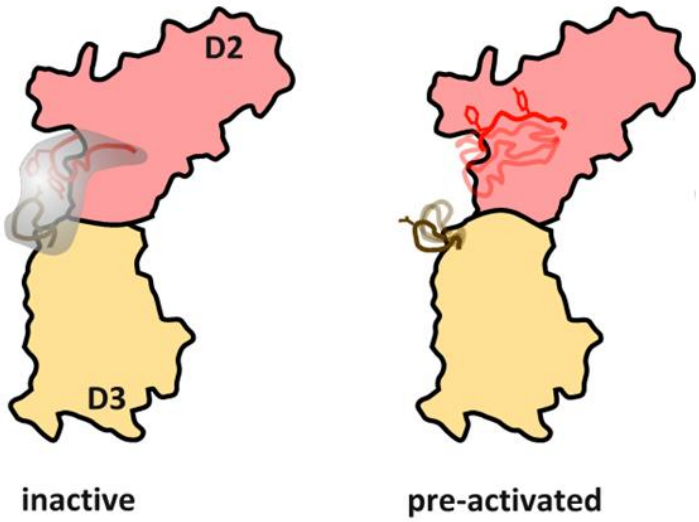

Figure 5.1: Model of gp130 activation I. Left: The inactive state of gp130 is stabilized by the formation of a hydrophobic core (grey) connecting the D2 EF loop (red) with the D3 BC loop (brown), limiting their flexibility. Right: Activating mutations either increase flexibility of the D2 EF loop, disconnecting it from D3 BC loop (C172S, D215G, deletion mutations) or directly disconnect the two loops by disturbing the hydrophobic core (V252G mutation). This leads to a pre-activated state of gp130. (Schuett *et al.*, submitted)

As ongoing work we want to validate the data achieved for the gp130 C172S mutant by replacing the counterpart C182. We furthermore generated gp130 mutants containing the substitutions E138A, V184P and V192P. The residue E138 exhibits ionic interactions to domain D3 of gp130, as seen in the crystal structure and we speculate that interference loosens the D2/D3 connectivity, which subsequently leads to activation. The residues V184 and V192 are flanking the EF loop. Substitution to proline, which exhibits a strong conformational rigidity, will alter the positioning of the whole loop, resulting presumably in autonomous activation of gp130. Moreover, the substitutions F191E and V252D, which lead to impaired activation of gp130 wt, will be introduced into the deletion mutant gp130 ΔYY to analyze its constituve activity (16, 107). Crystal structure reveals that V252 is partially hidden by the side chain of F191, which is located in the EF loop of domain D2, highlighting a connection of these two residues (106, 131). By interfering with F191 in domain D2, Planz *et al.* ruled out the importance of this residue for the IL-6 binding site II of gp130 (16). The mutation F191E did not interfere with the binding of the IL-6/sIL-6R

complex to gp130 but the mutant gp130 F191E was biologically inactive, judged by reporter assays where no significant activation of STAT1 was detectable. Co-immunoprecipitation studies revealed that the mutant gp130 F191E cannot form homodimers, which were crucial for the transmission of a signal transduction cascade (16). This mutation in the background of gp130 ΔYY will be analyzed, with respect to its constitutive activity. On the other hand, we generated the mutation F191G, expecting to observe a ligand independent activation, as we assumed that this mutation also disrupts the hydrophobic core.
In addition, Horsten *et al.* already showed that the substitution V252D led to impaired binding of the IL-6/sIL-6R complex compared to gp130 wt as well as to diminished biological activity, determined with a reporter assay (107). This underlines the importance of distinct residues in the binding interface of IL-6 for the activity of gp130. The fact, that replacement of the crucial residue V252 with aspartate led to an impaired gp130 signaling, whereas the substitution V252G showed autonomous gp130 activity is very interesting. We conclude that the hydrophobic property of valine is changed by introducing the small and unpolar residue glycine, whereas the introduction of aspartic acid could lead to alternative polar interactions and thereby abrogating gp130 activation. This hypothesis can be tested by the mutants gp130 F191G and gp130 ΔYY F191E, as well as gp130 ΔYY V252D.

5.3 Domain D1 is important for gp130 activation but dispensable for dimerization

Previous reports suggest a role of the immunoglobulin-like domain D1 in the binding of IL-6 and gp130 activation. Pflanz *et al.* showed that cells expressing gp130 lacking the domain D1 (gp130 ΔD1) were not able to bind IL-6/sIL-6R complexes. However, cells co-expressing the mutant gp130 ΔD1 and a gp130 mutant altered in domain D2 could respond well to IL-6 and soluble IL-6R (16). Therefore, it was postulated that domain D1 is absolutely required to initiate signal transduction, and that two different epitopes of gp130, one on each receptor chain, are sufficient for binding of the IL-6/sIL-6R complex. Obviously, these epitopes are cooperating due to asymmetrical binding of IL-6/sIL-6R. The importance of domain D1 for gp130 activation has been further underlined by Sommer *et al.*. In this study the deletion of domain D1 abolished the constitutive activation of the gp130 ΔYY mutant, highlighting that the D1 domain is involved in ligand independent activation of gp130 ΔYY (133). In this context we were interested, if partial deletion of domain D1 is sufficient to abrogate constitutive signaling of the gp130 ΔYY mutant. Gp130 crystal structure reveals that the N-terminus of domain D1 contacts IL-6 directly through intercalation into a groove of IL-6 (Fig. 4.12 B) (112). We assumed that the N-terminus contributes to the ligand independent activation of the gp130 ΔYY mutant in the way that domain D1 contacts a neighboring gp130 with this N-terminal peptide. To address the relevance of the N-terminus for gp130 activation, we deleted the first five residues E1 to P5 (ΔN1-5) in the gp130 ΔYY mutant. HEK 293 T cells expressing the mutant gp130 ΔYYΔN1-5 showed diminished activity of STAT3, in terms of phosphorylation, subsequent proliferation and activation of a STAT3 reporter. However, the constitutive activation of gp130 ΔYYwas not completely abolished due to the deletion ΔN1-5 as compared to cells expressing the mutant gp130 ΔYYΔD1. In addition, we generated mutants, which contain substitutions of

only one of these five amino acids (gp130 ΔYY E1A, L2G, L3G, D4A and P5G). None of the mutants led to reduced activity of STAT3 compared to the gp130 ΔYY mutant, indicating that a potential intermolecular contact is not mediated by a single residue (data not shown).

We speculate that domain D1 interferes with the binding site II of IL-6, located in the domain D2 of the second gp130 molecule. Thereby, the domain D1 pushes the IL-6/IL-6R complex in the D2/D3 groove. This pressure leads to a conformational change of this hydrophobic area as well as of the C-terminal part of gp130, which leads subsequently to activation of the Janus kinases. It is known that the gp130 ΔYY mutant can form homodimers and maybe domain D1 of the gp130 ΔYY mutant is sufficient to push the D2/D3 interface of another gp130 molecule without the help of an additional molecule, e.g. the IL-6/IL-6R complex (Fig. 5.2). The deletion of the N-terminus in the gp130 ΔYY mutant presumably reduces the force of domain D1 to exhibit pressure on the loosened D2/D3 interface and leads therefore to a reduced STAT3 activation.

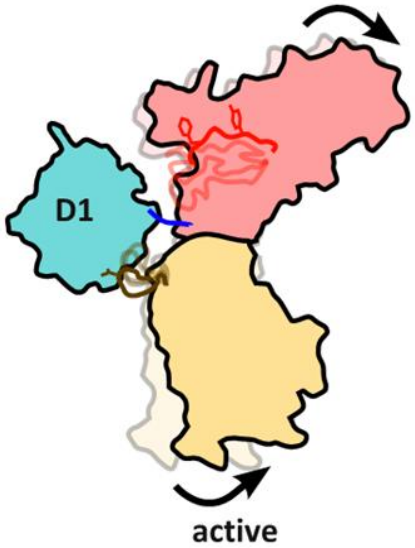

Figure 5.2: Model of gp130 activation II. The preactivated state (Fig. 5.1) needs the interaction to domain D1 of a second gp130 molecule, anchored by its N-terminal peptide (blue) in order to achieve fully fledged activation of gp130. (Schuett *et al.,* submitted)

This hypothesis can be proven by exchanging the D1 domain of the mutant gp130 ΔYY with globular domains (e.g. GFP) of different molecular weights, to monitor which size is adequate to keep the constitutive activity of the gp130 ΔYY mutant. The data generated by Sommer *et al.* showed that blocking of the domain D1 by the anti-gp130 antibody B-T2 did not influence autonomous proliferation of cells expressing the mutant gp130 ΔYY, whereas deletion of domain D1 led to abrogation of ligand independent proliferation (133). In context with our assumption, the anti-gp130 antibody B-T2 has no influence on ligand independent proliferation because the domain D1 is still present and can exhibit pressure to the D2/D3 interface of another gp130 molecule. Furthermore it is possible that the binding of the anti-gp130 antibody B-T2 even increases the tension. But with the complete loss of this plunger, the D2/D3 groove is unchanged, resulting in inactivation of the gp130 ΔYYΔD1 mutant. This leads to the conclusion, that a sterical correct orientation of domain D1 (or an appropriate domain) and its access to

the D2/D3 interface of a second gp130 molecule seems to be important for gp130 activation. It seems that the whole domain D1 is needed to achieve the right positioning of the D2/D3 area and subsequent activation of gp130, whereas the N-terminal tail of domain D1 helps to properly anchor the domain D1 to a second gp130 molecule (Fig. 5.3).

Moreover, it has been shown that dimerization of the gp130 ΔYY mutant was independent of the presence of domain D1, whereas gp130 wt lacking the domain D1 was not able to form homodimers (16). Sommer *et al.* speculated that homodimers of the gp130 ΔYY mutant were built through an interaction of the mutated domains D2. We studied the potential of the mutants gp130 ΔYY, gp130 ΔYYΔD1 and gp130 ΔYYΔN1-5 to form dimers. Using co-immunoprecipitation, we realized that co-expressed gp130 variants form homo- as well as heterodimers irrespective of their partners. All precipitated receptors showed phosphorylation of tyrosine residues, indicating that co-expression results in activation of gp130. Furthermore, we could show that the generated constitutive active mutants gp130 C172S, gp130 D215G and gp130 V252G were able to form homodimers and in consequence showed phosphorylation of tyrosine residues as well as activation of STAT3. Furthermore, we reproduced data showing that gp130 wt forms inactive homodimers. We hypothesize that the formation of homodimers is not sufficient to activate gp130 but rather the interference with the hydrophobic core of D2/D3 is crucial for the activation of associated Janus kinases and gp130 downstream signaling (Fig. 5.2, 5.3).

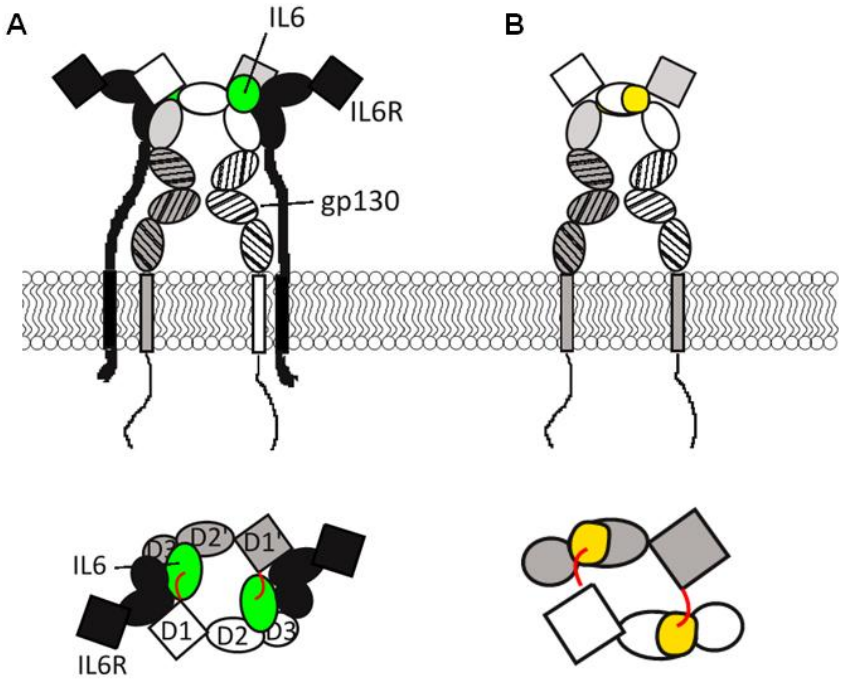

Figure 5.3: Schematic representation of gp130 signaling complexes. (A) The hexameric IL-6/IL-6R/$(gp130)_2$ complex, indicating the involvement of the gp130 D1 domain in contacting IL-6. In red are highlighted the first five N-terminal amino acids in gp130 D1 domain. (B) Potential dimer formation and ligand independent activation of gp130 deletion mutants like gp130 ΔYY. Areas of deletions are depicted in yellow. Domain D1 of gp130 is contacting the site of mutation. (Schuett *et al.*, submitted)

5.4 Expression of the constitutive active variant L-gp130 can be achieved *in vitro* and *ex vivo* using an inducible system

As reported by Stuhlmann-Laeisz *et al.* the expression of the constitutive active variant L-gp130 leads to sustained phosphorylation of STAT3 in HepG2 cells, ligand independent proliferation of Ba/F3-gp130 cells and suppresses the *in vitro* differentiation of murine embryonic stem cells (123). We took advantage of the Tet-system in order to achieve inducible expression of L-gp130 and firefly luciferase. Both systems, inhibition (Tet-off) and induction (Tet-on) of gene expression via doxycycline treatment were analyzed *in vitro* and *in vivo*. We could show in time course experiments that an induction time of 24 h is sufficient for both systems *in vitro*. Furthermore, we defined in a dose response curve that 1 μg/ml doxycycline is an adequate concentration for the induction of gene expression.

Transgenic mice expressing L-gp130 and firefly luciferase under the control of the tetracycline responsive promoter element (TRE) were generated in cooperation with the IBF (Heidelberg). Twelve L-gp130$^+$ strains were established, which presumably differ in site and amount of transgene integration. In order to find out, if expression of L-gp130 and luciferase can be induced via the Tet-system *ex vivo*, we generated murine embryonic fibroblasts (mEF cells) of L-gp130$^+$ tg mice. MEF cells from one L-gp130 strain (L11) showed luciferase activity in the absence of the transactivator, indicating a leakiness of the Tet-promoter. Consequently, mEF cells of different L-gp130 strains were stably transduced with the transactivator tTA and analyzed for L-gp130 and luciferase expression. Two out of four generated mEF cell lines from L-gp130$^+$ strains L2 and L5, showed transgene induction in response to tTA, which could be inhibited by doxycycline treatment. We assumed that these mouse strains (L2, L5) are suitable for breding with Tet-mice, expressing tTA or rtTA under the control of a tissue specific promoter.

5.5 Different Tet-inducer strains failed to induce the expression of L-gp130 and firefly luciferase *in vivo* due to promoter inactivity

We wanted to investigate the cell-autonomous activation of L-gp130 in the liver of transgenic mice, because previous reports showed that transgenic mice expressing IL-6 and sIL-6R in the liver developed liver hyperplasia and adenoma but no malignant tumors (51, 140). The same was reported for the gp130 deletion mutants found in human liver adenoma, which seem to be insufficient to induce malignant tumor formation. Initially, we analyzed luciferase activity in liver lysates of L-gp130$^+$ tg mice and detected background activity in two strains (L11 and L12). This result stands in line with the data obtained from L-gp130$^+$ mEF cells, indicating that the site of integration causes probably a leakiness of the promoter. To analyze the induction of L-gp130 expression *in vivo*, different L-gp130$^+$ tg mice strains were crossed with mice expressing the tetracycline transactivator (tTA) under control of the liver-enriched activator protein (Lap) promoter (Lap-tTA$^+$ tg mice). All mice, including breeding pairs, were kept on doxycycline supplemented nutrition for 3 - 8 weeks to prevent activation of L-gp130 at early stage, as it is known that gp130 is highly expressed in the murine uterus at day 3 and 4 of pregnancy and is essential for the implantation of mouse embryos in combination with the LIF receptor (141). Following an induction time

of 1 to 16 weeks, mice were analyzed at the age of 3 to 6 months. However, Lap-tTA$^+$/L-gp130$^+$ dtg mice did not show any expression of L-gp130 in the liver. In addition, luciferase expression was examined either in liver lysates or via *in vivo* imaging using a CCD camera. Induction of luciferase expression was absent in control mice, whereas the expression of luciferase in Lap-tTA$^+$/L-gp130$^+$ dtg mice was very low. However, literature reveals that luciferase expression needs to reach a specific threshold to ensure transgene expression, even if both genes are expressed under control of a bidirectional promoter element. Ernst *et al.* generated transgenic mice expressing a core protein of the hepatitis virus C as well as firefly luciferase under control of the Tet-specific promoter. These mice were crossed to Lap-rtTA$^+$ tg mice to achieve liver specific expression. They could examine that low luciferase activity correlates with undetectable protein levels of the transgene in Western blot analysis (142). Another reason for low or absent induction could be the long term treatment with doxycycline, which prevented transgene expression in early stages. It is postulated that doxycycline can be incorporated into the bones or the fat tissue, thereby building depots from where it is released at later time points (K. Schönig, ZI Mannheim, personal communication). Even low concentrations of doxycycline are enough to suppress transgene expression in the very sensitive Tet-off system. Due to undetectable levels of the tTA transcript in liver lysates of Lap-tTA$^+$ tg mice, we assumed that the transactivator is either not expressed or did not reach an appropriate concentration to induce gene expression. Crossing Lap-tTA$^+$ tg mice with LC-1 reporter mice, expressing luciferase and Cre-recombinase under control of the Tet-promoter, revealed that only one out of three Lap-tTA$^+$/LC-1 dtg mice showed luciferase induction. This data leads to the conclusion that the transactivator tTA is not homogenously expressed among the population of Lap-tTA$^+$ tg mice.
In cooperation with the group of Prof. Eithan Galun (Goldyne Savad Institute of gene therapy, Jerusalem, Israel) we analyzed the expression of the L-gp130 construct (pBI5-L-gp130) in the liver of Lap-tTA$^+$ tg mice via hydrodynamic injection. As control, wildtype mice were co-injected with pBI5-L-gp130 and a Tet-off vector (pTan-Pur). Mice were imaged for luciferase expression *in vivo* up to 6 days via CCD camera. The injected Lap-tTA$^+$ tg mice showed stronger and persistent expression of luciferase as compared to injected wildtype mice. These data indicate that the expression of L-gp130 can be induced in the liver via the tetracycline transactivator (tTA). However, by using hydrodynamic injection the number of gene copies is increased compared to transgenic mice, resulting in higher transgene expression. Furthermore, hydrodynamic injection leads only to a transient and not to a stable integration of the transgene in the liver such as in transgenic mice. We therefore conclude that the genomic integration in L-gp130$^+$ tg mice might impair the inducibility of the Tet-promoter.

For further experiments, we switched to the Tet-on system to avoid long doxycycline treatment. Using this system, comparable induction levels of L-gp130 and luciferase expression were achieved *in vitro*. The L-gp130$^+$ strain L2 was the most suitable to generate double transgenic mice, because mEF cells isolated of this strain were responsive to retrovirally transducted tTA. Initially, L-gp130$^+$ tg mice (L2) were crossed to hCMV-rtTA$^+$ tg mice to analyze the induction capability of the Tet-promoter via the reverse transactivator (rtTA) in general. To induce transgene expression, hCMV-rtTA$^+$/L-gp130$^+$ dtg mice were treated with doxycycline for 48 h, 7 days or up to 2 months and luciferase activity was detectable in several

tissues, as reported by Schönig *et al.* (126). However, no increase in luciferase expression due to long term induction could be detected and no expression of L-gp130 was measurable in any tissue. For liver tissue, this can be explained with the reduced activity of the hCMV promoter in hepatocytes. For other tissues however this might indicate a transcriptional silencing due to genomic integration. To analyze liver specific expression, L-gp130$^+$ mice were crossed with Lap-rtTA$^+$ tg micge and Lap-rtTA$^+$/L-gp130$^+$ dtg mice received doxycycline for one or two weeks to induce gene expression (143). However, no expression was detectable for L-gp130 and luciferase in Western blot analysis and luciferase assay, respectively. Even high dose i.p. injection of doxycycline into double transgenic mice did not result in the induction of the Tet-promoter. Although the expression of the reverse tetracycline transactivator (rtTA) was shown by RT-PCR and doxycycline was detectable in the sera of treated mice, the transgene expression was not induced. This leads to the conclusion that the Tet-promoter is not accessible for rtTA. We hypothesized that the random integration site of the transgene causes probably a silencing of the Tet-promoter by e.g. methylation.

Due to the fact that the generated L-gp130$^+$ tg mice were not capable to express the transgene in an inducible manner, this strain was terminated. New mice will be generated in the future in cooperation with T. Wunderlich (Cologne). A transgene containing a 5' floxed stop cassette followed by the L-gp130 cDNA will be introduced into the Rosa26 locus. Expression of L-gp130 will be induced by the Cre-mediated removal of the stop cassette. The liver specific expression of constitutive active L-gp130 will then be achieved using mice expressing Cre-recombinase in hepatocytes (e.g. Alfp-Cre, Alb-Cre). The liver will be the focus of further investigations, in respect to analyze formation of liver adenoma and liver regeneration after injury. As shown by Jenkins *et al.*, expression of constitutive active gp130 in mice resulted in gastric hyperproliferation and growth of spontaneously arising gastric adenomas (101). We expect an equal effect in the liver due to liver restricted expression. Previous studies revealed that IL-6 and gp130 play an essential role in liver regeneration as well as in tumor initiation. In addition, mice expressing the deletion mutant gp130 ΔYY in the liver are under ongoing investigation in our laboratory.

Taken together, to the best of our knowledge we present here for the first time data which helps to understand the molecular basis of gp130 activation. We could show that activating mutations increase the flexibility of the EF loop situated in domain D2. As a consequence hydrophobic interactions to domain D3 are lost, leading to the transmission of the activating signal via domains D4-D6 to the intracellular part. Further structure-function analyses as well as crystallisation of the deletion mutant gp130 ΔYY are needed to fully understand the mechanism of gp130 activation.

Although the participation of IL-6 and gp130 signaling to liver diseases has been shown, the consequences of a cell-autonomous hepatocellular gp130 activation are unclear. We therefore sought to develop a transgenic murine model system with a tetracycline-inducible expression of a constitutive active gp130 variant. Unfortunately our model hampered inducible expression so that we cannot draw any conclusions from the current mouse model. Therefore we are currently developing novel approaches to generate transgenic mice with hepatocellular expression of ligand independent gp130 variants. With those models we hope to deepen our knowledge about the participation of gp130 signaling in liver regeneration and liver tumor formation, resulting in novel concepts for therapeutic interventions.

6 SUMMARY

The IL-6 cytokine family is involved in inflammation, regeneration and tumor formation (23, 144). One characteristic of IL-6 signaling is the requirement of the alpha-subunit IL-6R, which exists as a membrane bound as well as a soluble form. The IL-6/IL-6R complex binds to the ubiquitously expressed, signal transducing beta-receptor gp130, leading to gp130 activation and downstream signaling via the intracellular associated Janus kinases (JAKs). Despite the fact that the binding sites of the IL-6/IL-6R complex to gp130 were identified by crystal structure analysis, the molecular mechanism underlying gp130 activation is barely understood.

Recently constitutive active deletion mutants of gp130 were found in patients with benign liver adenoma. Theses deletions differ in length as well as in position and cluster around the IL-6 contact site of domain D2. This contact area comprises the EF loop, stabilized by adjacent amino residues in wildtype gp130. Furthermore, the EF loop is connected to the BC loop of domain D3 via hydrophobic interactions. We hypothesized that an inactive gp130 conformation is stabilized via such interactions. Using a rational structure-based mutagenesis approach we could show, that an increased EF loop flexibility as well as interference with the hydrophobic interactions led to ligand independent activation of gp130. In addition we discovered that the D1 domain, in particular the first N-terminal residues were crucial for the ligand independent activity of the gp130 deletion mutants. Based on our results we present a model, which helps to explain the molecular basis of cytokine dependent as well as cytokine independent activation of gp130, presumably providing an insight into the molecular basis of cytokine receptor activation in general.

Moreover, we were interested in the physiological consequences of a cell-autonomous, ligand independent activation of gp130 in hepatocytes. We therefore generated transgenic mice, expressing a previously published artificial, constitutive active variant of gp130 (L-gp130) in a tetracycline inducible manner. We intended to use this murine model to study in more depth the impact of hepatocellular signaling on injury-induced liver regeneration and tumor promotion. Unfortunately we did not achieve an inducible expression of L-gp130 during our analysis, suggesting that the transgene was silenced after genomic integration. Therefore we are currently generating two alternative murine models to analyze the effect of a cell-autonomous hepatocellular expression of ligand independent gp130 variants.

7 ZUSAMMENFASSUNG

Die Familie der Interleukin-6 (IL-6) Zytokine spielt eine wichtige Rolle bei Entzündung, Regeneration und Tumorentstehung (23, 144). Die Besonderheit der IL-6 Signalgebung ist, dass IL-6 zuerst an seinen alpha-Rezeptor (IL-6R) binden muss, welcher in membrangebundener und löslicher Form existiert. Dieser Komplex bindet an den ubiquitär expremierten, signalgebenden beta-Rezeptor gp130 und aktiviert die intrazellulär gekoppelten Janus kinasen (JAKs). Obwohl die Bindungsstellen des IL-6/IL-6R Komplexes an gp130 anhand von Strukturanalysen aufgeklärt wurden, ist die molekulare Grundlage der gp130 Aktivierung nach wie vor unklar.

Kürzlich wurden konstitutiv aktive Deletionsmutanten von gp130 in Patienten mit benignen Leberadenomen gefunden (130). Die Deletionen variierten in Länge und Position, befanden sich jedoch alle in einem Bereich der D2 Domäne, die als Kontaktstelle für IL-6 identifiziert wurde. Dieser Bereich beinhaltet den EF loop, dessen Konformation durch angrenzende Aminosäuren in Wildtyp gp130 stabilisiert wird. Zudem ist der EF loop über hydrophobe Wechselwirkungen mit dem BC loop der D3 Domäne verbunden. Wir stellten die Hypothese auf, dass eine inaktive gp130 Konformation durch diese Wechselwirkungen stabilisiert wird. Durch rationale strukturbasierte Mutagenese konnten wir zeigen, dass eine erhöhte Flexibilität des EF loops, als auch die Unterbrechung der hydrophoben Interaktionen zu einer liganden-unabhängigen Aktivierung von gp130 führten. Zudem können wir zeigen, dass die D1 Domäne und insbesondere die ersten N-terminalen Aminosäurereste eine wichtige Rolle bei der liganden-unabhängigen Aktivierung der gp130 Deletionsmutanten spielt. Aufgrund unserer Befunde können wir ein Modell aufstellen, das versucht, die molekularen Grundlagen der Zytokin-abhängigen, als auch der Zytokin-unabhängigen gp130-Aktivierung zu erklären und somit einen generellen Einblick in die Aktivierung von Zytokinrezeptoren liefert.

Wir waren zudem an den physiologischen Konsequenzen einer zell-autonomen, liganden-unabhängigen hepatozytären gp130 Aktivierung interessiert. Wir generierten daher transgene Mäuse mit einer Tetrazyklin-induzierbaren Expression einer kürzlich publizierten artifiziellen, konstitutiv aktiven gp130 Variante (L-gp130). Die Auswirkungen auf die Leberregeneration nach Schädigung, sowie die Entstehung von Lebertumoren sollten anhand dieses murinen Modells ermittelt werden. Im Laufe unserer Analysen zeigte sich allerdings, dass die L-gp130 Expression nicht induzierbar war und der Promotor vermutlich im Genom nicht zugänglich vorliegt. Wir arbeiten daher gerade an zwei alternativen transgenen Mausmodellen zur zell-autonomen Expression liganden-unabhängiger gp130 Varianten.

8 REFERENCES

1. Lee, F.; Yokota, T.; Otsuka, T.; Meyerson, P.; Villaret, D.; Coffman, R.; Mosmann, T.; Rennick, D.; Roehm, N.; Smith, C. *(*1986) Isolation and characterization of a mouse interleukin cDNA clone that expresses B-cell stimulatory factor 1 activities and T-cell- and mast-cell-stimulating activities. *Proc. Natl. Acad. Sci. U.S.A.* 83:2061–2065.

2. Yokota, T.; Otsuka, T.; Mosmann, T.; Banchereau, J.; DeFrance, T.; Blanchard, D.; Vries, J. E. de; Lee, F.; Arai, K. *(*1986) Isolation and characterization of a human interleukin cDNA clone, homologous to mouse B-cell stimulatory factor 1, that expresses B-cell- and T-cell-stimulating activities. *Proc. Natl. Acad. Sci. U.S.A.* 83:5894–5898.

3. Heinrich, P.C.; Behrmann, I.; Müller-Newen, G.; Schaper, F.; Graeve, L. (1998) Interleukin-6-type cytokine signalling through the gp130/Jak/STAT pathway. *Biochem. J.* 334 (Pt 2):297–314.

4. Hirano, T.; Matsuda, T.; Nakajima, K. (1994) Signal transduction through gp130 that is shared among the receptors for the interleukin 6 related cytokine subfamily. *Stem Cells.* 12(3):262-77.

5. Boulanger, M.J. (2003) Hexameric Structure and Assembly of the Interleukin-6/IL-6 -Receptor/gp130 Complex. *Science* 300:2101–2104.

6. Somers, W.; Stahl, M.; Seehra J.S. (1997) 1.9 A crystal structure of interleukin 6: implications for a novel mode of receptor dimerization and signaling. *The EMBO Journal* 16:989–997.

7. Xu, G. Y.; Yu, H. A.; Hong, J.; Stahl, M.; McDonagh, T.; Kay, L. E.; Cumming, D. A. *(*1997) Solution structure of recombinant human interleukin-6. *J Mol Biol.* 268(2):468-81.

8. Burger, R.; Neipel, F.; Fleckenstein, B.; Savino, R.; Ciliberto, G.; Kalden, J. R.; Gramatzki, M. *(*1998) Human herpesvirus type 8 interleukin-6 homologue is functionally active on human myeloma cells. *Blood* 91:1858–1863.

9. Suthaus, J.; Tillmann, A.; Lorenzen, I.; Bulanova, E.; Rose-John, S.; Scheller, J. (2010) Forced homo- and heterodimerization of all gp130-type receptor complexes leads to constitutive ligand-independent signaling and cytokine-independent growth. *Mol. Biol. Cell* 21:2797–2807.

10. Chow, D.; He, X.; Snow A.L.; Rose-John S.; Garcia K.C. (2001) Structure of an extracellular gp130 cytokine receptor signaling complex. *Science* 291:2150–2155.

11. Giese, B.; Roderburg, C.; Sommerauer, M.; Wortmann, S. B.; Metz, S.; Heinrich, P. C.; Müller-Newen, G. (2005) Dimerization of the cytokine receptors gp130 and LIFR analysed in single cells. *J. Cell. Sci.* 118:5129–5140.

12. Tenhumberg, S.; Schuster, B.; Zhu, L.; Kovaleva, M.; Scheller, J.; Kallen, K. J.; Rose-John, S. (2006) gp130 dimerization in the absence of ligand: Preformed cytokine receptor complexes. *Biochem. Biophys. Res. Commun.* 346:649–657.

13. Ward, L. D.; Howlett, G. J.; Discolo, G.; Yasukawa, K.; Hammacher, A.; Moritz, R. L.; Simpson, R. J. (1994) High affinity interleukin-6 receptor is a hexameric complex consisting of two molecules each of interleukin-6, interleukin-6 receptor, and gp-130. *J. Biol. Chem.* 269:23286–23289.

14. Paonessa, G.; Graziani, R.; Serio, A. de; Savino, R.; Ciapponi, L.; Lahm, A.; Salvati, A. L.; Toniatti, C.; Ciliberto, G. (1995) Two distinct and independent sites on IL-6 trigger gp130 dimer formation and signalling. *EMBO J.* 14:1942–1951.

15. Grötzinger, J.; Kernebeck, T.; Kallen, K.J.; Rose-John, S. (1999) IL-6 type cytokine receptor complexes: hexamer, tetramer or both? *Biol. Chem.* 380:803–813.

16. Pflanz, S.; Kurth, I.; Grötzinger, J.; Heinrich, P.C.; Müller-Newen, G. (2000) Two different epitopes of the signal transducer gp130 sequentially cooperate on IL-6-induced receptor activation. *J. Immunol.* 165:7042–7049.

17. Kallen, K. J.; Grötzinger, J.; Lelièvre, E.; Vollmer, P.; Aasland, D.; Renné, C.; Müllberg, J.; Zum Myer Büschenfelde, K. H.; Gascan, H.; Rose-John, S. (1999) Receptor recognition sites of cytokines are organized as exchangeable modules. Transfer of the leukemia inhibitory factor receptor-binding site from ciliary neurotrophic factor to interleukin-6. *J. Biol. Chem.* 274:11859–11867.

18. Heinrich, P. C.; Behrmann, I. Haan, S.; Hermanns, H. M.; Müller-Newen, G. ; Schaper, F. (2003) Principles of interleukin (IL)-6-type cytokine signalling and its regulation. *Biochem. J.* 374:1–20.

19. Lust, J. A.; Donovan, K. A.; Kline, M. P.; Greipp, P. R.; Kyle, R. A.; Maihle, N. J. (1992) Isolation of an mRNA encoding a soluble form of the human interleukin-6 receptor. *Cytokine* 4:96–100.

20. Müllberg, J.; Schooltink, H.; Stoyan, T.; Günther, M.; Graeve, L.; Buse, G.; Mackiewicz, A.; Heinrich, P. C.; Rose-John, S. (1993) The soluble interleukin-6 receptor is generated by shedding. *Eur. J. Immunol.* 23:473–480.

21. Kallen K. (2002) The role of transsignalling via the agonistic soluble IL-6 receptor in human diseases. *Biochim. Biophys. Acta* 1592:323–343.

22. Drucker, C.; Gewiese, J.; Malchow, S.; Scheller, J.; Rose-John, S. (2010) Impact of interleukin-6 classic- and trans-signaling on liver damage and regeneration. *J. Autoimmun.* 34:29–37.

23. Scheller, J.; Chalaris, A.; Schmidt-Arras, D.; Rose-John, S. (2011) The pro- and anti-inflammatory properties of the cytokine interleukin-6. *Biochim. Biophys. Acta* 1813:878–888.

24. Fischer, M.; Goldschmitt, J.; Peschel, C.; Brakenhoff, J. P.; Kallen, K. J.; Wollmer, A.; Grötzinger, J.; Rose-John, S. (1997) I. A bioactive designer cytokine for human hematopoietic progenitor cell expansion. *Nat. Biotechnol.* 15:142–145.

25. Rakemann, T.; Niehof, M.; Kubicka, S.; Fischer, M.; Manns, M. P.; Rose-John, S.; Trautwein, C. (1999) The designer cytokine hyper-interleukin-6 is a potent activator of STAT3-dependent gene transcription in vivo and in vitro. *J. Biol. Chem.* 274:1257–1266.

26. Peters, M.; Blinn, G.; Jostock, T.; Schirmacher, P.; Zum Meyer Büschenfelde, K. H.; Gall, P. R.; Rose-John, S. (1998) In vivo and in vitro activities of the gp130-stimulating designer cytokine Hyper-IL-6. *J. Immunol.* 161:3575–3581.

27. Febbraio M.A.; Pedersen B.K. (2005) Contraction-induced myokine production and release: is skeletal muscle an endocrine organ? *Exerc. Sport. Sci. Rev.* 33:114–119.

28. Diehl A.M. (2000) Cytokine regulation of liver injury and repair. *Immunol. Rev.* 174:160–171.

29. Hirano, T.; Taga, T.; Nakano, N.; Yasukawa, K.; Kashiwamura, S.; Shimizu, K.; Nakajima, K.; Pyun, K. H.; Kishimoto, T. (1985) Purification to homogeneity and characterization of human B-cell differentiation factor (BCDF or BSFp-2). *Proc. Natl. Acad. Sci. U.S.A.* 82:5490–5494.

30. Muraguchi, A.; Hirano, T.; Tang, B.; Matsuda, T.; Horii, Y.; Nakajima, K.; Kishimoto, T. (1988) The essential role of B cell stimulatory factor 2 (BSF-2/IL-6) for the terminal differentiation of B cells. *J. Exp. Med.* 167:332–344.

31. Okada, M.; Kitahara, M.; Kishimoto, S.; Matsuda, T.; Hirano, T.; Kishimoto, T. (1988) IL-6/BSF-2 functions as a killer helper factor in the in vitro induction of cytotoxic T cells. *J. Immunol.* 141:1543–1549.

32. Chomarat, P.; Banchereau, J.; Davoust, J.; Palucka, A.K. (2000) IL-6 switches the differentiation of monocytes from dendritic cells to macrophages. *Nat. Immunol.* 1:510–514.

33. Kaplanski G, Marin V, Montero-Julian F, Mantovani A, Farnarier C (2003) IL-6: a regulator of the transition from neutrophil to monocyte recruitment during inflammation. *Trends Immunol.* 24:25–29.

34. Kimura, A.; Kishimoto, T. (2010) IL-6: Regulator of Treg/Th17 balance. *Eur. J. Immunol.* 40:1830–1835.

35. Komiyama, Yutaka; Nakae, Susumu; Matsuki, Taizo; Nambu, Aya; Ishigame, Harumichi; Kakuta, Shigeru; Sudo, Katsuko; Iwakura, Yoichiro (2006) IL-17 plays an important role in the development of experimental autoimmune encephalomyelitis. *J. Immunol.* 177:566–573.

36. Nakae, S.; Nambu, A.; Sudo, K.; Iwakura, Y. (2003) Suppression of immune induction of collagen-induced arthritis in IL-17-deficient mice. *J. Immunol.* 171:6173–6177.

37. Fattori, E.; Cappelletti, M.; Costa, P.; Sellitto, C.; Cantoni, L.; Carelli, M.; Faggioni, R.; Fantuzzi, G.; Ghezzi, P.; Poli, V. (1994) Defective inflammatory response in interleukin 6-deficient mice. *J. Exp. Med.* 180:1243–1250.

38. Dalrymple, S. A.; Lucian, L. A.; Slattery, R.; McNeil, T.; Aud, D. M.; Fuchino, S.; Lee, F.; Murray, R. (1995) Interleukin-6-deficient mice are highly susceptible to Listeria monocytogenes infection: correlation with inefficient neutrophilia. *Infect. Immun.* 63:2262–2268.

39. Okuda, Y.; Sakoda, S.; Bernard, C. C.; Fujimura, H.; Saeki, Y.; Kishimoto, T.; Yanagihara, T. (1998) IL-6-deficient mice are resistant to the induction of experimental autoimmune encephalomyelitis provoked by myelin oligodendrocyte glycoprotein. *Int. Immunol.* 10:703–708.

40. Castell, J. V.; Gómez-Lechón, M. J.; David, M.; Hirano, T.; Kishimoto, T.; Heinrich, P. C. (1988) Recombinant human interleukin-6 (IL-6/BSF-2/HSF) regulates the synthesis of acute phase proteins in human hepatocytes. *FEBS Lett.* 232:347–350.

41. Gauldie, J.; Richards, C.; Harnish, D.; Lansdorp, P.; Baumann, H. (1987) Interferon beta 2/B-cell stimulatory factor type 2 shares identity with monocyte-derived hepatocyte-stimulating factor and regulates the major acute phase protein response in liver cells. *Proc. Natl. Acad. Sci. U.S.A.* 84:7251–7255.

42. Kopf, M.; Baumann, H.; Freer, G.; Freudenberg, M.; Lamers, M.; Kishimoto, T.; Zinkernagel, R.; Bluethmann, H.; Köhler, G. (1994) Impaired immune and acute-phase responses in interleukin-6-deficient mice. *Nature* 368:339–342.

43. Sekiyama, K. D.; Yoshiba, M.; Thomson, A. W. (1994) Circulating proinflammatory cytokines (IL-1 beta, TNF-alpha, and IL-6) and IL-1 receptor antagonist (IL-1Ra) in fulminant hepatic failure and acute hepatitis. *Clin. Exp. Immunol.* 98:71–77.

44. Cressman, D. E.; Greenbaum, L. E.; DeAngelis, R. A.; Ciliberto, G.; Furth, E. E.; Poli, V.; Taub, R. (1996) Liver failure and defective hepatocyte regeneration in interleukin-6-deficient mice. *Science* 274:1379–1383.

45. Peters, M.; Blinn, G.; Jostock, T.; Schirmacher, P.; Zum Meyer Büschenfelde, K. H.; Galle, P. R.; Rose-John, S. (2000) Combined Interleukin 6 and Soluble Interleukin 6 Receptor Accelerates Murine Liver Regeneration. *Gastroenterology* 119:1663–1671.

46. Wuestefeld, T.; Klein, C.; Streetz, K. L.; Betz, U.; Lauber, J.; Buer, J.; Manns, M. P.; Müller, .; Trautwein, C. *(*2003) Interleukin-6/glycoprotein 130-dependent pathways are protective during liver regeneration. *J. Biol. Chem.* 278:11281–11288.

47. Streetz, K. L.; Luedde, T.; Manns, M. P.; Trautwein, C. (2000) Interleukin 6 and liver regeneration. *Gut* 47:309–312.

48. Moh, A.; Iwamoto, Y.; Chai, G.-X.; Zhang, S. S.-M.; Kano, A.; Yang, D. D.; Zhang, W.; Wang, J.; Jacoby, J. J.; Gao, B.; Flavell, R. A.; Fu, X.-Y. (2007) Role of STAT3 in liver regeneration: survival, DNA synthesis, inflammatory reaction and liver mass recovery. *Lab. Invest* 87:1018–1028.

49. Galun, E.; Zeira, E.; Pappo, O.; Peters, M.; Rose-John, S. S (2000) Liver regeneration induced by a designer human IL-6/sIL-6R fusion protein reverses severe hepatocellular injury. *FASEB J.* 14:1979–1987.

50. Hecht, N.; Pappo, O.; Shouval, D.; Rose-John, S.; Galun, E.; Axelrod, J. H. (2001) Hyper-IL-6 gene therapy reverses fulminant hepatic failure. *Mol. Ther.* 3:683–687.

51. Maione, D.; Di Carlo, E.; Li, W.; Musiani, P.; Modesti, A.; Peters, M.; Rose-John, S.; Della Rocca, C.; Tripodi, M.; Lazzaro, D.; Taub, R.; Savino, R.; Ciliberto, G. *(*1998) Coexpression of IL-6 and soluble IL-6R causes nodular regenerative hyperplasia and adenomas of the liver. *EMBO J.* 17:5588–5597.

52. Schirmacher, P.; Peters, M.; Ciliberto, G.; Blessing, M.; Lotz, J.; Zum Meyer Büschenfelde, K. H.; Rose-John, S. *(*1998) Hepatocellular hyperplasia, plasmacytoma formation, and extramedullary hematopoiesis in interleukin (IL)-6/soluble IL-6 receptor double-transgenic mice. *Am. J. Pathol* 153:639–648.

53. Malaguarnera, M.; Di Fazio, I.; Romeo, M. A.; Restuccia, S.; Laurino, A.; Trovato, B. A. (1997) Elevation of interleukin 6 levels in patients with chronic hepatitis due to hepatitis C virus. *J. Gastroenterol.* 32:211-5.

54. Sheron, N.; Bird, G.; Goka, J.; Alexander, G.; Williams, R. (1991) Elevated plasma interleukin-6 and increased severity and mortality in alcoholic hepatitis. *Clin. Exp. Immunol.* 84:449–453.

55. Deviere, J.; Content, J.; Denys, C.; Vandenbussche, P.; Schandene, L.; Wybran, J.; Dupont, E. (1989) High interleukin-6 serum levels and increased production by leucocytes in alcoholic liver cirrhosis. Correlation with IgA serum levels and lymphokines production. *Clin. Exp. Immunol.* 77:221–225.

56. Genesca, J.; Gonzalez, A.; Segura, R.; Catalan, R.; Marti, R.; Varela, E.; Cadelina, G.; Martinez, M.; Lopez-Talavera, J. C.; Esteban, R.; Groszmann, R. J.; Guardia, J. (1999) Interleukin-6, nitric oxide, and the clinical and hemodynamic alterations of patients with liver cirrhosis. *Am. J. Gastroenterol.* 94:169-77.

57. Giannitrapani, L.; Cervello, M.; Soresi, M.; Notarbartolo, M.; La Rosa, M.; Virruso, L.; D'Alessandro, N.; Montalto, G. *(*2002) Circulating IL-6 and sIL-6R in patients with hepatocellular carcinoma. *Ann. N. Y. Acad. Sci* 963:46–52.

58. Soresi, Maurizio; Giannitrapani, Lydia; D'Antona, Fabio; Florena, Ada-Maria; La Spada, Emanuele; Terranova, Angela; Cervello, Melchiorre; D'Alessandro, Natale; Montalto, Giuseppe (2006) Interleukin-6 and its soluble receptor in patients with liver cirrhosis and hepatocellular carcinoma. *World J. Gastroenterol* 12:2563–2568.

59. Goydos, J. S.; Brumfield, A. M.; Frezza, E.; Booth, A.; Lotze, M. T.; Carty, S. E. (1998) Marked elevation of serum interleukin-6 in patients with cholangiocarcinoma: validation of utility as a clinical marker. *Ann. Surg.* 227:398–404.

60. Malaguarnera, M.; Di Fazio, I.; Romeo, M. A.; Restuccia, S.; Laurino, A.; Trovato, B. A. (1997) Elevation of interleukin 6 levels in patients with chronic hepatitis due to hepatitis C virus. *J. Gastroenterol.* 32:211-5.

61. Becker, C.; Fantini, M. C.; WIRTZ, S.; Nikolaev, A.; Lehr, H. A.; Galle, P. R.; Rose-John, S.; Neurath, M. F. (2005) IL-6 signaling promotes tumor growth in colorectal cancer. *Cell Cycle* 4:217–220.

62. Senn, J. J.; Klover, P. J.; Nowak, I. A.; Mooney, R. A. (2002) Interleukin-6 induces cellular insulin resistance in hepatocytes. *Diabetes* 51:3391–3399.

63. Wallenius, V.; Wallenius, K.; Ahrén, B.; Rudling, M.; Carlsten, H.; Dickson, S. L.; Ohlsson, C.; Jansson, J.-O. *(*2002) Interleukin-6-deficient mice develop mature-onset obesity. *Nat. Med.* 8:75–79.

64. Grossman, R. M.; Krueger, J.; Yourish, D.; Granelli-Piperno, A.; Murphy, D. P.; May, L. T.; Kupper, T. S.; Sehgal, P. B.; Gottlieb, A. B. *(*1989) Interleukin 6 is expressed in high levels in psoriatic skin and stimulates proliferation of cultured human keratinocytes. *Proc. Natl. Acad. Sci. U.S.A.* 86:6367–6371.

65. Park, J. Y.; Pillinger, M.H. (2007) Interleukin-6 in the pathogenesis of rheumatoid arthritis. *Bull NYU Hosp Jt Dis*. 65 Suppl 1:S4-10.

66. Schieffer, B.; Selle, T.; Hilfiker, A.; Hilfiker-Kleiner, D.; Grote, K.; Tietge, U. J. F.; Trautwein, C.; Luchtefeld, M.; Schmittkamp, C.; Heeneman, S.; Daemen, M. J. A. P.; Drexler, H.(2004) Impact of interleukin-6 on plaque development and morphology in experimental atherosclerosis. *Circulation*. 110:3493-500.

67. Chung, Y,; Chang; Y: (2003) Serum interleukin-6 levels reflect the disease status of colorectal cancer. *J. Surg. Oncol*. 83:222–226.

68. Miki S *et al. (*1989) Interleukin-6 (IL-6) functions as an in vitro autocrine growth factor in renal cell carcinomas. *FEBS Lett*. 250:607–610.

69. Kawano, M.; Hirano, T.; Matsuda, T.; Taga, T.; Horii, Y.; Iwato, K.; Asaoku, H.; Tang, B.; Tanabe, O.; Tanaka, H. (1988) Autocrine generation and requirement of BSF-2/IL-6 for human multiple myelomas. *Nature* 332:83–85.

70. Dauer, Daniel J.; Ferraro, Bernadette; Song, Lanxi; Yu, Bin; Mora, Linda; Buettner, Ralf; Enkemann, Steve; Jove, Richard; Haura, Eric B. *(*2005) Stat3 regulates genes common to both wound healing and cancer. *Oncogene* 24:3397–3408.

71. Hirano, T.; Ishihara, K.; Hibi, M. (2000) Roles of STAT3 in mediating the cell growth, differentiation and survival signals relayed through the IL-6 family of cytokine receptors. *Oncogene*. 15;19(21):2548-56.

72. Niu, G.; Wright, K. L.; Huang, M.; Song, L.; Haura, E.; Turkson, J.; Zhang, S.; Wang, T.; Sinibaldi, D.; Coppola, D.; Heller, R.; Ellis, L. M.; Karras, J.; Bromberg, J.; Pardoll, D.; Jove, R.; Yu, H. *(*2002) Constitutive Stat3 activity up-regulates VEGF expression and tumor angiogenesis. *Oncogene* 21:2000–2008.

73. Abdulghani, J.; Gu, L.; Dagvadorj, A.; Lutz, J.; Leiby, B.; Bonuccelli, G.; Lisanti, M. P.; Zellweger, T.; Alanen, K.; Mirtti, T.; Visakorpi, T.; Bubendorf, L.; Nevalainen, M. T. *(*2008) Stat3 promotes metastatic progression of prostate cancer. *AM. J. Pathol*. 2(6):1717-28.

74. Bollrath, J.; Phesse, T. J.; Burstin, V. A. von; Putoczki, T.; Bennecke, M.; Bateman, T.; Nebelsiek, T.; Lundgren-May, T.; Canli, O.; Schwitalla, S.; Matthews, V.; Schmid, R.M.; Kirchner, T.s; Arkan, M. C.; Ernst, M.; Greten, F. R. *(*2009) gp130-mediated Stat3 activation in enterocytes regulates cell survival and cell-cycle progression during colitis-associated tumorigenesis. *Cancer Cell* 15:91–102.

75. Li, S.; Wang, N.; Brodt, P.; (2012) Metastatic cells can escape the proapoptotic effects of TNF-α through increased autocrine IL-6/STAT3 signaling. *Cancer Res*. 72:865–875.

76. Huang, H. F.; Murphy, T. F.; Shu, P.; Barton, A. B.; Barton, B. E. (2005) Stable expression of constitutively-activated STAT3 in benign prostatic epithelial cells changes their phenotype to that resembling malignant cells. *Mol. Cancer*. 12;4(1):2.

77. Wu, W.-Y.; Li, J.; Wu, Z.-S.; Zhang, C.-L.; Meng, X.-L. (2011) STAT3 activation in monocytes accelerates liver cancer progression. *BMC Cancer* 11:506.

78. Walker, S.R.; Nelson, E. A.; Zou, L.; Chaudhury, M.; Signoretti, S.; Richardson, A.; Frank, D. A. (2009) Reciprocal effects of STAT5 and STAT3 in breast cancer. *Mol. Cancer Res*. 7:966–976.

79. Barton, B.E.; Karras, J. G.; Murphy, T. F.; Barton, A.; Huang, H. F-S. (2004) Signal transducer and activator of transcription 3 (STAT3) activation in prostate cancer: Direct STAT3 inhibition induces apoptosis in prostate cancer lines. *Mol. Cancer. Ther*. 3(1):11-20.

80. Vogan, K. (2012) STAT3 activation in rare T-cell leukemia. *Nat Genet* 44:739.

81. Corvinus, F.M.; Orth, C.; Moriggl, R.; Tsareva, S. A.; Wagner, S.; Pfitzner, E. B.; Baus, D.; Kaufmann, R.; Huber, L. A.; Zatloukal, K.; Beug, H.; Ohlschläger, P.; Schütz, A.; Halbhuber, K.-J.; Friedrich, K. *(*2005) Persistent STAT3 activation in colon cancer is associated with enhanced cell proliferation and tumor growth. *Neoplasia.* 7(6):545-55

82. Jarnicki, A.; Putoczki, T.; Ernst, M. (2010) Stat3: linking inflammation to epithelial cancer - more than a "gut" feeling? *Cell Div* 5:14.

83. Grivennikov, S.; Karin, E.; Terzic, J.; Mucida, D.; Yu, G.-Y.; Vallabhapurapu, S.; Scheller, J.; Rose-John, S.; Cheroutre, H.; Eckmann, L.; Karin, M. (2009) IL-6 and Stat3 are required for survival of intestinal epithelial cells and development of colitis-associated cancer. *Cancer Cell* 15:103–113.

84. Yu, H.; Pardoll, D.; Jove, R. (2009) STATs in cancer inflammation and immunity: a leading role for STAT3. *Nat Rev Cancer* 9:798–809.

85. Pilati, C.; Amessou, M.; Bihl, M. P.; Balabaud, C.; van Nhieu, J. T.; Paradis, V.; Nault, J. C.; Izard, T.; Bioulac-Sage, P.; Couchy, G.; Poussin, K.; Zucman-Rossi, J. *(*2011) Somatic mutations activating STAT3 in human inflammatory hepatocellular adenomas. *J. Exp. Med.* 208(7):1359-66

86. He, G.; Karin M. (2010) NF-κB and STAT3 – key players in liver inflammation and cancer. *Cell Res* 21:159–168.

87. Besser, D.; Bromberg, J.F.; Darnell, J.E.; Hanafusa, H. (1999) A single amino acid substitution in the v-Eyk intracellular domain results in activation of Stat3 and enhances cellular transformation. *Mol. Cell. Biol.* 19:1401–1409.

88. Bromberg, J. F.; Wrzeszczynska, M. H.; Devgan, G.; Zhao, Y.; Pestell, R. G.; Albanese, C.; Darnell, J. E. (1999) Stat3 as an Oncogene. *Cell.* 98(3):295-303.

89. La Iglesia, N. de; Konopka, G.; Puram, S. V.; Chan, J. A.; Bachoo, R. M.; You, M. J.; Levy, D.E.; DePinho, R. A.; Bonni, A. *(*2008) Identification of a PTEN-regulated STAT3 brain tumor suppressor pathway. *Genes Dev.* 22:449–462.

90. Ecker, A.; Simma, O.; Hoelbl, A.; Kenner, L.; Beug, H.; Moriggl, R.; Sexl, V. *(*2009) The dark and the bright side of Stat3: proto-oncogene and tumor-suppressor. *Front. Biosci.* 14:2944-58.

91. Starr, R.; Willson, T. A.; Viney, E. M.; Murray, L. J.; Rayner, J. R.; Jenkins, B. J.; Gonda, T. J.; Alexander, W. S.; Metcalf, D.; Nicola, N. A.; Hilton, D. J. *(*1997) A family of cytokine-inducible inhibitors of signalling. *Nature* 387:917–921.

92. Lang, R.; Pauleau, A.-L.; Parganas, E.; Takahashi, Y.; Mages, J.; Ihle, J. N.; Rutschman, R.; Murray, P. J. (2003) SOCS3 regulates the plasticity of gp130 signaling. *Nat. Immunol.* 4:546–550.

93. Sasaki, A.; Yasukawa, H.; Suzuki, A.; Kamizono, S.; Syoda, T.; Kinjyo, I.; Sasaki, M.; Johnston, J. A.; Yoshimura, A. (1999) Cytokine-inducible SH2 protein-3 (CIS3/SOCS3) inhibits Janus tyrosine kinase by binding through the N-terminal kinase inhibitory region as well as SH2 domain. *Genes Cells* 4:339–351.

94. Kamura, T.; Sato, S.; Haque, D.; Liu, L.; Kaelin, W. G.; Conaway, R. C.; Conaway, J. W. (1998) The Elongin BC complex interacts with the conserved SOCS-box motif present in members of the SOCS, ras, WD-40 repeat, and ankyrin repeat families. *Genes Dev.* 12:3872–3881.

95. Zhang, J. G.; Farley, A.; Nicholson, S. E.; Willson, T. A.; Zugaro, L. M.; Simpson, R. J.; Moritz, R. L.; Cary, D.; Richardson, R.; Hausmann, G.; Kile, B. J.; Kent, S. B.; Alexander, W. S.; Metcalf, D.; Hilton, D. J.; Nicola, N. A.; Baca, M. (1999) The conserved SOCS box motif in suppressors of cytokine signaling binds to elongins B and C and may couple bound proteins to proteasomal degradation. *Proc. Natl. Acad. Sci. U.S.A.* 96:2071–2076.

96. Roberts, A. W.; Robb, L.; Rakar, S.; Hartley, L.; Cluse, L.; Nicola, N. A.; Metcalf, D.; Hilton, D. J.; Alexander, W. S. *(*2001) Placental defects and embryonic lethality in mice lacking suppressor of cytokine signaling 3. *Proc. Natl. Acad. Sci. U.S.A.* 98:9324–9329.

97. Takahashi, Yutaka; Carpino, Nick; Cross, James C.; Torres, Miguel; Parganas, Evan; Ihle, James N. (2003) SOCS3: an essential regulator of LIF receptor signaling in trophoblast giant cell differentiation. *EMBO J.* 22:372–384.

98. Ogata, H.; Kobayashi, T.; Chinen, T.; Takaki, H.; Sanada, T.; Minoda, Y.; Koga, K.; Takaesu, G.; Maehara, Y.; Iida, M.; Yoshimura, A. (2006) Deletion of the SOCS3 Gene in Liver Parenchymal Cells Promotes Hepatitis–Induced Hepatocarcinogenesis. *Gastroenterology* 131:179–193.

99. Ogata, H.; Chinen, T.; Yoshida, T.; Kinjyo, I.; Takaesu, G.; Shiraishi, H.; Iida, M.; Kobayashi, T.; Yoshimura, A. *(*2006) Loss of SOCS3 in the liver promotes fibrosis by enhancing STAT3-mediated TGF-beta1 production. *Oncogene* 25:2520–2530.

100. Tebbutt, N.C.; Giraud, A. S.; Inglese, M.; Jenkins, B.; Waring, P.; Clay, F. J.; Malki, S.; Alderman, B. M.; Grail, D.; Hollande, F.; Heath, J. K.; Ernst, M. *(*2002) Reciprocal regulation of gastrointestinal homeostasis by SHP2 and STAT-mediated trefoil gene activation in gp130 mutant mice. *Nat Med* 8:1089–1097.

101. Jenkins, B.J.; Grail, D.; Nheu, T.; Najdovska, M.; Wang, B.; Waring, P.; Inglese, M.; McLoughlin, R. M.; Jones, S.A.; Topley, N.; Baumann, H.; Judd, L.M.; Giraud, A. S.; Boussioutas, A.; Zhu, H.-J.; Ernst, M. *(*2005) Hyperactivation of Stat3 in gp130 mutant mice promotes gastric hyperproliferation and desensitizes TGF-β signaling. *Nat Med* 11:845–852.

102. Betz, U. A.; Bloch, W.; van den Broek, M.; Yoshida, K.; Taga, T.; Kishimoto, T.; Addicks, K.; Rajewsky, K.; Müller, W. *(*1998) Postnatally induced inactivation of gp130 in mice results in neurological, cardiac, hematopoietic, immunological, hepatic, and pulmonary defects. *J. Exp. Med.* 188:1955–1965.

103. Streetz, K. L.; Tacke, F.; Leifeld, L.; Wüstefeld, T.; Graw, A.; Klein, C.; Kamino, K.; Spengler, U.; Kreipe, H.; Kubicka, S.; Müller, W.r; Manns, M.l P.; Trautwein, C. (2003) Interleukin 6/gp130-dependent pathways are protective during chronic liver diseases. *Hepatology* 38:218–229.

104. Klein, C.; Wüstefeld, T.; Assmus, U.; Roskams, T.; Rose-John, S.; Müller, M.; Manns, M. P.; Ernst, M.; Trautwein, C. (2005) The IL-6-gp130-STAT3 pathway in hepatocytes triggers liver protection in T cell-mediated liver injury. *J. Clin. Invest.* 115:860–869.

105. Dierssen, U.; Beraza, N.; Lutz, H.H.; Liedtke, C.; Ernst, M.; Wasmuth, H. E.; Trautwein, C. (2008) Molecular dissection of gp130-dependent pathways in hepatocytes during liver regeneration. *J. Biol. Chem.* 283:9886–9895.

106. Bravo, J.; Staunton, D.; Heath, J.K.; Jones, E.Y. (1998) Crystal structure of a cytokine-binding region of gp130. *EMBO J.* 17:1665–1674.

107. Horsten, U.; Müller-Newen, G.; Gerhartz, C.; Wollmer, A.; Wijdenes, J.; Heinrich, P. C.; Grötzinger, J. *(*1997) Molecular modeling-guided mutagenesis of the extracellular part of gp130 leads to the identification of contact sites in the interleukin-6 (IL-6).IL-6 receptor.gp130 complex. *J. Biol. Chem.* 272:23748–23757.

108. Kurth, I.; Horsten, U.; Pflanz, S.; Timmermann, A.; Küster, A.; Dahmen, H.; Tacken, I.; Heinrich, P. C.; Müller-Newen, G. (2000) Importance of the membrane-proximal extracellular domains for activation of the signal transducer glycoprotein 130. *J. Immunol.* 164:273–282.

109. Lorenzen, I.; Shang, W.; Perbandt, M.; Petoukhov, M. V.; Svergun, D.I.; Waetzig, G. H.; Rose-John, S.; Hilgenfeld, R.; Grötzinger, J.*(*2011) The structure of the unliganded extracellular domain of the interleukin-6 signal transducer gp130 in solution. *Eur. J. Cell Biol.* 90:515–520.

110. Varghese, J. N.; Moritz, R. L.; Lou, M-Z; van Donkelaar, A.; Ji, H.; Ivancic, N.; Branson, K. M.; Hall, N. E.; Simpson, R. J. (2002) Structure of the extracellular domains of the human interleukin-6 receptor alpha -chain. *Proc. Natl. Acad. Sci. U.S.A.* 99:15959–15964.

111. Kurth, I.; Horsten, U.; Pflanz, S.; Dahmen, H.; Küster, A.; Grötzinger, J.; Heinrich, P. C.; Müller-Newen, G. (1999) Activation of the signal transducer glycoprotein 130 by both IL-6 and IL-11 requires two distinct binding epitopes. *J. Immunol.* 162:1480–1487.

112. Boulanger, M. J.; Garcia, K. C. (2004) Shared cytokine signaling receptors: structural insights from the gp130 system. *Adv. Protein Chem.* 68:107–146.

113. Chow, D.; Ho, J.; Nguyen Pham, T.L.; Rose-John, S.; Garcia, K.C. (2001) In Vitro Reconstitution of Recognition and Activation Complexes between Interleukin-6 and gp130. *Biochemistry* 40:7593–7603.

114. Boulanger, M.J.; Bankovich, A.J.; Kortemme, T.; Baker, D.; Garcia, K.C. (2003) Convergent mechanisms for recognition of divergent cytokines by the shared signaling receptor gp130. *Mol. Cell* 12:577–589.

115. Murakami, M.; Hibi, M.; Nakagawa, N.; Nakagawa, T.; Yasukawa, K.; Yamanishi, K.; Taga, T.; Kishimoto, T. (1993) IL-6-induced homodimerization of gp130 and associated activation of a tyrosine kinase. *Science* 260:1808–1810.

116. Kramer, J.M.; Hanel, W.; Shen, F.; Isik, N.; Malone, J. P.; Maitra, A.; Sigurdson, W.; Swart, D.; Tocker, J.; Jin, T.; Gaffen, S. L. *(*2007) Cutting edge: identification of a pre-ligand assembly domain (PLAD) and ligand binding site in the IL-17 receptor. *J. Immunol.* 179:6379–6383.

117. Naismith, J. H.; Brandhuber, B. J.; Devine, T. Q.; Sprang, S. R. (1996) Seeing double: crystal structures of the type I TNF receptor. *J. Mol. Recognit.* 9:113:7

118. Krause CD *et al. (*2006) Preassembly and ligand-induced restructuring of the chains of the IFN-gamma receptor complex: the roles of Jak kinases, Stat1 and the receptor chains. *Cell Res.* 16:55–69.

119. Chevalier, S.; Fourcin, M.; Robledo, O.; Wijdenes, J.; Pouplard-Barthelaix, A.; Gascan, H. *(*1996) Interleukin-6 family of cytokines induced activation of different functional sites expressed by gp130 transducing protein. *J. Biol. Chem.* 271:14764–14772.

120. Wijdenes, J.; Heinrich, P. C.; Müller-Newen, G.; Roche, C.; Gu, Z. J.; Clément, C.; Klein, B. *(*1995) Interleukin-6 signal transducer gp130 has specific binding sites for different cytokines as determined by antagonistic and agonistic anti-gp130 monoclonal antibodies. *Eur. J. Immunol.* 25:3474–3481.

121. Rebouissou, S.; Amessou, M.; Couchy, G.; Poussin, K.; Imbeaud, S.e; Pilati, C.; Izard, T.; Balabaud, C.; Bioulac-Sage, P.; Zucman-Rossi, J. *(*2008) Frequent in-frame somatic deletions activate gp130 in inflammatory hepatocellular tumours. *Nature* 457:200–204.

122. La Coste, A. de; Romagnolo, B.; Billuart, P.; Renard, C. A.; Buendia, M. A.; Soubrane, O.; Fabre, M.; Chelly, J.; Beldjord, C.; Kahn, A.; Perret, C. *(*1998) Somatic mutations of the beta-catenin gene are frequent in mouse and human hepatocellular carcinomas. *Proc. Natl. Acad. Sci. U.S.A.* 95:8847–8851.

123. Stuhlmann-Laeisz, C; Lang, S.; Chalaris, A.; Krzysztof, P.; Enge, S.; Eichler, J.; Klingmüller, U.; Samuel, M.; Ernst, M.; Rose-John, S.; Scheller, J.*(*2006) Forced dimerization of gp130 leads to constitutive STAT3 activation, cytokine-independent growth, and blockade of differentiation of embryonic stem cells. *Mol. Biol. Cell* 17:2986–2995.

124. Gossen, M.; Bujard, H. (1992) Tight control of gene expression in mammalian cells by tetracycline-responsive promoters. *Proc. Natl. Acad. Sci. U.S.A.* 89:5547–5551.

125. Shockett, P.; Difilippantonio, M.; Hellman, N.; Schatz, D.G. (1995) A modified tetracycline-regulated system provides autoregulatory, inducible gene expression in cultured cells and transgenic mice. *Proc. Natl. Acad. Sci. U.S.A* 92:6522–6526.

126. Schönig, K.; Schwenk, F.; Rajewsky, K.; Bujard, H. (2002) Stringent doxycycline dependent control of CRE recombinase in vivo. *Nucleic Acids Res.* 30:e134.

127. Hasan, M.T.; Schönig, K.; Berger, S.; Graewe, W.; Bujard, H. (2001) Long-term, noninvasive imaging of regulated gene expression in living mice. *Genesis* 29:116–122.

128. Ketteler, R.; Glaser, S.; Sandra, O.; Martens, U. M.; Klingmüller, U. (2002) Enhanced transgene expression in primitive hematopoietic progenitor cells and embryonic stem cells efficiently transduced by optimized retroviral hybrid vectors. *Gene Ther.* 9:477–487.

129. Auguste, P.; Guillet, C.; Fourcin, M.; Olivier, C.; Veziers, J.; Pouplard-Barthelaix, A.; Gascan, H. (1997) Signaling of type II oncostatin M receptor. *J. Biol. Chem.* 272:15760–15764.

130. Rebouissou, S.; Amessou, M.; Couchy, G.; Poussin, K.; Imbeaud, S.e; Pilati, C.; Izard, T.; Balabaud, C.; Bioulac-Sage, P.; Zucman-Rossi, J. *(*2008) Frequent in-frame somatic deletions activate gp130 in inflammatory hepatocellular tumours. *Nature* 457:200–204.

131. Kernebeck, T.; Pflanz, S.; Müller-Newen, G.; Kurapkat, G.; Scheek, R. M.; Dijkstra, K.; Heinrich, P. C.; Wollmer, A.; Grzesiek, S.; Grötzinger, J. *(*1999) The signal transducer gp130: solution structure of the carboxy-terminal domain of the cytokine receptor homology region. *Protein Sci.* 8:5–12.

132. Pflanz, S.; Kernebeck, T.; Giese, B.; Herrmann, A.; Pachta-Nick, M.; Stahl, J.; Wollmer, A.; Heinrich, P. C.; Müller-Newen, G.; Grötzinger, J. *(*2001) Signal transducer gp130: biochemical characterization of the three membrane-proximal extracellular domains and evaluation of their oligomerization potential. *Biochem. J.* 356:605–612.

133. Sommer, J.; Effenberger, T.; Volpi, E.; Waetzig, G. H.; Bernhardt, M.; Suthaus, J.; Garbers, C.; Rose-John, S.; Floss, D. M.; Scheller, J. *(*2012) Constitutively Active Mutant gp130 Receptor Protein from Inflammatory Hepatocellular Adenoma Is Inhibited by an Anti-gp130 Antibody That Specifically Neutralizes Interleukin 11 Signaling. *J. Biol.Chem.*287:13743–13751.

134. Wijdenes, J.; Heinrich, P. C.; Müller-Newen, G.; Roche, C.; Gu, Z. J.; Clément, C.; Klein, B. (1995) Interleukin-6 signal transducer gp130 has specific binding sites for different cytokines as determined by antagonistic and agonistic anti-gp130 monoclonal antibodies. *Eur. J. Immunol.* 25:3474–3481.

135. Chevalier, S.; Fourcin, M.; Robledo, O.; Wijdenes, J.; Pouplard-Barthelaix, A.; Gascan, H. (1996) Interleukin-6 family of cytokines induced activation of different functional sites expressed by gp130 transducing protein. *J. Biol. Chem.* 271:14764–14772.

136. Lebeau, B.; Montero Julian, F. A.; Wijdenes, J.; Müller-Newen, G.; Dahmen, H.; Chérel, M.; Heinrich, P. C.; Brailly, H.; Hallet, M. M.; Godard, A.; Minvielle, S.; Jacques, Y. *(*1997) Reconstitution of two isoforms of the human interleukin-11 receptor and comparison of their functional properties. *FEBS Lett.* 407:141–147.

137. Liu, F.; Song, Y.; Liu, D. (1999) Hydrodynamics-based transfection in animals by systemic administration of plasmid DNA. *Gene Ther.* 6:1258–1266.

138. Neurath, M.F.; Finotto, S. (2011) IL-6 signaling in autoimmunity, chronic inflammation and inflammation-associated cancer. *Cytokine Growth Factor Rev.* 22:83–89.

139. Bravo, J.; Staunton, D.; Heath, J. K.; Jones, E. Y. (1998) Crystal structure of a cytokine-binding region of gp130. *EMBO J.* 6:1665-1674

140. Schirmacher, P.; Peters, M.; Ciliberto, G.; Blessing, M.; Lotz, J.; Zum Meyer Büschenfelde, K. H.; Rose-John, S. (1998) Hepatocellular Hyperplasia, Plasmacytoma Formation, and Extramedullary Hematopoiesis in Interleukin (IL)-6/Soluble IL-6 Receptor Double-Transgenic Mice. *Am. J. Pathol.* 2:639-648.

141. Ni, H.; Ding, N.; Harper, M.J.; Yang, Z. (2002) Expression of leukemia inhibitory factor receptor and gp130 in mouse uterus during early pregnancy. *Mol. Reprod. Dev.* 63:143–150.

142. Ernst, E.; Schönig, K.; Bugert, J. J.; Bläker, H.; Pfaff, E.; Stremmel, W.; Encke, J. *(*2007) Generation of inducible hepatitis C virus transgenic mouse lines. *J. Med. Virol.* 79:1103–1112.

143. Dumortier, J.; Schönig, K.; Oberwinkler, H.; Löw, R.; Giese, T.; Bujard, H.; Schirmacher, P.; Protzer, U. (2005) Liver-specific expression of interferon γ following adenoviral gene transfer controls hepatitis B virus replication in mice *Gene Ther* 12:668–677.

144. Grivennikov, S.; Karin, M.(2008) Autocrine IL-6 Signaling: A Key Event in Tumorigenesis? *Cancer Cell* 13:7–9.

9 APPENDIX

9.1 Abbreviations

A	
Aa	Amino Acid
Ab	antibody
ADAM	A Disintegrin and Metalloprotease
APP	Acute Phase Protein
APR	Acute Phase Response
APS	Ammonium persulfate
Asp	Aspartatic Acid
B	
BiFC	bimolecular fluorescence complementation
bp	Base Pairs
BSA	Bovine Serum Albumin
C	
CBM	Cytokine Binding Module
cDNA	Complementary DNA
CIAP	Calf Intestine Al kali ne Phosphatase
CLC	Cardiotrophin-Like Cytokine
CNTF	Ciliary Neutrotrophic Factor
CRP	C-Reactive Protein
CT-1	Cardiothrophin-1
Cys	Cysteine
D	
dl	Deciliter
DNA	Deoxyribonucleic Acid
dNTP	2'-Desoxyribonucleotide-5'-Triphosphate
Dox	Doxycycline
DTT	Dithithreitol
E	
EAE	Experimental Autoimmune Encephalomyelitis
ECD	Extracellular domain
ECL	Electrochemiluminescence
EDTA	Ethylenediaminetetraacetic Acid
EGTA	Ethylene glycol tetraacetic acid
ELISA	Enzyme Linked Immunosorbent Assay

ERK	Extracellular Signal Regulated Kinase
F	
FACS	Fluorescence Activated Cell Sorter
Fc	Fragment Crystallizable
f.c.	final concentration
FCS	Fetal calf serum
FN III	Fibronectin Type III
FRET	Förster resonance energy transfer
G	
GFP	green fluorescent protein
Glu	Glutamic Acid
gp130	Glycoprotein 130
GPL	gp130-like receptor
Grb2	Growth Factor Receptor Bound Protein 2
H	
H	Hour
hCMV	Human cytomegalie virus
HEPES	2-(4-(2-Hydroxyethyl)-1-piperazinyl)-ethansulfonsäure
HepG2	hepatocellular carcinoma
HEK	human embryo kidney
HIL-6	Hyper-IL-6
I	
ICD	Intracellular Domain
IgD	Immunoglobulin-like Domain
IL	Interleukin
IL-6R	Interleukin-6 Receptor
IP	Immunoprecipitation
i.p.	Intraperitoneal Injection
IVC	Isolated Ventilated Cages
J	
JAK	Janus kinase
K	
kb	Kilobase Pairs
kDa	Kilodalton
kg	Kilogram
L	
L	Liter
LB	Lysogeny Broth

Lap	Liver enriched activator protein
LIF	leukemia inhibitory factor
Luc	Luciferase
M	
mAb	Monoclonal Antibody
MAPK	Mitogen-activated protein kinase
mEF	Mouse embryonic fibroblasts
mIL-3	Murine interleukine-3
min	Minute
mg	Milligram
ml	Milliliter
mRNA	Messenger RNA
MTT	3-(4,5-Dimethylthiazol-2-yl)-2,5-diphenyltetrazolium bromide
µ	micro
N	
NaF	Sodium fluoride
Na_3VO_4	Sodium orthovanadate
NP	Neuropoietin
NP-40	nonyl phenoxypolyethoxylethanol
n.t.	non-transfected/ non-transduced
O	
OD	Optic Density
OSM	Oncostatin M
P	
Phe	Phenylalanine
Pen/ Strep	Penicillin/ Streptomycin
P6	Pyridone 6
PBS	Phosphate Buffered Saline
PCR	Polymerase Chain Reaction
PMSF	Phenylmethanesulfonylfluoride
POD	Peroxidase
Pro	Proline
P-STAT3	Phospho-STAT3
PVDF	Polyvinylidene Fluoride
R	
RA	Rheumatoid Arthritis
RNA	Ribonucleic Acid
RLU	Relative light units

RT	Room Temperature
RT-PCR	Reverse Transcriptase PCR
S	
SAA	Serum Amyloid A
SDS	Sodium Dodecyl Sulfate
Ser	Serine
SFM	Serum free medium
SH2	Src homology domain 2
SHP-2	Src homology protein 2 tyrosine phosphatase-2
SIEM-Luc	sis-inducible element; STAT3 reporter with firefly luciferase
sIL-6R	soluble IL-6R
SOCS3	Suppressor of cytokine signaling 3
SSC	Saline-sodium citrate
STAT3	Signal transducer and activator of transcription 3
T	
TEMED	Tetramethylethylenediamine
Tet	Tetracycline
TetR	Tet repressor protein
TK-RL	Thymidin-Kinase-Renilla-Luciferase
TRE	Tetracycline responsive element
Tris	tris(hydroxymethyl)aminomethane
tTA	Tetracycline transactivator protein
rtTA	Reverse tetracycline transactivator protein
Tyr	Tyrosine
U	
U	Unit(s)
UV	Ultraviolet
V	
V	Volt
Val	Valine
v/v	Volume per Volume
vIL-6	Viral interleukin-6
VP16	Herpes simplex virus protein
W	
w/v	Weight per Volume
WT	Wildtype
WB	Western blot
w/o	without

Y

YFP	Yellow fluorescent protein

9.2 Publications

Paper

Selleng, K.; **Schütt, A.**; Selleng, S.; Warkentin, T.E.; Greinacher, A.: Studies of the anti-platelet factor 4/heparin immune response: adapting the enzyme-linked immunosorbent spot assay for detection of memory B cells against complex antigen. Transfusion. 2010 Jan; 50(1):32-9.

Poster

Schütt A., Scheller J., Rose-John S.: Constitutive active gp130 in the liver and its connection to chronic inflammation and carcinoma development. FALK Workshop Immunology and liver disease, Hannover, 10/2009

Schütt A., Horn S., Rose-John S. and Schmidt-Arras D.: Structural analysis of an oncogenic gp130 deletion mutant. FALK Workshop Inflammation and Cancer, Hamburg, 01/2012

Talks

Schütt A.: Transgenic model with liver specific cell autonomous gp130 activation: consequences for liver regeneration. Congress "Cytokines", Chicago, 10/2010

9.3 Curriculum vitae

Name:	Antje Michaela Schütt
Geburtstag:	06/04/1983
Geburtsort:	Lutherstadt Wittenberg
Staatsangehörigkeit:	deutsch

01/08 – 11/12	Anfertigung der Doktorarbeit im Biochemischen Institut der medizinischen Fakultät der Universität Kiel bei Prof. Dr. Rose-John Titel: "Biochemical and physiological analysis of oncogenic constitutive active variants of gp130"
10/06 – 10/07	Anfertigung der Diplomarbeit im Institut für Immunologie und Transfusionsmedizin der Universität Greifswald bei Prof. Dr. Greinacher Titel: „Etablierung eines Antigen-spezifischen ELISPOT-Assays zum Nachweis von PF4/Heparin-Antikörper produzierenden B-Zellen" (Note: 1,5)
10/02 – 10/07	Studium der Humanbiologie an der Universität Greifswald Abschluss: Diplom (Note: 1,6) Hauptfach: Immunologie Nebenfächer: Pharmakologie/Toxikologie, Funktionelle Morphologie des Menschen
08/93 - 04/02	Gymnasium Philipp-Melanchthon, Lutherstadt Wittenberg Abschluss: Abitur (Note 1,7)
08/91 - 08/93	Grundschule August-Bebel, Wittenberg
08/89 - 08/91	Grundschule Rosa-Luxemburg, Wittenberg

9.4 Acknowledgement

Sehr herzlich bedanken möchte ich mich bei Herrn Prof. Stefan Rose-John für die freundlich Aufnahme in seinem Institut sowie für die fachliche Unterstütztung während meiner Promotionszeit.

Besonderer Dank gilt auch Herrn Dr. Dirk Schmidt-Arras für die Übernahme und Betreuung dieser Promotion und die interessanten wie auch anregenden Diskussionen.

Ebenso möchte ich Herrn Prof. Dr. Thomas Röder herzlich danken für sein Interesse an meiner Arbeit sowie seiner Bereitschaft, das Korreferat zu übernehmen.

Bei meinen ehemaligen und derzeitigen Laborkollegen Athena Chalaris, Britta Hansen, Christoph Garbers, Claudia Broder, Jan Suthaus, Jessica Rabsch, Katja Möller, Kristina Bernoth, Marija Stevanovic, Miryam Müller, Nina Adam, Stefanie Schnell, Sven Malchow sowie unseren guten Seele Petra Voss möchte ich mich für die freundschaftliche und entspannte Zusammenarbeit im Labor und die netten Mittagspausen bedanken, die einem auch in schweren Phasen Motivation gegeben haben.

Bei Nico Schneider, Thies Reik und Silke Horn möchte ich mich für die Hilfe im Labor und im Tierstall bedanken.

Meiner Famile danke ich herzlich für ihre allzeit offenen Ohren und aufmunternden Worte! Insbesondere möchte ich meinen Eltern für ihre Unterstützung danken. Dank Ihnen war es mir überhaupt möglich diesen Weg zu gehen.

Zum Schluss möchte ich einer ganz besonderen Person in meinem Leben danken, ohne die ich nicht so weit gekommen wäre. Liebster Michel, ich bin dir unendlich dankbar für deine Unterstützung, dein Verständnis und deine Liebe in allen Lebenslagen. Ohne dich wäre mein Leben nicht annähernd so wunderbar.

9.5 Eidesstattliche Erklärung

Hiermit erkläre ich, Antje Michaela Schütt, dass ich die vorliegende Arbeit selbständig und nur mit Hilfe der angegebenen Hilfsmittel und Quellen unter Anleitung meiner akademischen Lehrer unter Einhaltung der Regeln guter wissenschaftlicher Praxis der Deutschen Forschungsgemeinschaft angefertigt habe.

Diese Dissertation wurde bisher an keiner anderen Fakultät vorgelegt.

Ich erkläre, kein anderes Promotionsverfahren ohne Erfolg beendet zu haben, und dass keine Aberkennung eines bereits erworbenen Doktorgrades vorliegt.

Die eingereichte schriftliche Fassung der Arbeit entspricht der auf dem elektronischen Speichermedium.

Kiel, den

Antje M. Schütt